

# **Leg 193 Preliminary Report**

Anatomy of an Active Felsic-Hosted  
Hydrothermal System, Eastern Manus Basin

7 November 2000–3 January 2001

Shipboard Scientific Party

Ocean Drilling Program  
Texas A&M University  
1000 Discovery Drive  
College Station TX 77845-9547  
USA

February 2001

## PUBLISHER'S NOTES

This report was prepared from shipboard files by scientists who participated in the cruise. The report was assembled under time constraints and does not contain all works and findings that will appear in the *Initial Reports* of the ODP *Proceedings*. Reference to the whole or to part of this report should be made as follows:

Shipboard Scientific Party, 2001. Leg 193 Preliminary Report. *ODP Prelim. Rpt.*, 93 [Online]. Available from World Wide Web:  
<[http://www-odp.tamu.edu/publications/prelim/193\\_prel/193PREL.PDF](http://www-odp.tamu.edu/publications/prelim/193_prel/193PREL.PDF)>. [Cited  
YYYY-MM-DD]

Distribution: Electronic copies of this series may be obtained from the Ocean Drilling Program's World Wide Web site at <http://www-odp.tamu.edu/publications>.

This publication was prepared by the Ocean Drilling Program, Texas A&M University, as an account of work performed under the international Ocean Drilling Program, which is managed by Joint Oceanographic Institutions, Inc., under contract with the National Science Foundation. Funding for the program is provided by the following agencies:

Australia/Canada/Chinese Taipei/Korea Consortium for Ocean Drilling  
Deutsche Forschungsgemeinschaft (Federal Republic of Germany)  
Institut National des Sciences de l'Univers-Centre National de la Recherche Scientifique (INSU-CNRS; France)  
Ocean Research Institute of the University of Tokyo (Japan)  
National Science Foundation (United States)  
Natural Environment Research Council (United Kingdom)  
European Science Foundation Consortium for Ocean Drilling (Belgium, Denmark, Finland, Iceland, Ireland, Italy, The Netherlands, Norway, Spain, Sweden, and Switzerland)  
Marine High-Technology Bureau of the State Science and Technology Commission of the People's Republic of China

## **DISCLAIMER:**

Any opinions, findings, and conclusions or recommendations expressed in this publication are those of the author(s) and do not necessarily reflect the views of the National Science Foundation, the participating agencies, Joint Oceanographic Institutions, Inc., Texas A&M University, or Texas A&M Research Foundation.



The following scientists were aboard the *JOIDES Resolution* for Leg 193 of the Ocean Drilling Program:

Fernando Barriga  
Co-Chief Scientist  
Departamento de Geologia  
Universidade de Lisboa  
Edificio C2, Piso 5  
Campo Grande  
1749-016 Lisboa  
Portugal  
Internet: f.barriga@fc.ul.pt  
Work: (35) 21-750-0066  
Fax: (35) 21-759-9380

Raymond A. Binns  
Co-Chief Scientist  
Division of Exploration and Mining  
CSIRO  
PO Box 136  
North Ryde NSW 1670  
Australia  
Internet: r.binns@syd.dem.csiro.au  
Work: (61) 2-9490-8741  
Fax: (61) 2-9490-8921

Jay Miller  
Staff Scientist  
Ocean Drilling Program  
Texas A&M University  
1000 Discovery Drive  
College Station TX 77845-9547  
USA  
Internet: miller@odpemail.tamu.edu  
Work: (979) 845-2197  
Fax: (979) 845-0876

Ryuji Asada  
Microbiologist  
Department of Earth Sciences  
Kanazawa University  
Kakuma, Kanazawa  
Ishikawa Prefecture 920-1192  
Japan  
Internet: rasada@kenroku.kanazawa-u.ac.jp  
Work: (81) 76-264-5732  
Fax: (81) 76-264-5746

Wolfgang Bach  
Petrologist  
Department of Marine Chemistry and  
Geochemistry  
Woods Hole Oceanographic Institution  
360 Woods Hole Road, Mail Stop #8  
Woods Hole MA 02543  
USA  
Internet: wbach@whoi.edu  
Work: (508) 289-2523  
Fax: (508) 457-2183

Anne C.M. Bartetzko  
LDEO Logging Scientist  
Angewandte Geophysik  
RWTH Aachen  
Lochnerstrasse 4-20  
52056 Aachen  
Germany  
Internet:  
A.Bartetzko@geophysik.rwth-aachen.de  
Work: (49) 241-804827  
Fax: (49) 241-8888-132

Liane G. Benning  
Geochemist  
School of Earth Sciences  
University of Leeds  
Leeds LS2 9JT  
United Kingdom  
Internet: liane@earth.leeds.ac.uk  
Work: (44) 113-233-5220  
Fax: (44) 113-233-5259

Terje Bjerkgård  
Petrologist/Structural Geologist  
Mineral Resources Division  
Geological Survey of Norway  
Leiv Eirikssons Vei 39  
N-7491 Trondheim  
Norway  
Internet: terje.bjerkgard@ngu.no  
Work: (47) 73-90-40-00  
Fax: (47) 73-92-16-20

Lizet Brokner Christiansen  
Physical Properties Specialist  
Department of Earth and Planetary Sciences  
Johns Hopkins University  
3400 North Charles Street  
Baltimore MD 21218  
USA  
Internet: lizet@jhu.edu  
Work: (410) 516-8543  
Fax: (410) 516-7933

Erika R. Elswick  
Geochemist  
Department of Geological Sciences  
Indiana University  
1001 East Tenth Street  
Bloomington IN 47405  
USA  
Internet: eelswick@indiana.edu  
Work: (812) 855-2493 or  
Fax: (812) 855-7899

Robert Findlay  
Science Observer/Structural Geologist  
Geological Survey of Papua New Guinea  
Department of Mining  
Private Bag  
Port Moresby National Capital District  
Port Moresby, Papua New Guinea  
Internet: director@daltron.com.pg  
Work: (675) 321-2422  
Fax: (675) 321-1360

Gerardo J. Iturrino  
Logging Staff Scientist  
Borehole Research Group  
Lamont-Doherty Earth Observatory  
Columbia University  
Route 9W  
Palisades NY 10964  
USA  
Internet: iturrino@ldeo.columbia.edu  
Work: (914) 365-8656  
Fax: (914) 365-3182

Hiroyuki Kimura  
Microbiologist  
Graduate School of Biosphere Sciences  
Hiroshima University  
1-4-4 Kagamiyama  
Higashi-Hiroshima, Hiroshima 739-8528  
Japan  
Internet: hirok@hiroshima-u.ac.jp  
Work: (81) 824-24-7986  
Fax: (81) 824-22-7059

John B. Kulange  
Science Observer/Sulfide Petrologist  
Geology Department  
University of Papua New Guinea  
PO Box 414, University  
N.C.D.  
Papua New Guinea  
Internet: kulange@yahoo.com  
Work: (675) 326 7395  
Fax: (675) 326 7187

Klas S. Lackschewitz  
Sedimentologist  
Fachbereich Geowissenschaften  
Universität Bremen  
Postfach 330440  
28334 Bremen  
Germany  
Internet: klacksch@uni-bremen.de  
Work: (49) 421-218-7763  
Fax: (49) 421-218-9460

Sang-Mook Lee  
Paleomagnetist  
Deep-Sea Research Center  
Korea Ocean Research and Development  
Institute  
Ansan PO Box 29  
Seoul 425-600  
Korea  
Internet: smlee@kordi.re.kr  
Work: (82) 31-400-6363  
Fax: (82) 31-418-8772

Andrew Masta  
Science Observer/Microbiologist  
Division of Biochemistry and Molecular  
Biology  
School of Medicine and Health Sciences  
University of Papua New Guinea  
PO Box 5623  
Boroko  
Papua New Guinea  
Internet: mastaany@upng.ac.pg  
Work: (675) 7324 3811  
Fax: (675) 3243 827

Holger Paulick  
Petrologist  
Institut für Mineralogie  
Technische Universität Bergakademie  
Freiberg Lehrstuhl für Lagerstättenlehre  
Brennhausgasse 14  
09599 Freiberg  
Germany  
Internet:  
holger.paulick@mineral.tu-freiberg.de  
Work: (49) 3731-392662  
Fax: (49) 3731-392610

Álvaro M. Pinto  
Sulfide Petrologist  
Departamento de Geologia  
Universidade de Lisboa  
Edifício C2, Piso 5  
Campo Grande  
1749-016 Lisboa  
Portugal  
Internet: alvaro-pinto@clix.pt or  
alvaro.pinto@somimcor.pt  
Work: (351) 21-750-0066  
Fax: (351) 21-759-0064

Stephen Roberts  
Sulfide Petrologist  
School of Ocean and Earth Sciences  
University of Southampton  
Southampton SO14 3ZH  
United Kingdom  
Internet: sr1@mail.soc.soton.ac.uk  
Work: (44) 23-80593246  
Fax: (44) 23-80593052

Steven D. Scott  
Sulfide Petrologist  
Department of Geology  
University of Toronto  
22 Russell Street  
Toronto ON M5S 3B1  
Canada  
Internet: scottsd@geology.utoronto.ca  
Work: (416) 978-5424  
Fax: (416) 978-3938

David A. Vanko  
Igneous Petrologist  
Department of Geology  
Georgia State University  
24 Peachtree Center Avenue  
Atlanta GA 30303  
USA  
Internet: dvanko@gsu.edu  
Work: (404) 651-2272  
Fax: (404) 651-1376

Ian Warden  
Science Observer/Sulfide Petrologist  
Nautilus Minerals Corporation  
397 Liverpool Street  
Darlinghurst NSW 2010  
Australia  
Internet: rosswarden@ozemail.com.au  
Work: (61) 02-9360-2941  
Fax: (61) 02-9380-5593

Christopher J. Yeats  
Sulfide Petrologist  
CSIRO Division of Exploration and Mining  
PO Box 136  
North Ryde NSW 1670  
Australia  
Internet: chris.yeats@dem.csiro.au  
Work: (61) 2-9490-8697  
Fax: (61) 2-9490-8921

## SCIENTIFIC REPORT

### ABSTRACT

Ocean Drilling Program Leg 193 undertook an exploration of the lateral, vertical, and temporal variability of a seafloor hydrothermal system hosted by felsic volcanic rocks in a convergent plate margin setting. In planning for this expedition, we knew we would encounter a myriad of technical challenges, so we brought with us an arsenal of tools, some still unproven, to help us achieve our objectives. Three sites on the crest of Pual Ridge in the Eastern Manus Basin were proposed as primary targets, one each in an area of high-temperature venting (a black smoker chimney field), a field of lower temperature diffuse venting, and at a reference site that, although proximal to a high-temperature venting area, showed no surficial evidence of hydrothermal activity. From the first core recovered to the last, and throughout our coring, wireline logging, and logging-while-drilling operations, the prophetic watchwords of the cruise—to “expect the unexpected”—rang true. With the material recovered, we expect to assess the interplay between magmatic-derived fluids and seawater and to examine fluid pathways with an eye toward establishing a comprehensive chemical and hydrologic model for this system. The intensity, degree, and distribution of alteration facies and details regarding the abundance of clay minerals and anhydrite chronicled in the Leg 193 Initial Reports volume directly address these objectives. We have intersected an actively forming base metal sulfide system. However, poor core recovery in the sulfide-rich interval precludes adequate assessment of the dimension of such mineralization. Detailed consideration of extensive downhole logging data, still being processed, will throw additional light on this issue. Our initial perception is that despite the pervasive alteration indicative of a long-lived hydrothermal system, we have glimpsed the prenatal development of a massive sulfide deposit, which, given continued maturation, could develop into a deposit on the order of those exploited for centuries in ancient ore environments. Additionally, we seek to develop a petrogenetic model for the volcanic rocks at Pual Ridge and evaluate the volcanic architecture of this edifice. Low recovery notwithstanding, the descriptions and analyses of the cores from all three types of sites drilled during this expedition define a fresh volcanic cap underlain by pervasively altered volcanic flows and breccias, albeit with short intervals of markedly less intense alteration, which reveal the nature of the growth and evolution of this edifice. Finally, we set out to determine the nature, extent, and habitat controls of microbial activity in this hydrothermal system. Direct counting and biological tracer analyses indicate the presence of a biomass to >100 m below seafloor. Cultivation experiments indicate that potential microbiological activity persists to much deeper and more harsh environments. We recognize that all of these scientific objectives rely on postcruise research to be fully realized. We are confident, however, that by integrating the results of that research with the detailed descriptions we have recorded and the array of continuous records provided by the logging tools, we will be able to make direct comparisons with not only other active seafloor hydrothermal areas, but with

ancient ore deposition environments as well, improving our understanding of these complex systems.

## **BACKGROUND AND OBJECTIVES**

### **Background**

Felsic volcanic sequences and their associated intrusive rocks, presumed to have erupted in convergent margin or what are broadly called island arc settings, have long been recognized as especially prospective for a variety of valuable hydrothermal ore deposits. These range from massive sulfide deposits rich in both base and precious metals to deep-seated porphyry copper-gold deposits. Understanding how such ore bodies were created in the past, by deciphering the interplay between igneous, structural, hydrothermal, and hydrologic processes in a close modern analog of such a setting, will improve the capability of future exploration geoscientists to recognize favorable signals of economic potential in ancient sequences.

The western margin of the Pacific plate displays numerous convergent segments or subduction zones, most of which, over the past two decades, have been shown to exhibit seafloor hydrothermal activity at one or more sites in their vicinity (Fig. 1). The first place where hydrothermal “chimney” deposits and associated vent fauna were discovered, other than on a mid-ocean spreading axis, was in the Manus Basin in the Bismarck Sea north of Papua New Guinea (Both et al., 1986). This was at a site now called Vienna Woods on the basaltic Manus spreading center, near the apex of a wedge of backarc oceanic crust (Fig. 2). By contrast, the Eastern Manus Basin has a more complex geological construction involving the creation of continental-type crust, and the Manus Basin accordingly shows closer affinities to ancient orebody settings. It contains the PACMANUS (Papua New Guinea-Australia-Canada-Manus) hydrothermal field, discovered in 1991 (Binns and Scott, 1993), where the host volcanic sequence is conspicuously siliceous. Now thoroughly surveyed at the seafloor surface, PACMANUS is the site where the first subsurface study of an active felsic-hosted convergent margin hydrothermal system was conducted during Leg 193. As anticipated, we found significant differences between this site and hydrothermal activity hosted by mafic volcanic rocks and sediments on divergent margins (seafloor spreading axes) previously drilled during Ocean Drilling Program (ODP) Leg 158 to the TAG hydrothermal area on the Mid-Atlantic Ridge and Legs 139 and 169 in the northeast Pacific, respectively. The differences are profoundly important in understanding chemical and energy fluxes in the global ocean, as well as for understanding mineral deposit geology.

The region that includes the Manus Basin is a highly mineralized sector of the Earth’s crust. Notable hydrothermal ore deposits of Neogene to Quaternary age in Papua New Guinea include the Panguna porphyry copper-gold deposit on Bougainville Island, the Ladolam epithermal gold deposit in the Tabar-Lihir-Tanga-Feni island chain north of New Britain, and, on the mainland,

the Porgera polygenetic gold deposit and the Ok Tedi and Grasberg porphyry copper-gold deposits. Combining these with modern mineralizing systems like PACMANUS, such fertility hints at an underlying cause, perhaps the presence of geochemically anomalous mantle lithosphere as the source of metals concentrated by hydrothermal processes in both continental and marine settings. The results of Leg 193 have added to our understanding of the processes involved in such ore formation. Although focused on the submarine environment, the knowledge gained will also have application to subaerial and transitional ore environments.

### **Regional Setting**

The Manus Basin is a rapidly opening (~10 cm/yr) backarc basin set between opposed fossil and active subduction zones (Manus Trench and New Britain Trench, respectively) within a complex zone of oblique convergence between the major Indo-Australian and Pacific plates (Fig. 2). Adjacent to the now-inactive Manus Trench or its antecedent, volcanism above an Eocene–Oligocene intraoceanic subduction zone within the Pacific plate (or at its boundary with an oceanic portion of the Indo-Australian plate, now represented by the Solomon microplate) formed an island arc represented by exposures of this age on New Ireland, New Hanover, Manus, and parts of New Britain (e.g. Hohnen, 1978; Stewart and Sandy, 1988). Paleomagnetic measurements (Falvey and Pritchard, 1985) indicate that these islands have been relocated to their present positions by an imperfectly understood sequence of backarc developments (Exon and Marlow, 1988). During the late Miocene or Pliocene, when arrival of the Ontong Java Plateau blocked subduction at the Manus Trench, convergence switched to the New Britain Trench. Here the Cretaceous oceanic Solomon microplate is moving under what is now the South Bismarck microplate (a unit separated from the Pacific plate by more recent backarc processes). Above the north-dipping Wadati-Benioff Zone associated with the New Britain Trench, a chain of young arc volcanoes has formed along the concave northern side of New Britain (Bismarck or New Britain Arc; Johnson, 1976).

The present-day configuration of spreading segments, extensional faults, and obliquely oriented transform faults in the Manus Basin (Fig. 3) is well established by bathymetric, sidescan sonar, seismic reflection, gravity, and magnetic surveys (Taylor, 1979; Taylor et al., 1991), and by microseismicity (Eguchi et al., 1989), which defines left-lateral movement on the transform faults. In contrast to the wedge-shaped Manus spreading center, where new backarc oceanic crust has been forming since the 0.78-Ma Brunhes/Matuyama boundary (Martinez and Taylor, 1996), the rift zone of the Eastern Manus Basin lying between the islands of New Ireland and New Britain, and between two major transform faults (Djaul and Weitin Faults), is a pull-apart zone of distributed extension on mostly low-angle faults approximately normal to the transforms. Martinez and Taylor (1996) infer ~80 km of extension across a 150-km-wide rift zone, mostly concentrated in the bathymetrically deeper portion of thinned crust (Fig. 4), which is coincident with an isostatic gravity high. They argue that this amount of extension is equivalent to that accomplished by a combination of backarc spreading and microplate rotation in the central

portion of the Manus Basin (Fig. 3). Bathymetry, gravity modeling, and reverse magnetization indicate that basement of the Eastern Manus Basin (called the Southeastern Rifts by Martinez and Taylor, 1996) is arc crust equivalent to the Eocene–Oligocene exposures on New Britain and New Ireland. Reflection seismic traverses across the Eastern Manus Basin (Fig. 5A; also B. Taylor and K.A.W. Crook, unpubl. data) show essentially undeformed graben and half-graben fills up to 0.3 s, equivalent to ~1 m.y. at current sedimentation rates. This is consistent with rifting in the Eastern Manus Basin covering a similar duration to spreading on the central Manus spreading center. The sediment fill is commonly tilted, denoting block rotation on listric master faults. The dredging of fault scarps, where seismic profiles indicate exposure of lower, more deformed sequences, has yielded fossiliferous calcareous mudstones and volcanoclastic sandstones ranging in age from early Miocene to the Pliocene/Pleistocene boundary. Although mainly of deeper marine origin, these are contemporaneous with the Miocene Lelet Limestone and Pliocene Rataman Formation, which overlie the Eocene–Oligocene Jaulu Volcanics of New Ireland (Stewart and Sandy, 1988), and with equivalent sequences on New Britain. Undated, mildly metamorphosed basalts dredged from inner nodal scarps near the active ends of the Djaul and Weitin transform faults may represent the presumed arc volcanic basement.

Built up on this nascent continental crust, and probably controlled by subtle, relatively recent changes in the extensional stress field, a series of high-standing neovolcanic edifices (eastern Manus volcanic zone; Binns and Scott, 1993) extends en echelon across the trend of the rift faults (Fig. 6). Because these edifices do not significantly disturb the negative regional magnetization derived from basement, they are considered to be superficial features (Martinez and Taylor, 1996). The neovolcanic edifices range from central eruptions of more mafic lavas (basalt and basaltic andesite) to linear ridges formed by fissure eruption of andesite, dacite, and rhyodacite. The westernmost volcanic feature of Figure 6 is a low axial ridge of basalts with compositions resembling mid-ocean-ridge basalt (MORB), set within a deep trough (Fig. 4). This is probably a failed spreading center. The other edifices, however, are variably but distinctly potassic. They have trace element and isotopic affinities comparable with the subaerial arc volcanoes of New Britain (Binns et al., 1996b; Woodhead and Johnson, 1993) rather than with the MORBs at the Manus spreading center (Woodhead et al., 1998), the Willaumez extensional transform fault (Taylor et al., 1994), and in the adjacent East Sherburne volcanic zone (R. Binns, unpubl. data) (Fig. 3). The eastern Manus volcanic zone appears to be a submarine segment of the New Britain arc, displaced from the main subaerial chain and erupted in the rifted backarc region.

The region is one of active seismicity, especially on transform faults. The major magnitude 8.2 earthquake of 16 November 2000 was typical. It occurred 25 km deep under the western active end of the Weitin Fault (Fig. 6), causing disruption in Rabaul and a consequent delay to commencement of drilling operations for Leg 193. Tregoning et al. (1998) measured 13 cm/yr of sinistral transcurrent movement on the Weitin fault, which is a major plate boundary.

The PACMANUS hydrothermal field targeted by Leg 193 is located near the crest of Pual Ridge, a 500- to 700-m-high felsic neovolcanic ridge with negligible sediment cover that trends northeast (Figs. 4, 6). This ridge is externally terraced and appears constructed of stacked subhorizontal lava flows 5–30 m thick, with negligible to minor sediment cover along the crest. Dacite and some rhyodacite block lavas with rough surface topography predominate, but there are also some smoother sheet flows and lobate flows of dacite (Waters et al., 1996). Consanguineous lobate flows of andesite occupy the lower reaches of Pual Ridge, whereas the 2200-m-deep valley to its east is floored by lobate flows of basaltic andesite (Fig. 6).

### **PACMANUS Hydrothermal Field**

Isolated hydrothermal deposits are scattered for at least 13 km along the main crestal zone of Pual Ridge (Binns and Scott, 1993; Binns et al., 1995, 1996a, 1997a, 1997b). The more significant, active deposits are in the center of this zone between two low knolls on the ridge crest (Fig. 7). Lavas in this central area are exclusively dacitic to rhyodacitic (65–71 wt% SiO<sub>2</sub>). Four principal fields of hydrothermal activity, including sulfide chimneys, and several smaller sites have been delineated and named. Much of the information cited below is currently unpublished and is derived from cruises listed in the caption of Figure 7.

Roman Ruins (1693–1710 m below sea level [mbsl] and 150 m across) contains many close-packed simple columnar chimneys that stand as high as 20 m and some complex multispired chimneys with numerous conduits. Commonly, these coalesce into wall-like constructions oriented north-south. Many chimneys are broken (seismic effects?) and some show later regrowth. Fallen chimneys form a 10-m-high pediment for the active structures including black smokers and diffuser-style chimneys that emit clear fluid. A smaller, deeper (1730–1740 mbsl) field to the north, Rogers Ruins, is linked to Roman Ruins by a zone of Fe oxyhydroxide deposits. Numerous small occurrences of the latter and of Mn oxides are common throughout the PACMANUS field.

Satanic Mills (1708–1720 mbsl and 200 m across) is an equivalent-sized field of rather more scattered chimneys and spires marked by clouds of dark particulate-rich hydrothermal fluid (“black smoke”). Both black to gray smokers and structures that are vigorously venting clear fluid are in close proximity. East of this field are north-south oriented fissures in dacite, encrusted with fauna, that are emitting clear fluid and are interpreted as juvenile vents soon to become smoker fields. To its south, Satanic Mills is linked by a zone of altered dacite with diffuse venting and scattered Fe-Mn oxide deposits to the smaller Marker 14 field, which, at 1745 mbsl depth, is the deepest hydrothermal site so far recognized at PACMANUS. Deflections of bathymetric contours beyond both the Roman Ruins-Rogers Ruins and Satanic Mills-Marker 14 lines suggest that both fields are located on north-northwest-trending fracture zones.

The Tsukushi field (1680–1686 mbsl) at the southwestern end of PACMANUS contains numerous actively venting chimneys as high as 30 m, many very slender but some as much as 10 m in diameter. This area was traversed by bottom camera in 1993 and by a *Shinkai-6500*



submersible dive in 1995 without sighting chimneys. However, chimneys were discovered during a 1996 *Shinkai-2000* submersible dive, and additional large chimneys were present in 1998. Hence, it might be very young. Fe oxyhydroxide and Fe-Mn oxide crusts are common in the zone that extends northeast from Tsukushi.

Snowcap Knoll (1654–1670 mbsl), the other major active hydrothermal site at PACMANUS, is very different in character. It occupies the crest and the flanks of a 10- to 15-m-high hill, 100 m × 200 m in size, bounded on its eastern side by a north-northeast-striking fault scarp 60–80 m high. Outcrops of altered dacite-rhyodacite lava and hyaloclastite predominate, locally covered with patches of both sandy sediment and metalliferous hemipelagic ooze (only millimeters thick). Gravity corer and grab operations revealed the sand to be altered lava disaggregated by bioturbation or hydrothermal fragmentation. Typical alteration assemblages at Snowcap Knoll are dominated by cristobalite, with lesser natroalunite, diaspore, and illite-montmorillonite with traces of pyrite, marcasite, chalcopyrite, enargite, and formerly molten globules of native sulfur. These reflect interaction at relatively low temperature between dacites and a highly acid, relatively oxidized hydrothermal fluid (“advanced argillic alteration”), indicating that SO<sub>2</sub>-bearing magmatic components were present in the fluid.

Diffuse low-temperature venting (6°C, compared with 3°C in ambient seawater) is extensive across the gently undulating to flat crest of Snowcap Knoll. More intense shimmer occurs at the edges of the occasional Mn-encrusted outcrop of altered dacite. The diffuse vent sites are marked by white surficial patches that probably include both microbial mat and methane hydrate deposits. Around the southwestern fringes of Snowcap Knoll are several small fields of actively smoking and inactive chimneys aligned in north-south trending clusters.

Fluid temperatures measured at the orifices of black or gray smokers and sulfide chimneys venting clear fluid are comparable for the Satanic Mills, Roman Ruins, and Tsukushi fields, ranging between 220° and 276°C. End-member vent fluids are very acid (pH = 2.5–3.5), show high K/Ca ratios reflecting equilibration with dacite wallrocks, are high in Mn and Fe relative to mid-ocean-ridge fluids, and have variable salinities (Gamo et al., 1996; Auzende et al., 1996; Charlou et al., 1996). The variable salinities imply subsurface phase separation, meaning hydrothermal temperatures exceed 350°C at indeterminate depths below the chimney fields. This is supported by mineralogical evidence of multiple fluid compositions in chimney assemblages (Parr et al., 1996). End-member gas compositions of 20–40 mM CO<sub>2</sub>, 20–40 μM CH<sub>4</sub>, and R/R<sub>A</sub>(He) = 7.4 denote significant contribution to the hydrothermal fluids from arc-type magmatic sources (Ishibashi et al., 1996). Douville et al. (1999) ascribe unusually high fluorine contents in the fluids to magmatic sources. Temperatures of 40° to 73°C have been measured in the shimmering clear fluid emitted from Fe oxyhydroxide deposits in the Tsukushi-Snowcap Knoll zone.

A very high thermal gradient of 15°C/m was measured at a sediment pocket on Snowcap Knoll adjacent to a 6°C shimmering water zone. Fluids collected near this by a funnel sampler

are close to seawater in composition but are enriched in Mn, Fe, and Al. All outcrops of altered dacite at Snowcap Knoll are encrusted by Fe-Mn oxide.

Chimneys collected from Roman Ruins and Satanic Mills are comparatively rich in precious metals (average Au = 15 ppm; average Ag = 320 ppm) and are composed predominantly of chalcopyrite and sphalerite, with subsidiary pyrite, bornite, tennantite, galena, and dufrenoyite (Scott and Binns, 1995; Parr et al., 1996). Barite is the principal gangue, but anhydrite substitutes in some samples. Chimneys at Roman Ruins typically contain less Cu than those at Satanic Mills. Fewer samples have been recovered from Tsukushi and the southwestern side of Snowcap Knoll, but these are virtually devoid of Cu and Au and contain more Pb and Ag. Their gangue includes appreciable amorphous SiO<sub>2</sub> as well as barite.

PACMANUS chimneys have elevated contents of “magmatophile” trace elements (e.g., As, Sb, In, Tl, and Te). Sulfur isotope ratios near zero per mil  $\delta^{34}\text{S}$  (Gemmell et al., 1995; 1996) indicate a larger magmatic-sourced component than found at mid-ocean-ridge hydrothermal sites and mature backarc spreading axes. Direct evidence for the importance of magmatic fluids is found in the Cu + Zn-rich gas-filled cavities within glass melt inclusions in the phenocrysts of Pual Ridge andesites (Yang and Scott, 1996), as well as in the gas compositions of collected vent fluids (see above).

The PACMANUS hydrothermal field supports an exceptionally abundant vent macrofauna broadly similar to those of other southwest Pacific sites (Hashimoto et al., 1999), dependent on chemosynthetic microbes. At Snowcap Knoll, dredged samples of altered dacite possess microscopic tube worms (unidentified species) along internal hairline fractures. These, and their presumed symbiotic microbes, were the first indication of the presence of a subsurface biosphere that was also investigated during Leg 193.

### **Scientific Objectives**

The overall aims of Leg 193 were to delineate the subsurface volcanic architecture, the structural and hydrologic characteristics, the deep-seated mineralization and alteration patterns, and the microbial activity of the PACMANUS hydrothermal field. From these data and subsequent laboratory analyses of samples and structural data, we planned to pursue the following specific scientific objectives.

1. Quantify the manner in which fluids and metals derived from underlying magmatic sources, and from leaching of wallrocks by circulated seawater, respectively, have combined within the PACMANUS hydrothermal system. This would be approached by applying geochemical and isotopic modeling to the vertical and lateral variations in hydrothermal alteration styles and sulfide mineral occurrences established by the drilling.
2. Evaluate the mechanisms of subsurface mineral precipitation, including comparison of exhalative and subhalative mineralizing processes, assessing the consequences of fluid

phase separation, and seeking explanations for the elevated contents of copper, zinc, silver, and gold in massive sulfide chimneys at the PACMANUS seafloor.

3. Delineate probable fluid pathways within the system and establish a hydrologic model by measuring and interpreting variations in physical properties and fracture patterns of fresh and altered bedrocks.
4. Test whether the volcanic construction of Pual Ridge is a simple “layer cake,” with potential older exhalative or subhalative massive sulfide horizons concealed by younger lavas or, alternatively, whether inflation of the volcanic edifice by lava domes or shallow intrusions is the predominant process in this submarine felsic volcanic environment.
5. Develop a petrogenetic model for Pual Ridge igneous rocks and seek evidence pertaining to the nature of the possible underlying source for magmatic components in the hydrothermal fluids.
6. By combining the above models, develop an integrated understanding of coupling between volcanological, structural, and hydrothermal phenomena in the PACMANUS system for comparison with equivalent hydrothermal phenomena at mid-ocean ridges and to provide a new basis for interpreting ancient ore environments.
7. Establish the nature, extent, and habitat controls of microbial activity within the hydrothermal system and interpret the differences encountered in diversity and biomass in terms of nutrient supplies and environmental habitats in the context of the geochemical and hydrologic understanding of the total hydrothermal system.

## **OPERATIONS SUMMARY**

Leg 193 was logistically different than most ODP expeditions in that all sites occupied were less than 1 km apart on the crest of Pual Ridge. Events in this operations summary are presented in chronological order (see Table 1).

### **Guam Port Call**

Leg 193 began with the first line passed ashore to the fueling dock at 1700 hr on 7 November 2000. Port call activities including loading the equipment required in support of the arsenal of tools we brought along to ensure the success of this expedition. These tools included, above and beyond all of our routine paraphernalia, two developmental systems, the advanced diamond core barrel (ADCB) and the hard-rock reentry system (HRRS). Engineering observers, scientific observers representing Papua New Guinea (PNG), and an observer representing the mining company holding a lease on our operational area sailed as part of the ship’s complement. At 0800 hr on 14 November the last line was cast off and we were under way at full speed for our first drilling target. During the entire transit to Manus Basin, we enjoyed fair weather.

**Site 1188**

Upon arrival at Site 1188 (Snowcap Knoll diffuse venting area) on the evening of 18 November, arrangements for customs and immigration clearance to PNG had not been finalized. We could not commence operations until clearance had been received, which resulted in delaying our start until 0845 hr on 19 November, when a helicopter carrying customs and immigration officials arrived on the *JOIDES Resolution* from Rabaul, Papua New Guinea. Our overall strategy was to drill a series of pilot holes in each of the three high-priority areas and to assess from those operations how best to pursue our scientific objectives. A short survey with the subsea camera identified our first target, and Hole 1188A was initiated at 1230 hr on 19 November with a jet-in test to determine the thickness of sediment cover and/or soft formation, which might dictate our operational approach. Coring continued until 0900 hr on 21 November, when the pipe stuck in the borehole while we recovered Core 193-1188A-23R (to 211.6 m below seafloor [mbsf]) (Table 2). This was the last of several episodes of stuck pipe, which along with poor recovery (slightly >10%) indicated poor hole conditions. Despite several hours of attempts to free the drill string, including releasing the bit, we eventually were forced to sever just below the seafloor, ending operations at this hole at 0830 hr on 22 November.

**Site 1189**

After assembling a new bottom-hole assembly (BHA), a second seafloor camera survey located a drilling location at our next high-priority site (Roman Ruins high-temperature area). A 3-m jet-in test at 1615 hr on 22 November was followed by continuous coring through Core 193-1189A-13R (to 125.8 mbsf). Once again, several incidents of stuck pipe and poor recovery (<7%) plagued operations, resulting in a second pipe-severing episode. The severed pipe cleared the rotary table at 2045 hr on 23 November, concluding operations in Hole 1189A.

**Site 1190**

Our third high-priority target was an area that was not known to host surficial evidence of extensive hydrothermal alteration. This area was far enough from known active venting that we hoped to use it a reference site. After a jet-in test failed to penetrate the surface, three holes (Holes 1190A, 1190B, and 1190C) were attempted between 0300 hr on 24 November and 0520 hr on 25 November. None of these holes penetrated >17 m, nor did they return more than three short intervals of core before hole conditions became the basis for abandonment.

**First Return to Site 1188**

With the arrival (via a second helicopter) of batteries for our logging-while-drilling/resistivity-at-bit (LWD/RAB) operations, we elected to attempt a RAB experiment at Site 1188. Our plan was to drill to ~75 mbsf to protect our BHA by keeping the decrease in drill string diameter (a potential spot for material to pinch off the drill string if the hole collapsed) above the level of the seafloor and establish a reentry site by deploying a free-fall-funnel (FFF).

We were to follow this with our first deployment of the ADCB, to determine if this method of coring provided improved hole conditions or recovery.

The RAB experiment went smoothly, starting at 1615 hr on 25 November, but the rate of penetration (ROP) decreased markedly at ~68 mbsf and we terminated penetration at 72 mbsf. We deployed a standard FFF, ran the vibration-isolated television (VIT) frame to bottom, and observed as the RAB tool was extracted from Hole 1188B without disturbing the FFF. The ADCB followed into Hole 1188B, but as there were several meters of fill in the bottom of the hole, we could make no new penetration. Attempts to deepen Hole 1188B were suspended at 1400 hr on 27 November. Despite not deepening Hole 1188B, the success of the RAB experiment in a hard-rock application was our first operational highlight.

### **Site 1191**

Having attempted rotary core barrel (RCB) coring at our primary sites, and recognizing that realizing our ultimate objectives would require significantly deeper penetration than we had been able to achieve with bare-rock spudding, we decided to attempt setting a casing string to prevent upper borehole wall collapse while we drilled deeper. Inasmuch as we were able to achieve >200 m of penetration at Hole 1188, and only just over 100 m in Hole 1189A, we decided our attempt at deep penetration should be at Site 1188, where we could set casing significantly deeper without missing a significant thickness of the section. Our engineers advised us that preparation for this deployment would take as much as a day. Because we had not brought any core on deck during operations at Hole 1188B, we chose to utilize the time required for assembling a reentry system by attempting another bare-rock spud at Satanic Mills, an alternate high-temperature venting site.

Hole 1191A was spudded at 2045 hr on 27 November, and RCB coring continued through to a depth of 20.1 mbsf before the pipe stuck fast. The driller was eventually able to free the pipe and recover the core barrel, but on deployment of the subsequent barrel there were indications that something was amiss. Low-circulation pressures indicated the core barrel was not seating properly, but indicators on the core barrel latching assembly appeared normal. In the meantime, the borehole started to collapse (indicated by >3 m of fill), and even through we were eventually able to attain 20 mbsf again, we could not advance the hole. By this time we were ready to begin our deep penetration attempt, so we abandoned operations at this site.

### **Second Return to Site 1188**

Considering the challenges we had faced during operations in our pilot holes, designing a reentry and deep penetration assembly introduced numerous complications to our standard deployment. Variability in local topography and in the depth of soft material covering hard volcanic rocks and the tendency of the borehole walls to be unstable were factored into our design. We foresaw the requirement for a minimum of at least 50–60 m of large diameter casing

in our initial deployment to offer the best chance of success of eventually casing to the approximate depth of Hole 1188A (211 mbsf).

Based on these considerations, we decided to deploy the conventional reentry cone/casing hanger in an unconventional manner. Because we needed to select a drilling target based on the assurance we could jet in at least 3 m of casing below the seafloor away from any obstructions, we could not emplace the reentry cone by running it on the end of the pipe and releasing it. In our standard configuration, it is impossible to see around the cone with our VIT camera and pick a specific target on the seafloor. Additionally, because we were limited in the number of attempts we could perform by the amount of casing hanger hardware in stock, if we deployed the cone only to discover later that we could not drill a hole, we would potentially lose our opportunity for deep penetration. Our innovative strategy was to drill a large-diameter (14.75 in) borehole to an intermediate depth for our initial casing deployment, drop the standard reentry cone in free-fall mode, and round trip the pipe to install our first casing string.

Three attempts at drilling a large diameter borehole (Holes 1188C, 1188D, and 1188E) were not successful at achieving our desired depth (confirming the merit of our strategy), but our fourth attempt (Hole 1188F) yielded the best hole conditions and drilling parameters we had enjoyed to date. By 0745 hr on 2 December, we had drilled to a depth of 104.0 mbsf (as deep as we could drill without placing the top of the BHA in jeopardy below the seafloor) with no significant indications of hole instability. Pulling the pipe to just below seafloor, the reentry cone was dispatched through the moonpool and made for the most rapid conventional reentry cone installation in ODP history (under 9 min at 187 m/min). After tripping the pipe, we decided that our best chance at installing a second casing string would rely on having a hole with the largest diameter possible to our target depth, so another 14.75-in bit was assembled, this time with a much longer BHA. By 0230 hr on 4 December, the hole had reached a total depth of 195.0 mbsf, although we experienced several intervals of minor hole blockage. Because the stability of the borehole was suspect, we adapted the fluid hammer HRSS to precede the large-diameter casing into the hole as a hole-cleaning system. This deployment was not without complications, requiring a couple of iterations and additional hole-cleaning operations, but by late in the evening of 8 December we had installed the casing to a depth of ~59 mbsf, with ~2.5 m of casing protruding above the throat of our standard reentry cone.

Although in other circumstances our inability to fully insert the casing string into the hanger might have been disastrous, our engineers immediately realized that the geometry of our casing assembly (out of the throat of our reentry cone and sticking up ~2.5 m above the casing hanger) was identical in concept to the design of our HRSS. A quick adaptation to the FFF and centralizer guide was all that was required to create a nested funnel system that was installed without complication. We commenced hole cleaning beneath the large-diameter casing string, and after several intervals of stuck pipe, we were prepared to deploy our second casing string. Our second casing run went without incident and by 1205 hr on 12 December, we had a hole

cased to 190 mbsf, cemented at the bottom for stabilization, and cleaned to a total depth of 218 mbsf in preparation for continuous coring.

At 1645 hr on 12 December we initiated ADCB coring in Hole 1188F with slow circulation rates while the drillers and engineers monitored our drilling progress. Slow coring rates were maintained at first to learn operational parameters, and recovery was intermittent, although on occasion excellent. Inasmuch as our goal was to achieve maximum penetration, we did not spend much time attempting to optimize our coring process for recovery. This resulted in poorer-than-expected average recovery, exacerbated by the fragmented formation. Continuous ADCB coring proceeded until reaching a depth of 327.2 mbsf. A failure in a core barrel landing ring necessitated a slightly premature bit trip, but as it turned out, the bit was worn and performance deterioration would have required a change in any case.

A second ADCB run (temporarily interrupted by another core barrel landing failure) continued through Core 193-1188F-47Z to a depth of 386.7 mbsf. At that point a steadily decreasing ROP (<1.0 m/hr) and no recovery for the last three cores prompted us to terminate ADCB coring. ADCB coring in Hole 1188F averaged nearly 20%, despite intensely fragmented core and core catchers not optimized for recovery of such material. ROP was as high as 4.5 m/hr and averaged ~3 m/hr. One of the primary lessons we took from this operation was how difficult it can be to optimize bit and core catcher design as well as coring parameters in variable lithologies. Further details of the ADCB deployment in Hole 1188F can be found in the Operation Manager's report for Leg 193 (available from ODP); however, the success of this endeavor should not be underestimated. The casing installation was accomplished with innovation and adaptation, and our earlier attempts at coring with an RCB system indicated to us that we would not have achieved our science objectives at this site without the development tools we employed. Coring operations at Hole 1188F were augmented by a series of wireline logging runs, following which we moved to Hole 1188B to attempt to measure borehole temperature and collect a water sample. Alas, neither the temperature tool nor the water sampler would pass an obstruction a few meters below the seafloor.

### **Return to Site 1189**

Yet another technical highlight of operations during Leg 193 was the first deployment of the complete HRRS. At 0015 hr on 23 December, we began a brief camera survey and initiated Hole 1189B in the middle of a chimney field. This hole was spudded with >30 m of casing using our developmental hammer-in-casing system. Although penetration rates were variable (as we expected from our previous coring operations in fresh and altered rocks), the casing was installed much faster than we anticipated (33 hr from start to finish), and resulted in a reentry hole, cased to 31 mbsf, in an area of extremely rugged local topography where no conventional reentry system would have had much chance for success. RCB coring through the HRRS commenced at 0815 hr on 24 December. Although recovery was poor (~8% for Cores 193-1189B-1R through 18R), coring continued without incident to a depth of 206.0 mbsf. At that point hole conditions

began to deteriorate, and because we were within 2 m of the maximum depth we could achieve without placing the top of the drill collars below the bottom of the casing, we decided to terminate operations in this hole. Wireline logging commenced at 2015 hr on 25 December and were complete by early afternoon on 26 December, ending operations in this hole.

### **Third Return to Site 1188**

With the logging assembly near the seafloor, we planned to collect a second temperature profile with the ultra-high temperature multisensor memory (UHT-MSM) tool and a water sample with the water-sampling temperature probe (WSTP). The temperature run indicated the borehole had heated up significantly since our logging operation (from ~100° to >300°C in 5 days), but we were not able to rapidly estimate a temperature gradient, resulting in a water sample from a much lower temperature interval than we had hoped.

### **Second Return to Site 1189**

Building on our successes, we decided to perform another LWD/RAB penetration, this time within the confines of the Roman Ruins chimney field. We had seen no evidence of high-temperature fluids in our earlier operations and were confident that our drilling fluid circulation would keep the borehole cool. The RAB experiment was designed to penetrate beneath a distinct lithology change and concomitant depth marker in wireline logging data from Hole 1189B ( $\pm 25$  m away). After reaching 166 mbsf in Hole 1189C, we decided to multiply our achievement by dropping a FFF and adding wireline logging in this hole to our operations strategy. This experiment provides not only the deepest LWD/RAB penetration within hard rock in ODP history, but it also represents the first time we will have the opportunity to directly compare wireline logging and RAB data in a hole drilled in fresh and altered volcanic rock on the seafloor.

### **Final Return to Site 1188**

With only a few days left for operations, we decided to attempt temperature profiles and water-sampling runs in Holes 1188B and 1189B, followed by another attempt to core at Site 1190. Although the first of these objectives was accomplished, a compassionate leave emergency required us to suspend operations and transit to the port of Rabaul. Upon arrival in Rabaul, PNG authorities opted to clear the vessel from their waters 2 days early (being the millennium change weekend) and required our immediate departure without further subsea operations.

## **SITE 1188**

### **Site Objectives**

Site 1188 is located on the Snowcap Knoll hydrothermal field, which straddles a low knoll on



the crest of Pual Ridge. The location is characterized by scattered outcrops of intensely altered to fresh dacite-rhyodacite and intervening areas of sediment with patches of dark Fe-Mn oxide crust and areas covered by white material, thought to be either microbial mat or clathrate deposits. Previous gravity coring of the sediment showed it to be composed predominantly of disaggregated altered dacite, formed by bioturbation and/or hydrothermal fragmentation. Temperatures of 6°C were measured by a submersible at one of the many shimmering water sites, most of which are close to the edge of rock outcrops.

The principal objectives of drilling at Site 1188 were to establish subsurface alteration and mineralization patterns, and their variation with depth, beneath this area of low-temperature diffuse venting and acid sulfate alteration at the seafloor. Other objectives included defining fluid pathway structures, testing the possible existence of “subhalative” massive sulfide layers, establishing the volcanic architecture, if allowed by the alteration, and delineating the extent and characteristics of subsurface microbial life. These objectives required relatively deep penetration, our aim being 500 m with the possibility of even deeper drilling if conditions were suitable.

### **Igneous Petrography**

Holes 1188A and 1188F are only ~30 m apart (Fig. 8), so together they provide a vertical section to a depth of 386.7 mbsf of the lithologic architecture beneath the low-temperature diffuse Snowcap Knoll hydrothermal field located within the PACMANUS hydrothermal area of Pual Ridge (Figs. 9, 10). Volcanic rocks from the upper part of Hole 1188A are unaltered rhyodacite (Fig. 11). Plagioclase (optically identified as labradorite) is the most common phenocryst phase with subordinant titanomagnetite (Fig. 12). Unaltered plagioclase crystals in the deeper altered rocks also have the optical properties of labradorite. Most of the rocks are either vesicular or amygdaloidal, with instances of open or incompletely filled vesicles persisting to some of the deepest units (Fig. 13). The groundmass of all the igneous rocks is uniformly fine grained, and porphyritic rocks contain relatively few and relatively small plagioclase phenocrysts (generally only 1%–2% and 1–2 mm long). Thus, all of the rocks are interpreted as volcanic, there being no coarser-grained rocks or textures such as microgranitic ones that might indicate a hypabyssal origin.

Occurrences of perlitic texture (Fig. 14), spherulitic texture, flow banding (Fig. 15), and volcanic brecciation and autobrecciation all attest to the success of the coring program in sampling various coherent and brecciated portions of the volcanic rocks that built up the upper 387 m of Pual Ridge. Occurrences of hydrothermal breccia and pseudoclastic textures illustrate details about the subsequent lithologic modifications that overprint the volcanic rocks when they are subjected to subseafloor hydrothermal activity.

### **Hydrothermal Alteration**

Alteration varies with depth and is complicated by overprinting relationships (Fig. 16). A 34-m-thick cap of fresh rhyodacite to dacite, possibly intercalated with altered units that have not

been recovered, is underlain by a sequence of deeply altered volcanic rocks from that depth in Hole 1188A to the bottom of Hole 1188F (387 mbsf). The original volcanic nature of the rock can often be recognized (Fig. 17). Pseudoclastic textures are frequently developed (Fig. 18). The earlier, more pervasive alteration (greenish) comprises silica forms and polymorphs varying successively from opaline silica (above) through cristobalite to quartz (below) accompanied by clays. Clays are mostly illite (Fig. 19) with chlorite, the latter especially at depth. Mixed-layer chlorite-smectite and pyrophyllite are also common. A second type of alteration (generally white), seldom truly pervasive and generally as veins or vein controlled, is composed of silica (as above), clays, pyrophyllite, and variable amounts of pyrite and anhydrite (Fig. 18). Deeper in the site (Hole 1188F), quartz and chlorite become more important, as a later silicification event (+ clays) overprints the two previous ones. Late anhydrite-pyrite-quartz veins are ubiquitous throughout (Fig. 20).

### **Sulfide and Oxide Petrography**

Pyrite is the dominant sulfide mineral at Site 1188. The first appearance of pyrite correlates with the onset of hydrothermal alteration of the uppermost dacitic volcanics in Hole 1188A. Within the hydrothermally altered rocks, pyrite is predominantly present in trace amounts (0%–5%) within four distinct settings: associated with anhydrite-silica-filled fractures (most common), as vesicle linings associated with anhydrite and silica, in silica-anhydrite-magnetite veins, and disseminated throughout the variably altered igneous protoliths.

Chalcopyrite is a minor phase throughout the core from Site 1188. Chalcopyrite first appears in trace amounts within a chloritized interval as small inclusions in quartz. Deeper within the section, chalcopyrite is present as isolated anhedral grains and, in a few places, as partial replacements of pyrite (Fig. 21). Chalcopyrite is also present in a few vesicles.

Pyrrhotite is a trace mineral in cores from Hole 1188F (but not in samples from Hole 1188A). Pyrrhotite is present exclusively as small (0.006 to 0.01 mm), pink, anhedral to equant subhedral inclusions within pyrite grains (Fig. 22).

Sphalerite is rare, observed only macroscopically in vesicles, in some cases perched on pyrite crystals that it clearly postdates. Iron-poor honey-yellow crystals are most common, but a black variety was also described, in one case in the same vesicle as the honey-yellow type.

Titanium magnetite is an accessory and, in places, a liquidus phase of the relatively unaltered dacitic rocks that cap the sequence of highly altered rocks. Hydrothermal magnetite, some with octahedral habit and typically 0.2 mm in diameter, is first found in the lower part of Hole 1188A within altered volcanic rocks. The magnetite is invariably observed within veinlets with silica and anhydrite and in vugs together with green clay, anhydrite, and pyrite. The downhole distribution of magnetite in thin section shows maxima at 150–165 m in Hole 1188A and 355–375 m in Hole 1188F. These maxima coincide with peaks in pyrite abundance, probably because of the prevalence of both veins and, in the case of magnetite, vein halos.

## Structure

The structures identified in these cores are primary volcanic layering, orientations of veins, and vein relationships. Original layering was identified from the orientation of elongate flattened and stretched vesicles in some of the massive lavas and, in other parts of the core, from millimeter-scale color banding attributed to flow (Fig. 13). Several features of the veins are worthy of note. Anhydrite and pyrite are the most common mineral assemblages in the veins and are present from 48 mbsf in Hole 1188A and to 378.5 mbsf in Hole 1188F (Fig. 23). Cristobalite-bearing veins were only encountered in the upper part of the system (i.e., above ~126 mbsf). Magnetite-bearing veins are at two depth intervals: between 146 and 184 mbsf in Hole 1188A and between 322 and 378.50 mbsf in Hole 1188F. Crack-seal veins and alteration halos showing multiple zonation were only observed below 218 mbsf. Furthermore, the alteration halos around the veins consisting of quartz and clay minerals tend to be more intense in Hole 1188F compared to Hole 1188A. Crosscutting relationships between veins are more abundant in Hole 1188F than in Hole 1188A. Brecciation and network veining are only present in Hole 1188A above 110 mbsf, and such structures were not observed in Hole 1188F. There are no systematic trends with respect to dips of veins with depth, and the vein paragenesis is very complex as a result of several episodes of fluid infiltration (Fig. 24).

## Geochemistry

Onboard chemical analyses were performed on 42 altered rocks from Site 1188, mostly of homogeneous rocks but including some with anhydrite-dominated veins or breccia matrices. Some analyses of the latter display elevated contents of CaO. More generally, CaO is similar to or lower than its content in fresh dacites depending on whether relict igneous plagioclase has been preserved, and Na<sub>2</sub>O shows a similar behavior. Enrichment in MgO relative to likely parents is a common phenomenon, particularly in chloritic rocks. Depending on the relative abundance of illite, K<sub>2</sub>O varies from severely depleted to modestly enriched. On a relative basis, MnO is always extremely depleted. Sulfur is distinctly enriched reflecting the presence of pyrite, or of pyrite and anhydrite. Both enrichment and depletion of iron (total as Fe<sub>2</sub>O<sub>3</sub>) occur, but some pyritic samples have similar Fe contents to those of unaltered dacites and rhyodacites, which indicates that pyrite has commonly formed by a sulfidation process. Immobile behavior is apparent for Al<sub>2</sub>O<sub>3</sub>, TiO<sub>2</sub>, Zr, and Y and less certainly for P<sub>2</sub>O<sub>5</sub>.

## Microbiology

Both direct bacterial counting and adenosine-triphosphate (ATP) analysis established the presence of microbial biomass within core samples from ~34 and 49 mbsf, respectively, but not on a sample from 60 mbsf or others deeper in Holes 1188A and 1188F. Samples were successfully cultivated at various temperatures under both aerobic and anaerobic conditions to 25° and 90°C from samples taken at 10 and 34 mbsf and at 25°C under anaerobic conditions

from the 49 mbsf sample. Aerobic microbes were also cultivated at 25°C from very deep rock samples at 222 and 225 mbsf, but these are believed to arise from seawater contamination.

### **Physical Properties**

Magnetic susceptibility varies greatly over the length of the recovered core, but generally increases downsection. The average compressional wave velocity for all samples from this site is 4.1 km/s; however, the more massive volcanic rocks commonly have higher compressional velocities than the brecciated and flow-banded rocks. Thermal conductivity is higher in brecciated rocks (average =  $>2$  W/(m·K) than in massive altered dacite (usually  $<2$  W/(m·K)). Average measured solid density differs somewhat between Holes 1188A and 1188F (2.65 and 2.82 g/cm<sup>3</sup>, respectively). This may reflect a higher abundance of veins (anhydrite + pyrite) in samples from the lower part of the cored interval. Porosity is highly variable, from  $<1\%$  to nearly 45%, but with an overall trend toward decreasing porosity with depth.

### **Rock Magnetism**

The top 35 m of the cored material is characterized by high magnetic susceptibility and remanent intensity. This depth corresponds to the relatively fresh dacite-rhyodacite section at the top of the core. The magnetic measurement values show a considerable drop from 35 to ~135 mbsf, representing the high alteration in Hole 1188A. A sudden increase in both the susceptibility and remanent intensity is present below 135 mbsf. The cause of this change is unclear. However, the presence of a large amount of paramagnetic minerals, such as pyrite, can increase the magnetic susceptibility. Thermal demagnetization experiments indicate the dominant magnetic carrier in the upper part of the section is titanomagnetite with variable degrees of alteration. Deeper in the core, magnetite and possibly maghemite may be the important sources of magnetization. One of the most notable features in the magnetic character of this section is a sharp rise in the susceptibility values below 275 mbsf. The high magnetization intensity at the bottom of the hole is consistent with the presence of magnetite, which was identified by X-ray diffraction and optical microscopy.

### **Downhole Measurements**

Maximum borehole temperature during the drilling of Hole 1188A was 4°C as recorded with the developmental Lamont-Doherty Earth Observatory core barrel temperature tool (CBTT). Borehole temperatures were also measured with the wireline logging temperature tool in Hole 1188F, registering 100°C a few hours after coring ended. Five days later the UHT-MSM tool measured a maximum temperature of 304°C in the bottom of Hole 1188F. A final temperature run in Hole 1188F with the UHT-MSM tool on the last day of operations recorded a maximum of 312°C. Water samples were collected from Hole 1188B and 1188F. The sample from Hole 1188B was taken only a few meters below seafloor because of a blockage in the hole, and a concomitant temperature measurement was 6°C. Water samples also followed each UHT-MSM

run in Hole 1188F, but difficulties in rapidly estimating the temperature gradient to avoid high temperatures that would have damaged the WTSP resulted in water samples taken at 12°C (107 mbsf) and 22°C (206 mbsf). Hole 1188B was drilled with the LWD/RAB BHA, and the data provide a 360° image of the borehole resistivity characteristics that might be used for lithologic correlation. Wireline logging in Hole 1188F indicates that the borehole has a much larger diameter (in excess of 17 in) than we expected from drilling with the 7.5-in-diameter diamond bit. High U in spectral gamma-ray measurements was recorded at 197–209 mbsf, and a smaller peak was recorded at 239–245 mbsf.

## SITE 1189

### Site Objectives

The geological objectives at Site 1189 were to delineate the vertical profile of alteration and mineralization patterns, and their variations with depth, beneath an area of focused high-temperature venting—the Roman Ruins hydrothermal field. The data obtained on cored samples and by logging will allow assessments of the chemical and hydrological processes at this “end-member” location, whereas comparison of this site with Site 1188 at the low-temperature diffuse vent field at Snowcap Knoll will provide an understanding of lateral variations.

In addition, Site 1189 was designed as a test of the nature and extent of microbial life, particularly hyperthermophilic bacteria, at such a high-temperature hydrothermal site, together with delineation of the conditions conducive to such deep biomass.

### Igneous Petrography

Holes 1189A and 1189B (Fig. 25) provide a first-order understanding of the volcanic origin of the upper 200 m of Pual Ridge at the Roman Ruins high-temperature black smoker vent field. The only fresh rocks recovered are aphyric dacite in the uppermost core from Hole 1189A. Although all other cores from this site show high to complete alteration, abundant evidence for extrusive volcanic features shows that the whole sequence is either volcanic or volcanoclastic in origin.

Sparse relict plagioclase phenocrysts or pseudomorphs thereof are preserved in several of the Holes 1189A and 1189B lithologic units (Figs. 26). Clinopyroxene (almost always replaced) and titanomagnetite are much more rare. Fresh plagioclase, especially in Hole 1189B, is characteristically rounded (Fig. 27), suggesting a period of phenocryst instability and dissolution prior to or during eruption. Many coherent volcanic units from Site 1189 are vesicular, with the degree of vesicularity ranging up to ~20 vol% (Fig. 28). Hydrothermal alteration has commonly resulted in vesicle filling by secondary minerals, resulting in an amygdaloidal texture. The lithologic succession at Hole 1189A is comprised of alternating coherent volcanic rock units and brecciated units. Several units show fragmental textures that have been logged as hydrothermal

breccia because conclusive evidence for a volcanoclastic origin (e.g., grading, layering, rounding, or polymict composition) is lacking.

In the cored part of Hole 1189B, below 31 mbsf, the rocks recovered alternate between coherent volcanic units and brecciated units. Above ~70 mbsf, many of the breccias have stockwork-like veining. Below 70 mbsf, and particularly below 137 mbsf, the volcanic rocks are, on average, less altered and richer in relict plagioclase. One moderately vesicular rock unit from Hole 1189B (from ~138 mbsf) is noteworthy for its highly stretched vesicles, all of which have steep stretching orientations ranging from ~70° to 90°, indicative of subvertical flow. An upper limit on the thickness of eruptive units can be estimated at ~50 m by the presence of several intervals of polymict breccias, indicating paleoseafloor positions. Based on this evidence, it appears Pual Ridge was built up in at least five eruptive episodes.

### **Hydrothermal Alteration**

The two holes cored (Holes 1189A and 1189B), although very close together (~30 m) show rather distinct alteration features with respect to each other, under a thin crust of fresh, hard dacite (cored in Hole 1189A). The main alteration features are summarized in Figure 29.

Alteration in Hole 1189A is similar to that found at Site 1188, but the presence of cristobalite is restricted here to the upper 25 mbsf, suggesting a higher geothermal gradient. Below the cristobalite-bearing interval, there is abundant quartz in all three main associations found at Site 1189 (early pervasive greenish quartz + clay, subsequent white quartz + clay ± anhydrite, and late silicification + clay). Small amounts of pyrite (1%–5%) are found in all samples and assemblages. As at Site 1188, late quartz-pyrite-anhydrite veins are ubiquitous.

Hole 1189B intersected the only massive sulfide mineralization found during Leg 193. Very poor recovery precludes detailed interpretations, but massive and semimassive sulfides are hosted in anhydrite (±gypsum) at least partially replacing volcanic rock (Fig. 30). Underneath, there is a zone of stockwork-related alteration (to 119 mbsf) in which the rock clasts show complete alteration into greenish quartz + clay and are embedded in vein networks variably rich in anhydrite, quartz, pyrite, and hematite. Anhydrite predominates down to ~60 mbsf. Hematite is locally present disseminated in quartz as jasperoidal cement (Fig. 31). The amount of silicification increases downward through the upper sequence (especially below 70 mbsf).

Hole 1189B intersected a lower sequence below 127 mbsf comprising moderately to highly altered coherent volcanic rocks, highly to completely altered monomict breccias, and polymict volcanoclastic breccias and sandstones. In Hole 1189B, cristobalite is restricted to the least altered (generally coherent) volcanic rocks, rich in relict plagioclase, and is interpreted to be the result of simple devitrification. However, some cristobalite-bearing breccias contain complex alteration assemblages that include different clays (illite, chlorite, smectite, and mixed-layer varieties). Intense alteration produced some striking textures, including contrasting color banding attributed to the enhancement of flow banding and pseudoclastic textures (Fig. 32).

### **Sulfide and Oxide Petrography**

In the cores from Holes 1189A and 1189B, pyrite is the dominant sulfide. Pyrite is disseminated within the groundmass of the volcanic rocks, within quartz-anhydrite veins, and finally as linings and cores to vesicle fill. Some accessory sulfides, namely sphalerite and chalcopyrite, are more abundant in Hole 1189B than in Hole 1189A. Marcasite, galena, tennantite, and covellite are rare, and the latter have only been identified in cores from Hole 1189B. In addition, the oxides magnetite, hematite, and possibly ilmenite (one example) are present. Semimassive sulfide mineralization comprising ~50% sulfides was recovered in Section 193-1189A-12R-1, 120–128 cm (Fig. 33). The relationships between the accessory sulfides and pyrite provide evidence for at least two generations of pyrite-quartz precipitation (Fig. 34). Chalcopyrite is also observed in some late crosscutting veins. Pyrite is both intergrown with and includes chalcopyrite. Sphalerite in Hole 1189B provides convincing evidence for two generations of sphalerite deposition, before and after a period of pyrite formation. Nevertheless, the overall sulfide content of this site is low and should be considered as only a very weakly mineralized stockwork sequence.

### **Structure**

The structures identified in Holes 1189A and 1189B were primary volcanic layering, brecciation of volcanic rocks, orientation of veins, and age relationship between veins. There are several interesting similarities and differences between the two holes with respect to vein structures.

The brecciated rocks in the two holes are very similar, consisting of variably altered volcanic fragments, crosscut by vein networks of quartz with pyrite and minor anhydrite. However, the volcanic rocks recovered from Hole 1189B are more brecciated than the rocks from Hole 1189A. Additionally, the vein intensity is higher and intervals of vein network (stockwork) are thicker in Hole 1189B (Figs. 35, 36). In contrast to Hole 1189A, magnetite and hematite in Hole 1189B are in the networks as minor components and sphalerite and chalcopyrite are present as trace minerals. In both holes, late coarse-grained anhydrite veins crosscut vein networks and brecciated rocks. More than 95% of the veins recovered from both holes were <1 cm thick, indicating that we did not intersect any major fluid pathways feeding the sulfide deposits.

### **Geochemistry**

One fresh volcanic rock from Hole 1189A was analyzed and is dacitic in composition, similar to fresh samples from other sites but with distinctly lower SiO<sub>2</sub> (64.25 wt%) and Zr/TiO<sub>2</sub> (~130 vs. ~250). All other analyses were performed on altered rocks, and these analyses generally reflect the transformations described in the alteration mineralogy sections of this report. In Hole 1189A, green, silica-clay altered rocks have high water and sulfur contents and increases in Fe<sub>2</sub>O<sub>3</sub> and MgO correspond to increases in reported chlorite, clay minerals, and

pyrite. In Hole 1189B, SiO<sub>2</sub>, CaO, and Na<sub>2</sub>O increase with depth, in agreement with the observed increase in plagioclase content.

### **Microbiology**

Bacteria were not detected by direct count below 50 mbsf in cores from Hole 1189A, and no bacteria were detected by this method in any core below the first core (31 mbsf) from Hole 1189B. Enrichment cultivations of samples from Hole 1189A showed growth of bacteria in both aerobic and anaerobic conditions to 25°C and as high as 90°C in anaerobic conditions. Samples from Hole 1189B exhibit growth of bacteria in anaerobic cultures from as deep as 130 mbsf and at temperatures to 90°C.

### **Physical Properties**

Magnetic susceptibility decreases from top to bottom in the cored section from Hole 1189A. A similar pattern is expressed in data from the lower part of Hole 1189B, albeit the overall susceptibility is distinctly higher. Compressional wave velocity averages 4.4 km/s at ambient pressure. Thermal conductivity is relatively constant at ~2 W/(m·K), with the exception of one pyrite-rich sample that has a value of >5 W/(m·K). Solid rock density is constant in all samples measured from both holes, averaging 2.7 g/cm<sup>3</sup>. As in samples from Site 1188, porosity is highly variable, from 15% to nearly 70%.

### **Paleomagnetism**

In terms of rock magnetic behavior, Site 1189 shares many common features with Site 1188. The uppermost part of the section at both sites is characterized by high susceptibility and high remanent intensity caused by abundant magnetite and titanomagnetite. At both sites, the upper few tens of meters are underlain by an interval of low remanent intensity. Below this is a zone of high susceptibility and high remanent intensity. Inasmuch as the maximum remanent intensity is present in this lowermost interval, it is conceivable that this lower zone is equally important, if not more so, as the source of the magnetic anomalies measured from the sea surface. Some significant differences also exist between Sites 1188 and 1189 in terms of magnetic behavior. The highest measured magnetization intensity is deeper at Site 1189 than at Site 1188. However, susceptibility and remanent intensity are both generally lower at Site 1189. This may reflect more intense high-temperature alteration at Site 1189.

### **Downhole Measurements**

Site 1189 will likely turn out to be the highlight of downhole measurements for Leg 193. Continuous wireline logs were collected in Hole 1189B with excellent tool response as a result of good borehole condition. Formation MicroScanner (FMS) data are particularly striking, imaging different patterns of fracturing and local dissemination of sulfide minerals. Our second LWD/RAB experiment, Hole 1189C, was drilled to 166 mbsf, past a distinct lithology change described in cores and potentially imaged in Hole 1189B wireline logging data. Following



completion of RAB drilling, we dropped a FFF and conducted wireline logging of the same hole. This marks the first time in ODP history that we have the opportunity to correlate directly between wireline logging and RAB data from the same drilled interval in hard rock.

## SITE 1190

### Site Objectives

The objectives for Site 1190 (see Figs. 7, 25) were obtaining information on the volcanic architecture of Pual Ridge and fresh material for comparisons with the altered rocks recovered at other sites. Additionally, results obtained earlier during Leg 193 suggested that hydrothermal alteration might be more intense and widespread than previously thought. It is possible that at Site 1190 below a few tens of meters of fresh or incipiently altered rocks lie deeply altered counterparts. However, because of technical and logistic difficulties we were not able to fully address these objectives.

### Igneous Petrography

Holes 1190A, 1190B, and 1190C provided a total of 110 cm of core, representing material from the upper 17 m of the volcanic edifice of Pual Ridge. Almost all of the rocks recovered are fresh, black, glassy, moderately vesicular, plagioclase-clinopyroxene  $\pm$  magnetite phyrlic rhyodacite (Fig. 37), but a couple of pieces show incipient bleaching. The felsic composition of the samples has been confirmed by measurements of the refractive index of the glass, which indicate a SiO<sub>2</sub> content of ~71–72 wt%. Clusters of several phenocrysts, including two or three phenocryst phases, are common, and the glassy groundmass that occupies interstitial and concave spaces in and around these clusters is usually free or nearly free of microlites, in contrast to the microlite-rich glassy mesostasis elsewhere in the rocks (Fig. 38). The chemical composition of the single sample analyzed from this site is comparable to the fresh rocks from Site 1188 but is slightly enriched in SiO<sub>2</sub> (69.37 wt%) with respect to the fresh sample analyzed from Site 1189.

### Hydrothermal Alteration

The limited alteration exhibited by material recovered from Site 1190 is nearly absent, similar to that observed in fresh, near-surface volcanic rocks from Sites 1188 and 1189. The alteration at this site is manifested by poorly developed silica  $\pm$  clay films on vesicle walls and fracture surfaces and rare fine-grained zeolites lining vesicle walls.

## SITE 1191

### Site Objectives

Site 1191 is located among chimneys at the Satanic Mills high-temperature hydrothermal

field (see Fig. 7). The main objective of drilling at this site was to complement the more extensive characterization of a high-temperature venting field at the Roman Ruins site (Site 1189). Limited penetration resulted in only recovering the uppermost part of the lithologic section at Site 1191. However, as little time was consumed drilling here (profiting from a gap arising from other drill-rig operations), we consider the exercise as valuable because it provided some constraints on the distribution of alteration through Pual Ridge as well as additional fresh volcanic samples.

### **Igneous Petrography**

We drilled within the hard crust of vesicular dacite/rhyodacite found at the previous sites, without passing through it. Drilling intersected fresh to mildly altered dacite-rhyodacite (69–70 wt% SiO<sub>2</sub> on an anhydrous basis) for the entire hole depth to 20.1 mbsf. This is moderately vesicular and aphyric in hand specimen (Fig. 39). Large vesicles, up to 4 cm long, are severely stretched (Fig. 40).

### **Hydrothermal Alteration**

Alteration increases gradually downward from slight to moderate. It consists of both replacement of the vitreous matrix and vesicle and fracture fillings. The igneous groundmass is replaced in patches by cristobalite and clay (Fig. 41). Vesicles become lined by a silica + sulfide + clay coating, in which, in most vesicles, euhedral zeolites grow (possibly clinoptilolite and, much less abundant, phillipsite). Below ~11 mbsf, fractures and vesicles are lined by subhedral marcasite, which incorporate framboids of pyrite or greigite (Fig. 42). The alteration differs from that found near the top of previous holes drilled through hydrothermally active sites in two main aspects: the absence of anhydrite (abundant at Sites 1188 and 1189) and the presence of abundant zeolites.

### **Structure**

The structures identified in the core from Hole 1191A were primary volcanic layering, elongation of vesicles, and marcasite-pyrite veins. Original layering was identified from the orientation of elongate flattened and stretched vesicles in some of the massive lavas and, in other parts of the core, from millimeter-scale color banding attributed to flow. The stretching and flattening of vesicles most probably were formed during flow of the viscous lava and thereby define the direction of flow. Only 16 silica-pyrite veins were intersected, all of which were 1 mm or less in thickness.

### **Geochemistry**

The samples from Hole 1191A have similar compositions to the unaltered dacite-rhyodacites from Sites 1188, 1189, and 1190. A CIPW normative mineralogy calculated for these samples gave a quartz-normative composition.

## Microbiology

Active bacterial cells were found by direct counting on two samples from depths of ~10 and 15 m, respectively. Anaerobic bacterial cultivation tests on both samples yielded positive results at temperatures reaching 90°C.

## Physical Properties

Magnetic susceptibility is high in all samples, although only small amounts of titanomagnetite were observed in thin sections. The natural gamma measurement values from this site are similar to those of Hole 1188A on average and are significantly lower than those of Hole 1189A. Thermal conductivity measurements are consistent with measurements for unaltered dacite from Holes 1188A and 1189A (average = 1.45 W/(m·K)). There is little variation in the solid density data, ranging from 2.5 to 2.6 g/cm<sup>3</sup>, again consistent with measurements for unaltered dacites from Sites 1189 and 1190. The porosity values range from 7.1% to 11.5%.

## Rock Magnetism

Site 1191 samples provided a reliable estimation of the magnetic inclination (−16°) significantly different from the present-day value of ~7.7° for the region. Although this may result from slight deviation during drilling with the rotary coring system, the more or less consistent magnetic inclination among sites and the young age of Pual Ridge suggests the presence of a tilted block.

## SYNTHESIS

During Leg 193, ODP explored for the first time the subsurface parts of an active, mineralized hydrothermal system in submarine felsic volcanic rocks at a convergent plate margin setting. At the outset, we knew we faced many technical challenges, such as commencing holes on a topographically rugose seabed, the undetermined geotechnical properties of the various rock types we expected to intercept, and the high borehole temperatures inherent to active hydrothermal systems. The operations summary sections in the Leg 193 *Initial Reports* volume will demonstrate how problematic these proved and how successfully they were overcome.

Along the way, we recorded a number of operational breakthroughs for ODP. These included the first deployment in hard rock of the ADCB and the first application of a hammer drill in a new strategy for hard-rock reentry as well as an innovative adaptation that allowed us to case an existing hole. We achieved the first free-fall deployment of a standard reentry cone, enabling a deep hole to be commenced exactly on a small target selected under drill stem video observation. Another innovation was the nesting of a FFF above the reentry cone, allowing dual casing strings to be set after the first one failed to seat properly. On the logging side, we achieved the first hard-rock application by ODP of LWD technology. We also performed the first direct comparison in

hard rock of geophysical profiles obtained by two different tools—formation images obtained by the RAB tool during drilling, followed by wireline logging and formation images acquired with the FMS. These initiatives were vital to the scientific outcomes of the leg and will have long-term benefits for the program and its successor. Great credit is due to the drilling engineers and rig crew for their initiative and persistence.

Our scientific task was, in essence, to document the third dimension of the hydrothermal system responsible for development of massive sulfide chimneys and mounds at the PACMANUS site on felsic volcanic Pual Ridge. Thereby we would better understand the interplay between fluid pathways and fluid-wallrock interaction that governs the nature and location of mineral deposition within an environment representing a modern, actively forming analog of the settings of many orebodies in ancient geological sequences. Subsequent deformation and metamorphism commonly obscure genetic evidence pertaining to the latter. In addition, we would delineate the extent to which microbial life flourishes in the subsurface of such a hydrothermal system, contributing to ODP's "Deep Biosphere" initiative. The choice of location was governed by prior understanding of the tectonic and volcanological setting of most ancient massive sulfide ore deposits and by the detail with which the PACMANUS site had been surveyed by surface vessels and manned submersibles since its 1991 discovery.

Prior isotopic and geochemical research on the PACMANUS chimneys had indicated that magmatic fluids and metal sources represented a significant component of the system. Unraveling the relative importance of these and of seawater-dominated leaching of metals from country rocks was to be a main aim of drilling and the postcruise research to follow.

Our strategy was to drill as deeply as possible at four sites, including two along the crest of Pual Ridge representing hydrothermal outflow zones characterized by low-temperature diffuse venting (Site 1188) and high-temperature focused venting, respectively (Site 1189, augmented by Site 1191), plus a nearby background or reference site where no past or present hydrothermal activity was known (Site 1190). The fourth site was a presumed fault at the base of Pual Ridge, where major ingress of seawater into the lower parts of the hydrothermal system seemed likely. The very first cores returned showed that seawater influences were major even at the upper levels of the system, so plans to drill this fourth site were abandoned very early during the leg.

Several unsuccessful attempts were made to drill the reference site, which achieved a new relevance as a consequence of early drilling, namely assessing just how far the unexpected intense alteration extended under the newly revealed cap of fresh dacite lavas. Premature termination of the leg after an emergency port call to Rabaul prevented a final attempt to penetrate this difficult site. Fortunately its initial purpose, to assess the volcanic architecture of Pual Ridge and to provide samples for comparison with products of hydrothermal alteration, was nonetheless achieved because igneous fabrics were well preserved at the two main sites, especially within an intersection of relatively less altered dacitic lavas and clastic rocks in the lower part of Hole 1189B.

The proponents of Leg 193 expected that, under both outflow sites and especially at the one with higher temperature focused venting, there would be interleaving between altered and unaltered rocks, the former representing preferred fluid pathways and possibly being associated with mineralized layers and veins affiliated with the seafloor deposits. Marked changes were anticipated in the alteration patterns, both vertically and laterally, reflecting different temperature gradients and fluid chemistries. Several major outcomes of the drilling came as a surprise, although the unexpected results were, of course, welcome as a means of advancing our knowledge. The first surprise was the intensity and extent of subsurface hydrothermal alteration. Beneath a capping of unaltered dacite and rhyodacite lava equivalent to surficial dredged samples, ranging from <10 to 40 m thick at the different hole sites, there was a rapid transition to pervasively and thoroughly altered derivatives. These continued without interruption to the bottom of all four holes cored to depths between 100 and nearly 400 mbsf. Some igneous plagioclase is preserved in the lower section of Hole 1189B and at several thin intervals in other holes, but even these rocks bear the clear imprint of hydrothermal alteration.

A second surprise was the predominance of clay minerals in altered rocks throughout all levels of the cored sequence in places accompanied by or substituted by chlorite. The assemblages differed little between the high- and low-temperature sites, although there was telescoping at the former (and also from the fringe to the center of this site) of a vertical progression believed to reflect thermal gradient overall although kinetic effects probably related to fluid:rock ratios also play a role. The progression, obscured somewhat by superimposed bleaching in which pyrophyllite appears a significant phase, is marked by a change with increasing depth from cristobalite to quartz as the accompanying silica mineral and by increasing silicification. The predominance of clays at the low-temperature site is broadly consistent with a borehole temperature of 312°C measured there at 360 mbsf after allowing 8 days for rebound after drilling. Their persistence in holes at the high-temperature site, especially in country rock fragments within a stockwork zone under a chimney mound at the high-temperature site, was less expected. Here we were unable to define ambient temperature at depth, although borehole temperatures at the base of this stockwork (near 125 mbsf) increased from ~45°C soon after drilling to 68°C in our final logging run <12 hr later.

Yet another surprise was the measured porosity of the altered rocks and qualitative indications of their high permeability. Excepting some especially vesicular and brecciated samples, average porosity is near 25%, decreasing slightly downhole in the more silicified assemblages. Furthermore, intense fracturing is endemic, as indicated by semicoherent core returned by ADCB drilling, especially by borehole imaging, and in retrospect by the intervals of very poor or zero core recovery in both ADCB and RCB holes. These characteristics will require profound modifications to our original expectation of how mineralizing fluids might pass upward through the system. The volume of hydrothermal pseudoclastic rocks, and of closely related hydrothermal breccias recovered at Sites 1188 and 1189, is striking. They may represent creation and evolution of major fluid pathways in hydrothermal systems, so far poorly understood.

The frequency of anhydrite in veins and breccia matrices, as vesicle fillings, and particularly within bleached intervals as disseminations in altered wallrock, was also unexpected in the drilled portion of the PACMANUS hydrothermal system. The anhydrite abundance falls with depth in holes at the diffuse vent site (Site 1188) and under the fringe of the focused vent site (Site 1189), yet it remains a conspicuous vein mineral even in the deepest intersections. The presence of anhydrite implies a major role for seawater infiltrated or swept into the rising column of hot hydrothermal fluid. The aforesaid porosity, permeability, and fractured nature of the altered volcanic rocks provides a likely explanation for this exceptionally significant feature of the system.

Pyrite is a conspicuous disseminated mineral at the 1% to 5% level in the altered rocks at both main sites, except in the lower, somewhat less altered succession in Hole 1189B, which possibly represents something akin to what economic geologists might call an outer, propylitic zone less influenced by passage of mineralizing fluids. Pyrite is also present in thin veins and vein networks throughout the system and is especially prominent in the stockwork zone underlying the elevated mound portion of the high-temperature chimney site where, locally, it forms centimeter-scale pods and veins of massive pyritic sulfide. Chalcopyrite and sphalerite are virtually nonexistent in core from the diffuse venting site, trace to minor components in the fringe Hole 1188A under the focused venting site, and conspicuous only in an interval of semimassive sulfide (represented by a single specimen) cored immediately beneath casing placed to 36 mbsf at the chimney mound (Hole 1189B).

Although diffusive fluid flow through porous rocks and fractures might explain the low temperature venting characteristics at Site 1188, we failed to core any structure likely to represent a major conduit (or its fringing halo) enabling focused venting of 280°C fluids at the chimney site (Site 1189). The cored stockwork zone appears rather too subdued in this respect and too free of minerals other than pyrite. However, core recovery was particularly poor in this stockwork zone, so such a feature might not have been sampled. Further evaluation of logging data may resolve this discrepancy, although it must also be emphasized that a vertical drill hole could easily miss altogether a subvertical feeder conduit, even though our holes at Site 1189 were spudded near the base of active seafloor chimneys.

Concerning the architecture of Pual Ridge, delineation of which was a subsidiary objective of Leg 193, we have established by drilling that the upper two-thirds of this volcanic edifice is constituted of felsic lavas (dacite and rhyodacite). Altered equivalents of massive vesicular units, and flow-banded units that are commonly brecciated or show clear autoclastic structures, comprise the greater bulk. Less frequent intervals with palimpsest perlitic structure denote formerly vitreous rocks, possibly lava rinds. Unequivocal volcanoclastic breccia and former volcanoclastic sandstone layers define paleoseafloor positions. At least five and probably more such horizons were recognized in Hole 1189B, defining a maximum value of 50 m for the average thickness of flow units. This compares favorably with the 30-m average thickness deduced from terracing on the crest and eastern flank of Pual Ridge. No evidence was found for

the presence of slowly cooled intrusive units, but possible occurrences of relatively thin dikes are not ruled out.

Data acquired on the physical properties of rocks cored at the PACMANUS site will constitute major aids to future modeling of future marine geophysical surveys in island arc and convergent margin terrains. In particular, we have measured the first compressional wave velocities for intensely altered felsic volcanic rocks, albeit at atmospheric pressure. We also found that whereas surficial unaltered dacite lavas will contribute to surface and deep-tow magnetic intensity anomalies, a greater effect may arise from deeply buried horizons of altered rocks with hydrothermal magnetite. At the PACMANUS site, these are characterized by high natural remanent magnetism as well as high magnetic susceptibility.

Another major success of Leg 193 was confirmation that microbes flourish in subsurface rocks of the PACMANUS hydrothermal system. Bacteria were confirmed by direct counting and by ATP analyses in cores recovered from depths to 80 m under the diffuse venting at Site 1188 and to 129 m under the chimney field at Site 1189. Cultivation experiments on board proved that these deep biota flourish under anaerobic conditions in seawater at temperatures as high as 90°C, and higher temperature experiments will be conducted on shore.

The results of Leg 193 and the postcruise research to follow will impact on our ability to correctly interpret ancient geological environments in which orebodies are found and to develop improved strategies for finding them. They will also clarify a number of issues regarding thermal and chemical fluxes between the seafloor and the oceans in volcanic arc environments at convergent plate margins. Some 2000 samples have been taken ashore by the scientific participants for a variety of studies employing frontier as well as conventional analytical techniques. The results of these endeavors will flow into the scientific literature over coming years. Unraveling the sources and mixing behaviors of metals and fluids and establishing whether the PACMANUS hydrothermal field represents a growing ore system or a minor manifestation now in decline will be key topics in these enquiries.

In the long term, two requirements apply to further PACMANUS seafloor research. One is the need for close-spaced shallow drilling to delineate more fully the main hydrothermal conduits at the high-temperature chimney site. Such a program using the portable remotely operated diamond drill was intended to precede Leg 193, but it was abandoned for technical reasons. It is by no means unnecessary now. The other is for deeper drilling. Leg 193, with its innovations such as nested casing and hammer-in casing, has shown that the technology is in hand to attempt deeper penetrations than the near 400 m we achieved.

Penetrating the deepest, very high-temperature levels of a seafloor hydrothermal system has been proposed as a priority for IODP, and the PACMANUS hydrothermal field must now be considered a prime candidate for that activity. If the thermal gradient measured in Hole 1188F accurately represents rock temperatures, then we might predict that the igneous intrusion evidently responsible for the heat energy needed to drive this system, and arguably a significant

source of metals and hydrothermal fluid, might lie as shallow as 1.5 km below the crest of Pual Ridge.



**REFERENCES**

- Auzende, J.-M., Urabe, T., and Scientific Party of ManusFlux Cruise, 1996. Submersible observation of tectonic, magmatic and hydrothermal activity in the Manus Basin (Papua New Guinea). *Eos*, 77:W115.
- Binns, R.A., and Scott, S.D., 1993. Actively forming polymetallic sulfide deposits associated with felsic volcanic rocks in the eastern Manus back-arc basin, Papua New Guinea. *Econ. Geol.*, 88:2226–2236.
- Binns, R.A., Parr, J.M., Scott, S.D., Gemmell, J.B., and Herzig, P.M., 1995. PACMANUS: An active seafloor hydrothermal field on siliceous volcanic rocks in the Eastern Manus Basin, Papua New Guinea. In Mauk, J.L. and St George, J.D. (Eds.), *Proc. 1995 PACRIM Congress*, Australasian Inst. Mining and Metallurgy, Melbourne, 49–54.
- Binns, R.A., Parr, J.M., Waters, J.S., Gemmell, J.B., Moss, R., Scott, S.D., Naka, J., Charlou, J.-L., Gena, K., and Herzig, P.M., 1996a. Actively-forming sulfide deposits at the PACMANUS hydrothermal field, Eastern Manus Basin, Papua New Guinea. *Eos*, 77:W115–116.
- Binns, R.A., Waters, J.C., Carr, G.R., and Whitford, D.J., 1996b. A submarine andesite-rhyodacite lineage of arc affinity, Pual Ridge, eastern Manus back-arc basin, Papua New Guinea. *Eos*, 77:W119–120
- Binns, R.A., Scott, S.D., and Gemmell, J.B., 1997a. Modern analogue of a mineral field: Seafloor hydrothermal activity hosted by felsic volcanic rocks in the Eastern Manus Basin, Papua New Guinea. *Soc. Econ. Geol., Neves Corvo Field Conf.*, Abstracts and Program, 33.
- Binns, R.A., Scott, S.D., Gemmell, J.B., and Crook, K.A.W.C., and Shipboard Party, 1997b. The SuSu Knolls hydrothermal field, Eastern Manus Basin, Papua New Guinea. *Eos*, 78:F772.
- Both, R., Crook, K., Taylor, B., Brogan, S., Chappell, B., Frankel, E., Liu, L., Sinton, J., and Tiffin, D., 1986. Hydrothermal chimneys and associated fauna in the Manus backarc basin, Papua New Guinea, *Eos*, 67:489–490.
- Charlou, J.L., Donval, J.P., Fouquet, Y., Henry, K., Jean-Baptiste, P., Auzende, J.-M., Gamo, T., Ishibashi, J., and Shipboard Party, 1996. Variability in the chemistry of hydrothermal fluids from the Manus back-arc basin, Papua New Guinea. *Eos*, 77:W116
- Douville, E., Bienvenu, P., Charlou, J.-L., Donval, J.-P., Fouquet, Y., Appriou, P., and Gamo, T.,

1999. Yttrium and rare earth elements in fluids from various deep-sea hydrothermal systems, *Geochim. Cosmochim. Acta*, 63:627–643.
- Eguchi, T., Fujinawa, Y., and Ukawa, M., 1989. Earthquakes associated with the back-arc opening in the eastern Bismarck Sea: activity, mechanisms, and tectonics. *Phys. Earth Planet. Int.*, 56:189–209.
- Exon, N.F., and Marlow, M.S., 1988. Geology and offshore resources potential of the New Ireland-Manus region—a synthesis. *Circ.-Pac. Counc. Energy Mineral Resour., Earth Sci. Ser.*, 9:241–262.
- Falvey, D.A., and Pritchard, T., 1985. Preliminary paleomagnetic results from northern Papua New Guinea: Evidence for large microplate rotations. *Trans. Circ.-Pac. Counc. Energy Mineral Resour.*, 3:593–600.
- Gamo, T., Okamura, K., Kodama, Y., Urabe, T., Auzende, J.-M., Shipboard Party, and Ishibashi, J., 1996. Chemical characteristics of hydrothermal fluids from the Manus back-arc basin, Papua New Guinea, 1. Major chemical components. *Eos*, 77:W116
- Gemmell, J.B., 1995. Comparison of volcanic-hosted massive sulphide deposits in modern and ancient back-arc basins; examples from the southwest Pacific and Australia. In Mauk, J.L. and St George, J.D. (Eds.), *Proc. 1995 PACRIM Congress*: Melbourne, 227–231.
- Gemmell, J.B., Binns, R.A., and Parr, J.M., 1996. Comparison of sulfur isotope values between modern back-arc and mid-ocean ridge seafloor hydrothermal systems. *Eos*, 77:W117
- Hashimoto, J., Ohta, S., Fiala-Médioni, A., Auzende, J.-M., Kojima, S., Segonzac, M., Fujiwara, Y., Hunt, J.C., Gena, K., Miura, T., Kikuchi, T., Yamaguchi, T., Toda, T., Chiba, H., Tsuchida, S., Ishibashi, J., Henry, K., Zbinden, M., Pruski, A., Inoue, A., Kobayashi, H., Birrien, J.-L., Naka, J., Yamanaka, T., Laporte, C., Nishimura, K., Yeats, C., Malagun, S., Kia, P., Oyaizu, M., and Katayama, T., 1999. Hydrothermal vent communities in the Manus Basin, Papua New Guinea: Results of the BIOACCESS cruises in '96 and '98. *InterRidge News*, 8:12–18.
- Hohnen, P.D., 1978. Geology of New Ireland, Papua New Guinea. *BMR J Aust. Geol. Geophys.*, 194.

- Ishibashi, J., Wakita, H., Okamura, K., Gamo, T., Shitashima, K., Charlou, J.L., Jean-Baptiste, P., and Shipboard Party, 1996. Chemical characteristics of hydrothermal fluids from the Manus back-arc basin, Papua New Guinea., II. Gas components. *Eos*, 77:W116.
- Johnson, R.W., 1976. Late Cainozoic volcanism and plate tectonics at the southern margin of the Bismarck Sea, Papua New Guinea. In Johnson, R.W. (Ed), *Volcansm in Australasia*: Amsterdam (Elsevier), 101–116.
- Martinez, F., and Taylor, B., 1996. Fast backarc spreading, rifting and microplate rotation between transform faults in the Manus Basin, Bismarck Sea. In Auzende, J.-M., and Collot, J.-Y., (Eds.), *Seafloor mapping in the West, Southwest and South Pacific*. Mar. Geol. Res., Spec. Issue, 18:203–224.
- Parr, J.M., Binns, R.A. and Gemmell, J.B., 1996. Sulfide chimneys from the Satanic Mills site in the PACMANUS hydrothermal field, Eastern Manus Basin, Papua New Guinea. *Eos*, 77:W120.
- Scott, S.D. and Binns, R.A. 1995. Hydrothermal processes and contrasting styles of mineralization in the western Woodlark and eastern Manus basins of the western Pacific. In Parson, L.M., Walker, C.L., and Dixon, D.R. (Eds.), *Hydrothermal Vents and Processes*. Geol. Soc. Spec. Pub., 87:191–205.
- Stewart, W.D. and Sandy, M.J., 1988. Geology of New Ireland and Djual Islands, northeastern Papua New Guinea. In Marlow, M.S., Dafisman, S.V., and Exon, N.F., (Eds.), *Geology and Offshore Resources of Pacific Island Arcs, - New Ireland and Manus region, Papua New Guinea*, Circ.-Pac. Counc. Energy and Mineral Resour., Earth Sci. Ser., 9:13–30.
- Taylor, B., 1979. Bismarck Sea: evolution of a back-arc basin. *Geology*, 7:171–174.
- Taylor, B.J., Crook, K.A.W., Sinton, J.L., and Petersen, L. 1991. Manus Basin, Papua New Guinea. *Pacific Sea Floor Atlas* (Hawaii Inst. Geophys.), Sheets 1–7.
- Taylor, B., Crook, K.A.W., and Sinton, J., 1994. Extensional transform zones and oblique spreading centres. *J. Geophys. Res.*, 99:19707–19718.
- Taylor, B., Goodliffe, A., Martinez, F., and Hey, R., 1995. Continental rifting and initial sea-floor spreading in the Woodlark basin. *Nature*, 374:534–537.

- Tregoning, P., Lambeck, K., Stolz, A., Morgan, P., McClusky, S., van der Beek, P., McQueen, H., Jackson, R., Little, R., Laing, A., and Murphy, B., 1998. Estimation of current plate motions in Papua New Guinea from Global Positioning System observations, *J. Geophys. Res.*, 103:12,181–12,203.
- Waters, J.C., Binns, R.A., and Naka, J., 1996. Morphology of submarine felsic volcanic rocks on Pual Ridge, Eastern Manus Basin, Papua New Guinea. *Eos*, 77:W120.
- Woodhead, J.D., Eggins, S.M., and Johnson, R.W., 1998. Magma genesis in the New Britain island arc: Further insights into melting and mass transfer processes. *J. Petrol.*, 39:1641–1668.
- Woodhead, J.D., and Johnson, R.W., 1993. Isotopic and trace-element profiles across the New Britain island arc, Papua New Guinea. *Contrib. Mineral. Petrol.*, 113:479–491.
- Yang, K., and Scott, S.D., 1996. Possible contribution of a metal-rich magmatic fluid to a sea-floor hydrothermal system. *Nature*, 383:420–423.

## TABLE CAPTIONS

**Table 1.** Chronologic operations summary.

**Table 2.** Site summary information, Leg 193.

## FIGURE CAPTIONS

**Figure 1.** Major active hydrothermal sites at convergent margins of the western Pacific Ocean. Large arrows = plate movements.

**Figure 2.** Regional tectonic setting of the PACMANUS site drilled during Leg 193. The Manus Basin occupies a backarc position relative to present-day subduction on the New Britain Trench to its south. Creation of new oceanic crust occurs at the Manus spreading center and at smaller segments to its west. Major transform faults are somewhat oblique to the spreading segments. The eastern Manus rift zone is a pull-apart structure between two of the major transform faults. It is underlain by thinned older Tertiary arc crust, equivalent to exposures on New Ireland to the north and New Britain to the south. This older crust was generated during subduction on the now-inactive Manus Trench. Active volcanoes of the Bismarck arc, above the New Britain subduction–Benioff zone are indicated; submarine volcanism in the eastern Manus rifts lies well off the trend of this chain. Yellow boxes = known hydrothermal sites. Thick blue arrows = plate motions. Curved blue arrows = the sense of rotation on microplates as defined by Global Positioning System geodesy (Tregoning et al., 1998) or by the opening and westward propagation of the Woodlark Basin (Taylor et al., 1995).

**Figure 3.** Tectonic model for the Manus Basin (adapted from Martinez and Taylor, 1996). About 80 km of extension by low-angle normal faulting and crustal thinning has occurred in the Eastern Manus Basin between the Weitin and Djaul transform faults. The same amount of movement occurred on the Willaumez transform fault, where a slight obliquity between extension direction and fault strike allowed volcanism in the extensional transform zone. Between the Willaumez and Djaul transforms, equivalent movement was accommodated by wedge-shaped opening of the Manus spreading center and compensating counter-clockwise rotation of the Manus microplate. Mid-ocean-ridge basin (MORB)-type basaltic volcanism dominates the Manus spreading center, the extensional transform zone, the East Sherburne Zone that overlies a sediment basin, and limited activity in the Southern Rifts. By contrast, the Eastern Manus Basin is dominated by arc-type volcanism.

**Figure 4.** Bathymetry of the Eastern Manus Basin from multibeam data compiled by Institut Francais de Reserche pour l'Exploration de la Mer (IFREMER). The southeast-trending Djaul transform is conspicuous. The northeast-trending deep on the western side is a failed spreading segment. The PACMANUS site lies at the crest of a northeast-trending ridge of dacite (Pual Ridge).

**Figure 5.** High-resolution single channel seismic profile of (A) the section across Pual Ridge at the position of the PACMANUS hydrothermal field and (B) interpretation. All Leg 193 sites lie on the crest of Pual Ridge. Data from the *Sonne* cruise 94, Leg 2, single channel seismic line 07.

**Figure 6.** Seafloor geology of the Eastern Manus Basin. Edifices of the Eastern Manus Volcanic Zone, which extends between the active ends of the Djaul and Weitin transform faults, range from picritic basalt to rhyodacite in composition. Red dots = known hydrothermal sites, including the three main active sites of PACMANUS, Deep Sea Monitoring System (DESMOS), and Susu Knolls. Red lines = extensional fault scarps.

**Figure 7.** Distribution of hydrothermal deposits within the PACMANUS field along the crest of Pual Ridge, with the names assigned to active sites containing massive sulfide chimneys. Based on bottom-tow photography and submersible dive observations from the PACMANUS cruises (*Frankin*, 1991, 1993, 1996, 1997), EDISON-I cruise (*Sonne*, 1994), ManusFlux cruise (*Yokosuka*, 1995), BIOACCESS cruises (*Natsushima*, 1996, 1998), and KODOS'99 cruise (*Onnuri*, 1999).

**Figure 8.** Calculated course of vibration-isolated television (VIT) survey during the site survey prior to spudding of Hole 1188A and observed seafloor character. Bathymetric contours (5-m intervals) within the survey area are based on VIT cable measurement and sonar altimetry, calibrated to the actual drill pipe measurement depth of Hole 1188A. Contours outside the survey area are derived from submersible dives and have been added to show the general shape of Snowcap Knoll. Only the track from the initial survey is shown, but additional seafloor cover information from other surveys has been added. Global Positioning System averaged locations for all of the ODP holes at Site 1188 are also shown.

**Figure 9.** Key to lithology symbols used in the graphic summary log.

**Figure 10. A.** Graphic summary log for Hole 1188A showing the lithologic characteristics of the various units including alteration. **B.** Graphic summary log for Hole 1188F showing the lithologic characteristics of the various units including alteration. NR = no recovery.

**Figure 11.** Close-up photograph of fresh, black moderately vesicular rhyodacite from the upper part of Hole 1188A (interval 193-1188A-4R-1, 0–13 cm).

**Figure 12.** Photomicrograph in cross-polarized light of a fresh plagioclase phenocryst set in groundmass containing 35 vol% fresh plagioclase microlites, 35 vol% quartz, 25 vol% brown clay, and 5 vol% pyrite (Sample 193-1188F-31Z-1, 1–3 cm; field of view = 2.75 mm).

**Figure 13.** Many amygdules in altered dacite are filled by mosaic quartz  $\pm$  pyrite  $\pm$  anhydrite. In this photomicrograph they are <1 mm, and elongate amygdules define a general orientation of alignment (interval 193-1188F-1Z-3, 86–89 cm; field of view = 2.75 mm).

**Figure 14.** Close-up photograph of a perlitic texture of aphyric dacite (Unit 2) indicates that the groundmass originally consisted of volcanic glass (interval 193-1188A-5R-1, 35–49 cm). Alteration proceeded preferentially along and outward from the perlitic cracks generating a pseudoclastic texture in some domains of the sample. **A.** In hand specimen this unit has a sugary appearance. The arcuate perlitic cracks are enhanced by alteration generating light gray “islands” in a dark gray, irregular network of clay, silica, and minor pyrite forming an apparent matrix. **B.** In thin section, well-preserved perlitic texture is present within the “islands,” which, hence, represent remnants of the originally glassy groundmass (field of view = 2.75 mm).

**Figure 15.** Flow banding is commonly present in the altered volcanic rocks. In this case, the flow banding is folded and crosscut by silica-anhydrite-pyrite veins (interval 193-1188A-12R-2, 36–52 cm). **A.** Photograph of hand specimen. **B.** Line drawing sketch of the specimen highlighting folds and fractures.

**Figure 16.** Summary of lithostratigraphic units, alteration style, and distribution of alteration phases at Site 1188. Occurrences of relict igneous plagioclase are also represented (on the right side). Pyrite is present in all samples studied and is not represented on the figure. Clay phases are mentioned where detected by X-ray diffraction (XRD); no indication of their abundance relative to other phases is implied. EOH = end of hole.

**Figure 17.** Close-up photograph of pervasively bleached vesicular volcanic rock with a zoned alteration pattern toward a darker gray, less strongly bleached kernel (interval 193-1188A-9R-1, 16–29 cm).

**Figure 18.** Close-up photograph of a green silica-clay altered rock with a remnant perlitic texture and anhydrite-(silica-pyrite) stockwork veining (interval 193-1188A-8R-1, 108–140 cm). The large white patch near the center of the photographed piece is bleaching surrounding a late irregular anhydrite-pyrite vein.

**Figure 19.** Photomicrograph in cross-polarized light of a plagioclase phenocryst completely replaced by fine-grained illite (birefringent mineral) and possible halloysite (gray) (Sample 193-1188F-14Z-1, 102–105 cm; field of view = 0.7 mm).

**Figure 20.** Photomicrograph in plane-polarized light of anhydrite-pyrite veining with well-developed siliceous halo hosted in green silica-clay altered volcanic rock. The vein has cut and filled two vesicles (Sample 193-1188A-8R-1, 124–127 cm; field of view = 0.7 mm).

**Figure 21.** Photomicrograph in reflected light of chalcopyrite (light gray) partially enclosing and replacing pyrite (white) (Sample 193-1188F-37Z-2 [Piece 3, 31–33 cm]; field of view = 0.28 mm).

**Figure 22.** Photomicrograph in reflected light of pyrrhotite inclusion (diameter = 0.006 mm) with smaller magnetite inclusions in pyrite (Sample 193-1188F-1Z-3 [Piece 3, 86–89 cm]; field of view = 0.14 mm).

**Figure 23.** Photomicrograph in plane-polarized light of anhydrite-pyrite vein with pyrite surrounding anhydrite. Note the fine-grained pyrite at the outer fringes of the gray halo of silica around the veins (Sample 193-1188A-7R-2 [Piece 2, 39–41 cm]; field of view = 1.40 mm).

**Figure 24.** Interval 193-1188F-14Z-1 (Piece 6, 98.5–110 cm). **A.** Close-up photograph. **B.** Sketch of complex vein relationships (246.86 mbsf). The veins in this piece consist predominantly of anhydrite and pyrite. The two thicker veins, Va and Vb, are surrounded by 1- to 2-mm-thick gray siliceous halos that grade outward into 1- to 2-mm-thick light gray halos more rich in clay minerals (illite?). A thinner siliceous halo is present around vein Vc. In all veins, except for the thickest vein (Va) and the thinnest veins (Vj–Vp), pyrite occupies the center of the veins and is rimmed by anhydrite. Vein Va has coarse anhydrite in the center of the vein, rimmed by thin veinlets of pyrite, followed by a thin rim of anhydrite. The thinnest veins are either pyrite veins (Vj–Vm) or veinlets of anhydrite (Vn–Vp). Some of the thinner veins branch off from the thicker veins (e.g., Vk and Vl from Vb; Vi and Vm from Va; and Vg and Vj from Vc). Veins Vc and Vd are probably part of the same vein, crosscut by Vb. This is evinced by the anhydrite selvages of veins Vc and Vd, which are overprinted by the siliceous halo around Vb (Point A). Furthermore, the right-lateral offset between Vc and Vd matches the space of the extensional jog filled with pyrite of Vb (Point B). Finally, the anhydrite crystals are aligned east-west in the vein intersection at Point A, indicating an east-west extension. Microscopic examination shows that Ve cuts across the halos around both Va and Vb, indicating it to be later. Although these veins show crosscutting relationships, on the basis of their mineralogy and nature of alteration halos, most of the veins in this specimen are considered to be part of the same main veining event. On the basis of mineralogy and nature of the alteration



halos, this is considered to be the event that formed most of pyrite-anhydrite veins throughout all of Hole 1188F.

**Figure 25.** Hole locations for Sites 1189 and 1190. Shaded area around Site 1189 (Roman Ruins) = the approximate area of outcrop of chimney structures mapped by submersible and camera tow.

**Figure 26. A.** Graphic summary log for Hole 1189A showing the lithologic characteristics of the various units including alteration. **B.** Graphic summary log for Hole 1189B showing the lithologic characteristics of the various units including alteration. See Figure 9 for the lithology key.

**Figure 27.** Close-up photograph in cross-polarized light of rounded plagioclase phenocrysts in altered volcanic rock from Hole 1189B (Sample 193-1189B-16R-1 [Piece 6, 36–39 cm]; field of view = 2.75 mm).

**Figure 28.** Photograph of moderately vesicular aphyric volcanic rock. The groundmass shows a spotty hieroglyphic texture caused by incomplete hydrothermal alteration with white, angular shard-shaped domains representing remnants of less altered groundmass (interval 193-1189B-16R-1, 114–130 cm).

**Figure 29.** Summary of lithostratigraphic units, alteration style, and distribution of major (heavy lines) and minor to trace (light lines) alteration phases for **(A)** Hole 1189A and **(B)** Hole 1189B. Intervals where remnant igneous plagioclase was detected by X-ray diffraction (XRD) are also indicated on the right side. Pyrite is present in all samples analyzed and is not included in the plot. Clay phases are indicated where detected in XRD analyses; no indication of their abundance relative to other phases is implied. Shaded intervals = no recovery.

**Figure 30.** Close-up photomicrograph in plane-polarized light of gypsum partly replacing anhydrite, which has partially replaced altered volcanic clasts (Sample 193-1189B-2R-1 [Piece 2, 11–14 cm]; field of view = 1.4 mm).

**Figure 31.** Close-up photomicrograph in cross-polarized reflected light of jasperoidal quartz showing strong red internal reflections (Sample 193-1189B-6R-1 [Piece 2, 13–15 cm]; field of view = 1.4 mm).

**Figure 32.** Photograph of coherent flow-banded core piece, with a pseudobreccia appearance created by silica-clay alteration halos around a feeble network of silica veins (interval 193-1189B-15R-1, 130–135 cm).

**Figure 33. A.** Photograph of semimassive sulfide consisting of pyrite and chalcopyrite grains in an anhydrite-silica matrix. Angular white fragments are altered volcanic rock (interval 193-1189A-12R-1, 120–128 cm). **B.** Photomicrograph of volcanic clasts with fibrous, laminate internal texture, which are abundant in this sulfide-rich interval (Sample 193-1189A-12R-1 [Piece 16, 122–125 cm]; field of view - 1.4 mm).

**Figure 34.** Close-up photograph of pyrite crystals (white) in the center, nucleated around quartz and overgrown by marcasite crystals (light gray), which, in turn, are overgrown by more pyrite.

**Figure 35.** Photograph of a network of quartz-pyrite veins (dark gray) crosscutting earlier patchy silica-sulfate alteration (light gray) (interval 193-1189A-10R-1 [Piece 10, 88.5–100 cm]).

**Figure 36.** Photograph of breccia with highly altered volcanic fragments in a matrix of quartz with minor pyrite. Note the breccia is matrix supported (Sample 193-1189B-7R-1 [Piece 1, 0–5 cm]).

**Figure 37.** Close-up photograph of hand specimen shows fresh to slightly altered dacite recovered from Site 1190 is black, moderately vesicular, and superficially aphyric in hand specimen. However, careful observation and thin section petrography show that the glassy to microcrystalline groundmass contains up to 3 vol% of plagioclase, clinopyroxene, and minor magnetite phenocrysts (interval 193-1190B-2R-1, 28–35 cm).

**Figure 38.** Photomicrograph of glomerophytic clasts of phenocrysts (here, plagioclase, clinopyroxene, and magnetite) and a nearby microvesicle, which are a common feature of Unit 1. Interstitial spaces around these aggregates typically consist of microlite-free volcanic glass (Sample 193-1190B-2R-1 [Piece 7, 40–43 cm]; field of view = ~1.8 mm).

**Figure 39.** Photograph of fresh (interval 193-1191A-1R-1, 9.5–11.5 cm) to slightly altered (interval 193-1191A-1R-1, 12–18.5 cm) aphyric rhyodacite from the top part of Hole 1191A. The main stretching orientation of the vesicles is normal to the surface of the sample (interval 193-1191A-1R-1, 9–19 cm).

**Figure 40.** Photograph of altered rhyodacite with a spotty appearance and a strongly elongated tabular vesicle lined with fine zeolite crystals. The spotty appearance is caused by partial alteration of the volcanic groundmass forming very fine grained silica and clay minerals (interval 1191A-1R-1, 65–71 cm).

**Figure 41.** Photomicrograph in plane-polarized light illustrating cristobalite-clay alteration (colorless patches) of pale brown volcanic glass in a moderately altered volcanic rock from Site

1191 (interval 193-1191A-2R-2, 103–106 cm). Note that microlitic plagioclase and magnetite (fine opaque spots) are unaffected by the alteration (field of view = 0.7 mm).

**Figure 42.** Oil-immersion photomicrograph in reflected light of framboids of pyrite (or possible greigite,  $\text{Fe}_3\text{S}_4$ ) in a vein dominated by marcasite (Sample 193-1191A-2R-2 [Piece 16, 103–106 cm]; field of view = 0.14 mm).

Table 1. Chronologic operations summary.

Date		Location	Task
Start (2000)	Finish (2000)		
7 Nov	14 Nov	Port call	
14 Nov	18 Nov	Transit	
18 Nov	22 Nov	Hole 1188A	RCB coring
22 Nov	23 Nov	Hole 1189A	RCB coring
23 Nov	25 Nov	Holes 1190A, 1190B, 1190C	RCB coring
25 Nov	27 Nov	Hole 1188B	RAB/LWD/ADCB
27 Nov	28 Nov	Site 1191	RCB coring
28 Nov	1 Dec	Holes 1188C, 1188D, 1188E	No coring
1 Dec	12 Dec	Hole 1188F	Casing
12 Dec	21 Dec	Hole 1188F	ADCB coring/logging
21 Dec	22 Dec	Hole 1188F	Water-sampling/temperature measurements
22 Dec	26 Dec	Hole 1189B	HRRS casing/RCB coring/logging
27 Dec	29 Dec	Hole 1189C, Hole 1188F	RAB/LWD/ logging, temperature measurements/water sampling

Note: RCB = rotary core barrel, RAB = resistivity at bit, LWD = logging while drilling, ADCB = advanced diamond core barrel, HRRS = hard-rock reentry system.

Table 2. Site summary information, Leg 193.

Hole	Latitude	Longitude	Depth (mbrf)	Number of Cores	Cored interval (m)	Core recovered (m)	Core recovered (%)	Depth drilled (m)	Total penetration	Time on hole (hr)	Time on hole (days)
1188A	03°43.696' S	151°40.196' E	1651.0	23	211.6	21.93	10.4	0.0	211.6	87.00	3.63
1188B	03°43.696' S	151°40.198' E	1653.0	0	0.0	0.00	n/a	72.0	72.0	67.00	2.79
1188C	03°43.694' S	151°40.174' E	1654.0	0	0.0	0.00	n/a	44.0	44.0	20.00	0.83
1188D	03°43.667' S	151°40.178' E	1645.0	0	0.0	0.00	n/a	15.0	15.0	9.50	0.40
1188E	03°43.684' S	151°40.190' E	1652.0	0	0.0	0.00	n/a	16.0	16.0	10.25	0.43
1188F	03°43.685' S	151°40.190' E	1653.0	45	168.7	30.89	18.3	218.0	386.7	616.50	25.69
Site 1188 totals:				68	380.3	52.82	13.9	365.0	745.3	810.25	33.76
1189A	03°43.243' S	151°40.492' E	1701.0	13	125.8	8.58	6.8	0.0	0.0	36.25	1.51
1189B	03°43.236' S	151°40.508' E	1693.0	18	175.0	13.69	7.8	31.0	206.0	105.25	4.39
1189C	03°43.241' S	151°40.524' E	1700.0	0	0.0	0.00	n/a	166.0	166.0	56.00	2.33
Site 1189 totals:				31	300.8	22.27	7.4	197.0	372.0	197.50	8.23
1190A	03°43.292' S	151°40.582' E	1714.0	1	9.1	0.03	0.3	0.0	9.1	9.50	0.40
1190B	03°43.314' S	151°40.616' E	1712.0	1	8.6	0.24	2.8	1.5	10.1	4.75	0.20
1190C	03°43.303' S	151°40.610' E	1707.0	3	17.2	0.40	2.3	0.0	17.2	18.50	0.77
Site 1190 totals:				5	34.9	0.67	1.9	1.5	36.4	32.75	1.36
1191A	03°43.608' S	151°40.337' E	1705.0	3	20.1	3.36	16.7	0.0	20.1	45.00	1.88
Site 1191 totals:				3	20.1	3.36	16.7	0.0	20.1	45.00	1.88
Leg 193 totals:				107	736.1	79.12	10.7	563.5	1173.8	1085.5	45.23

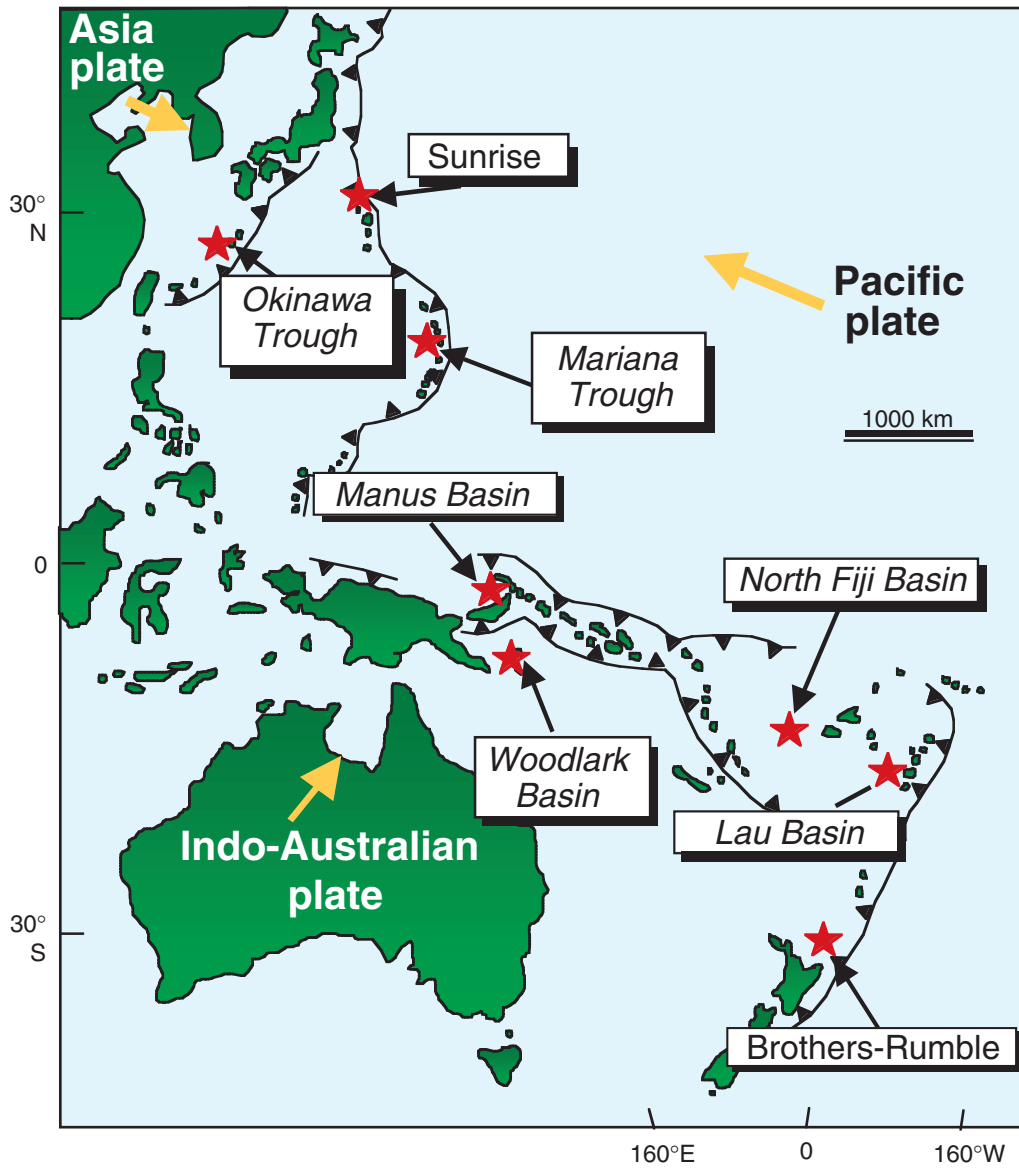


Figure 1

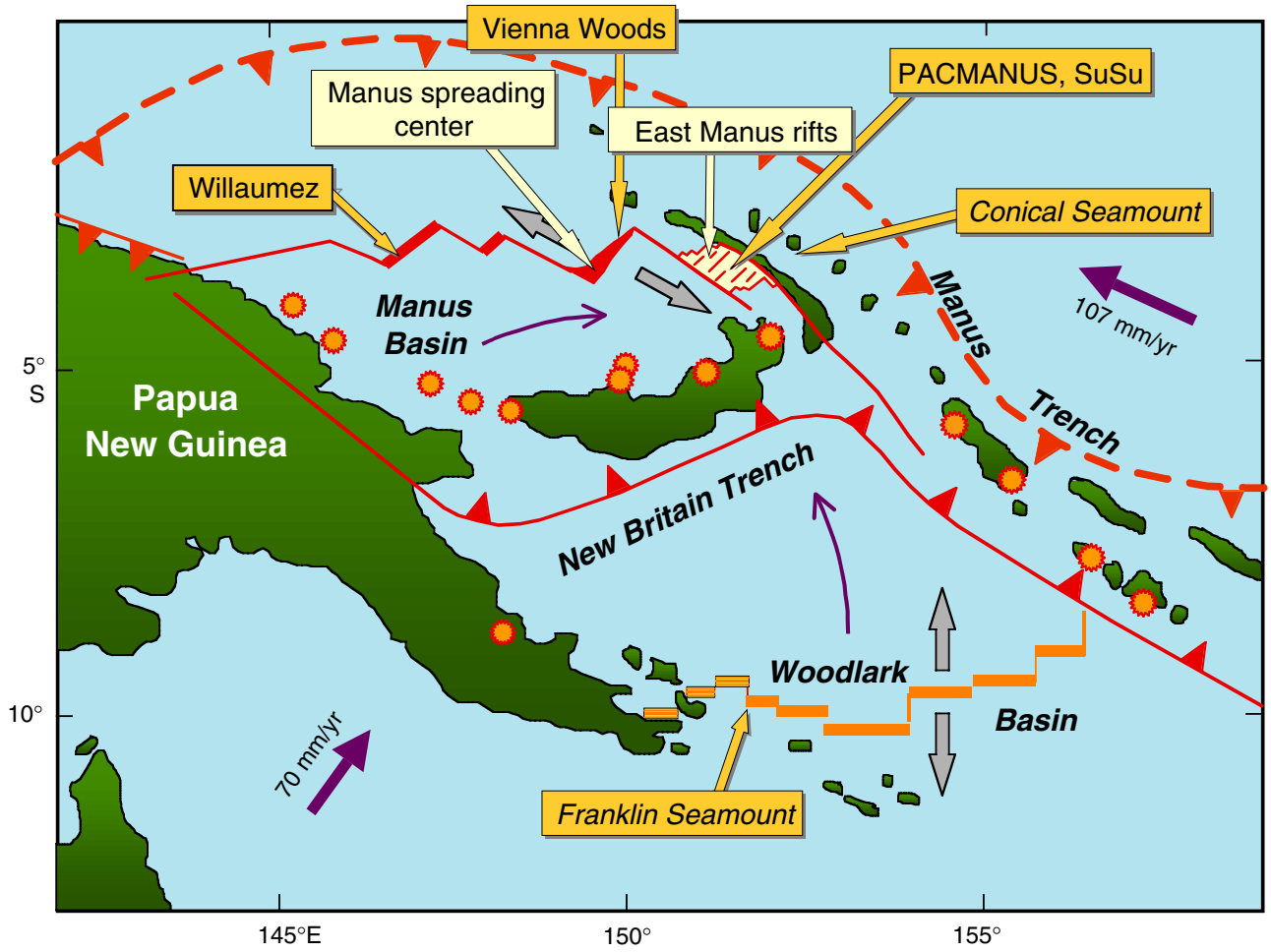


Figure 2

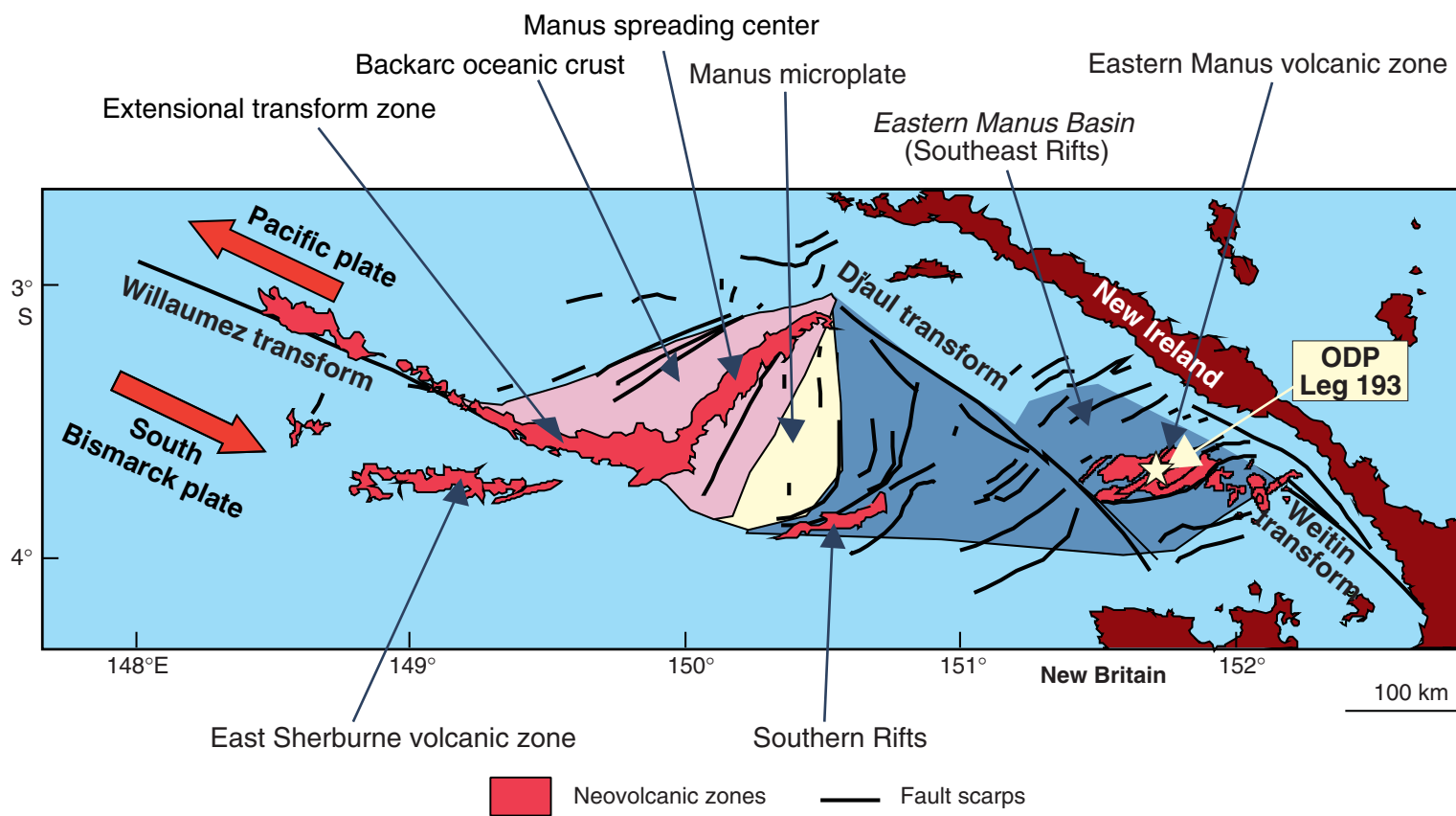


Figure 3



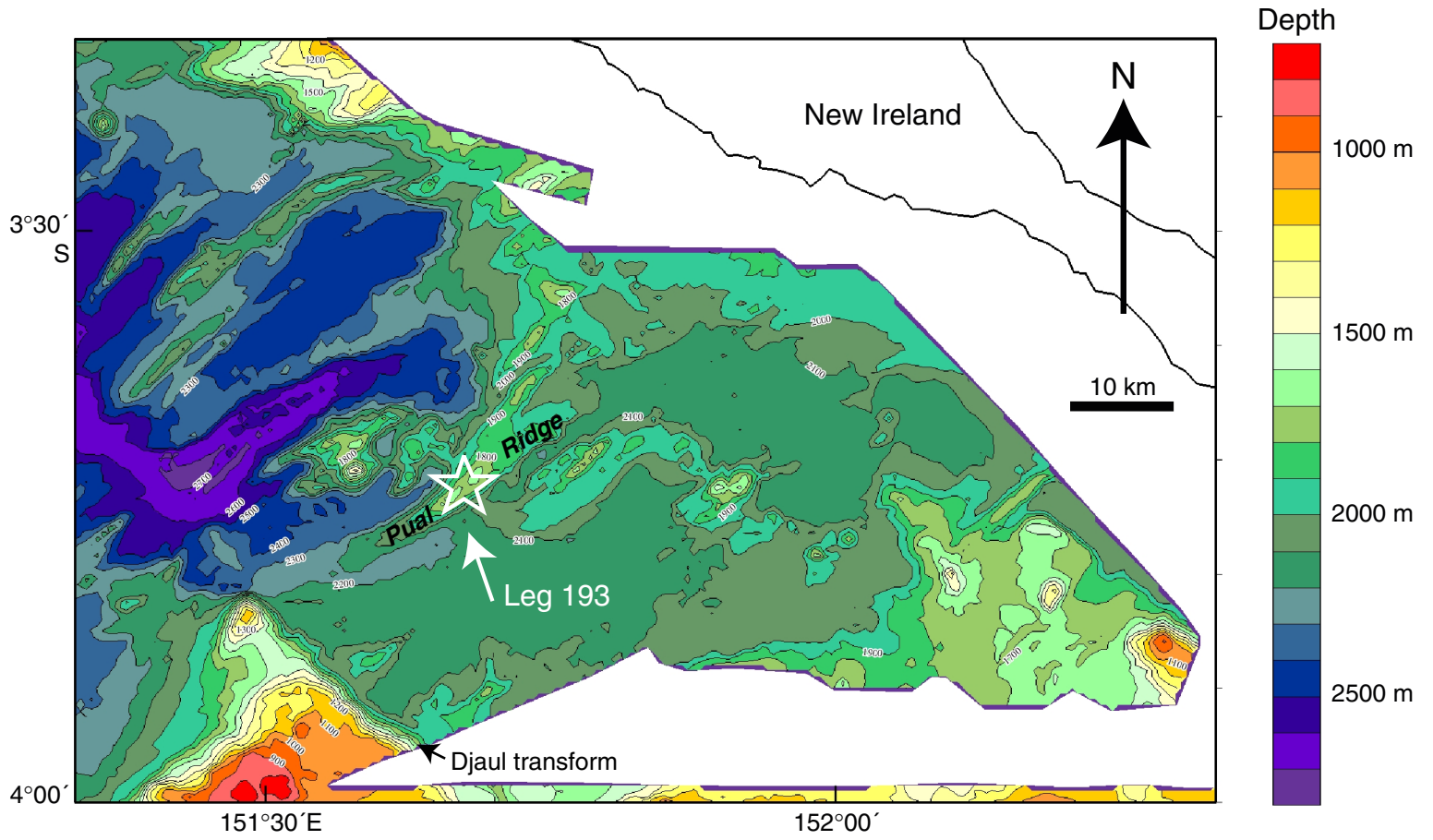


Figure 4

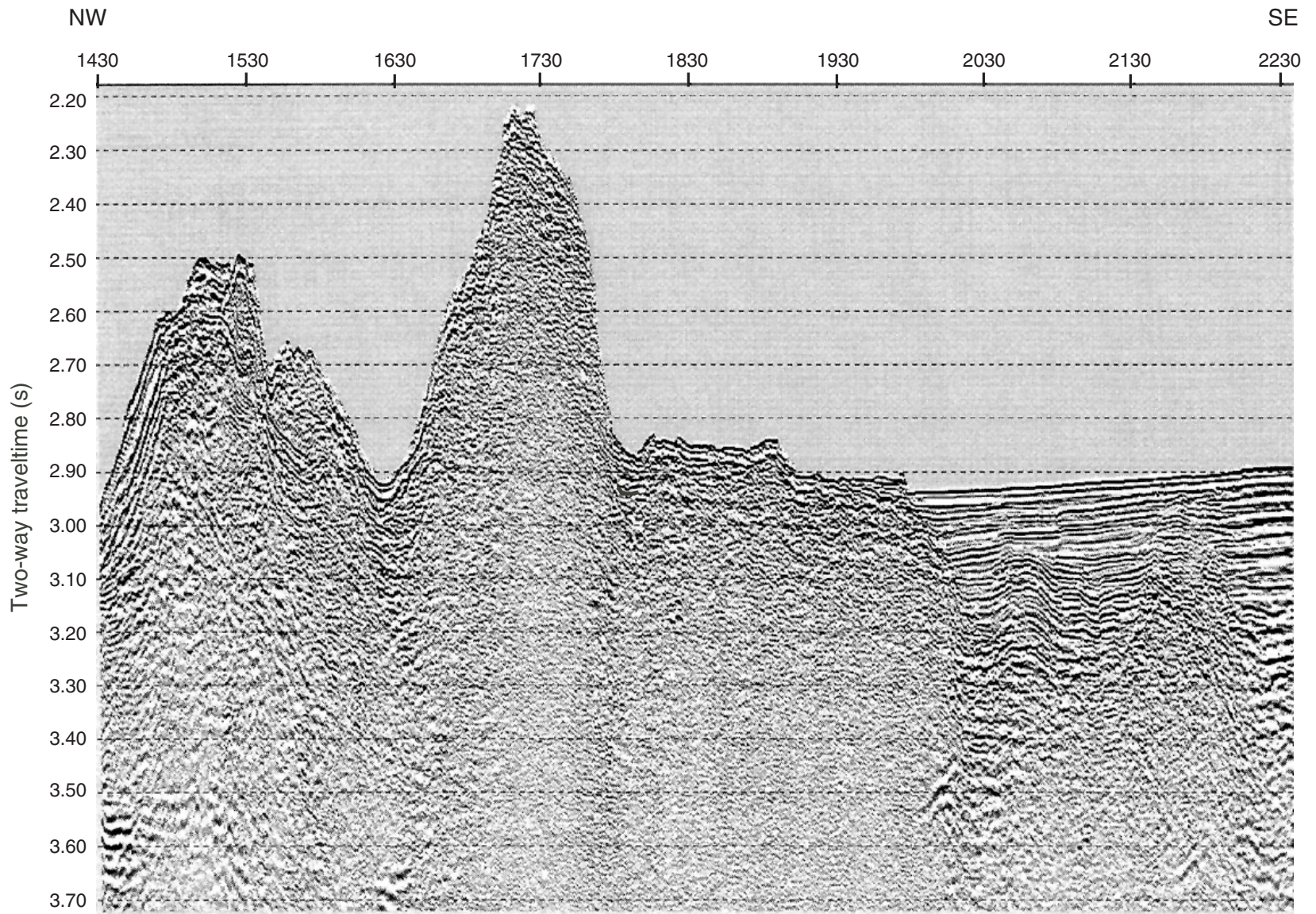


Figure 5A



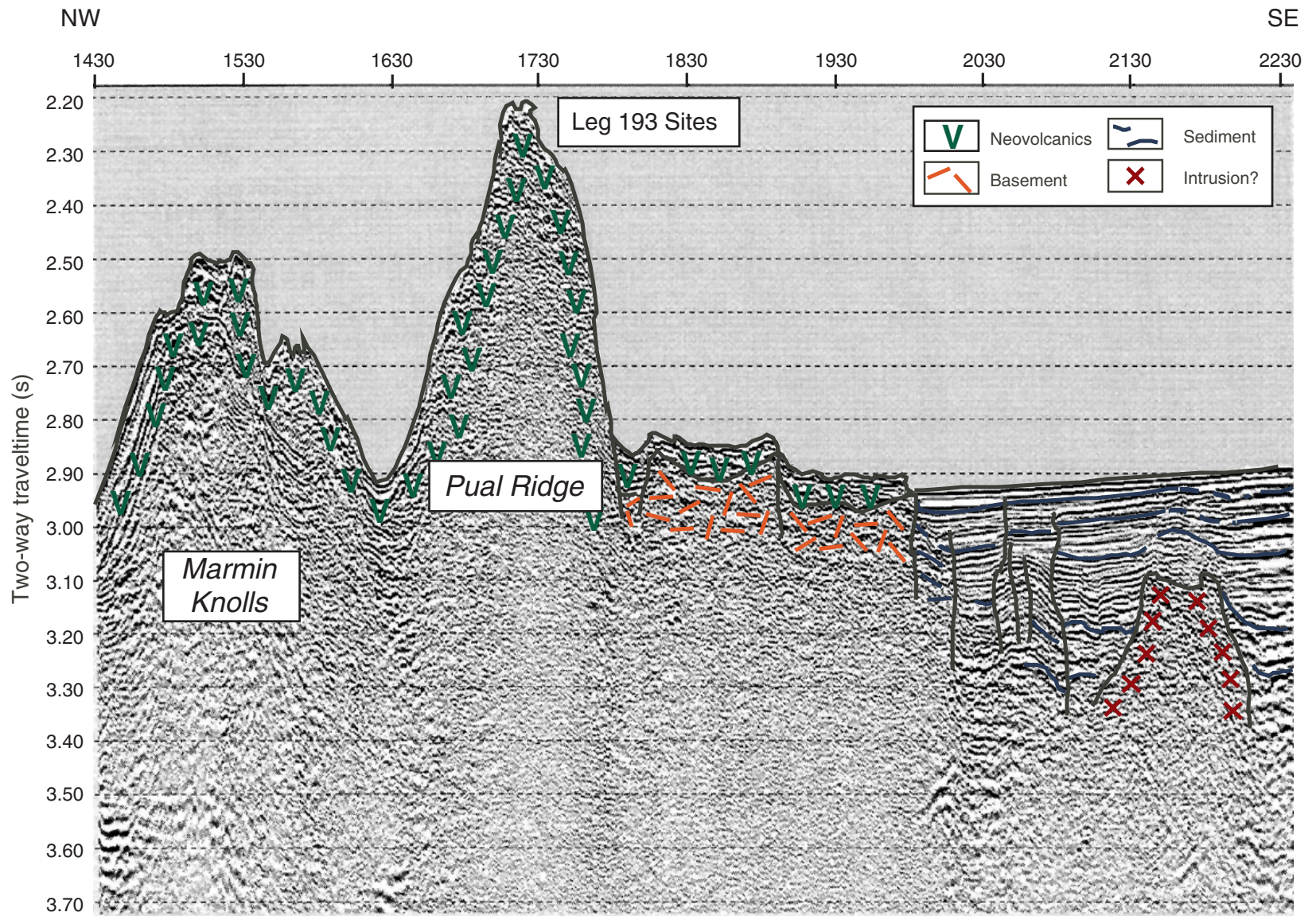


Figure 5B

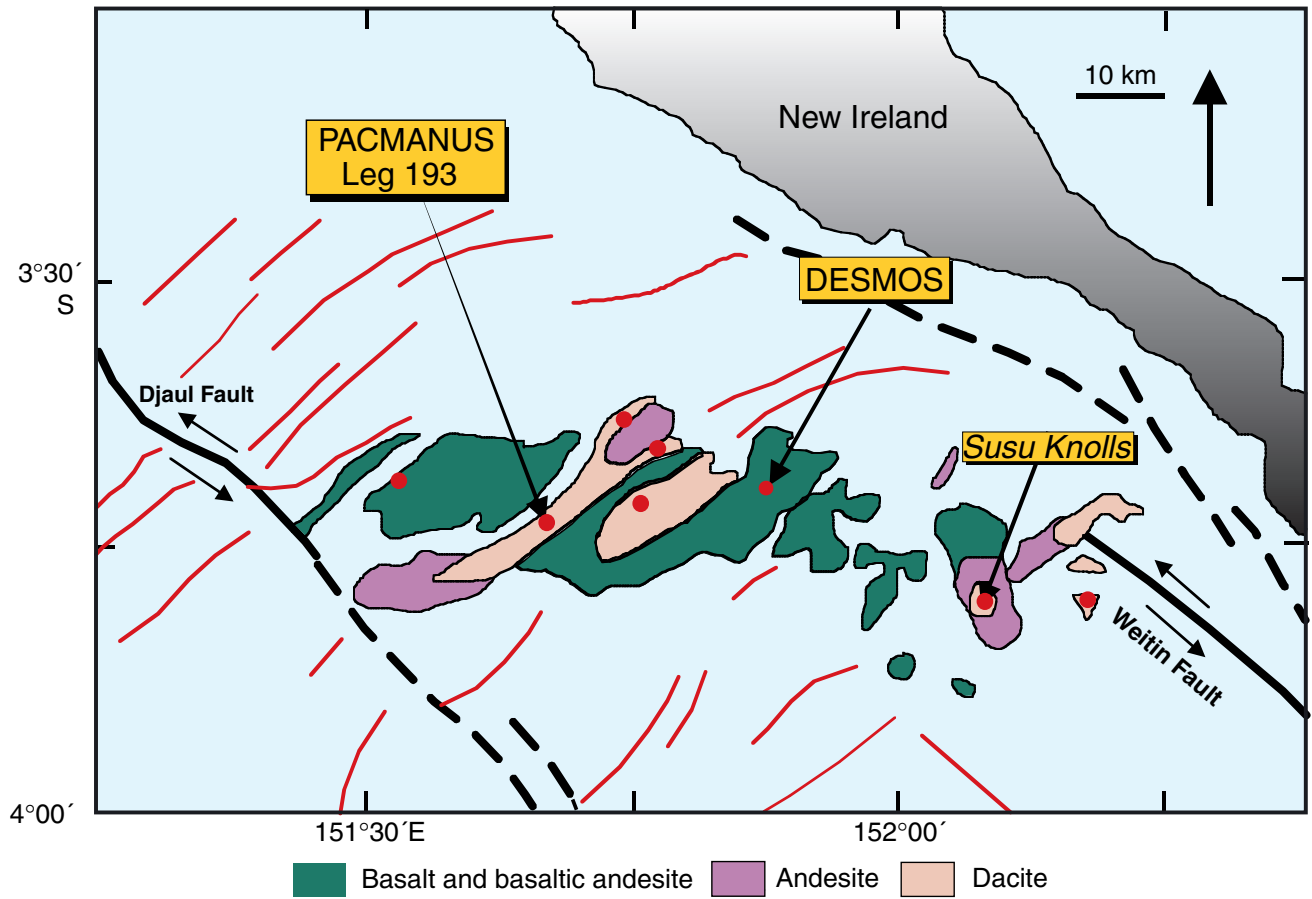


Figure 6

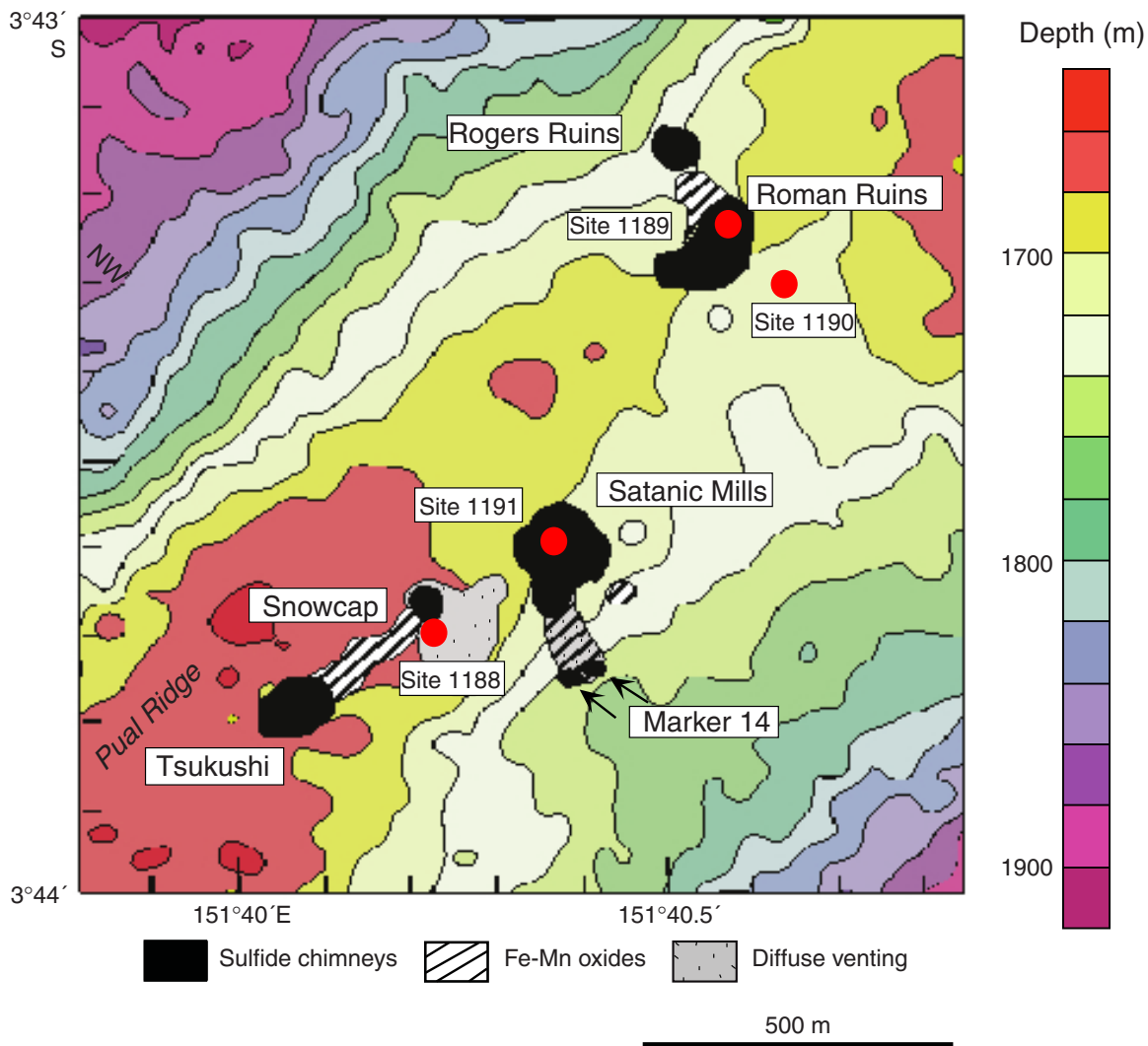


Figure 7

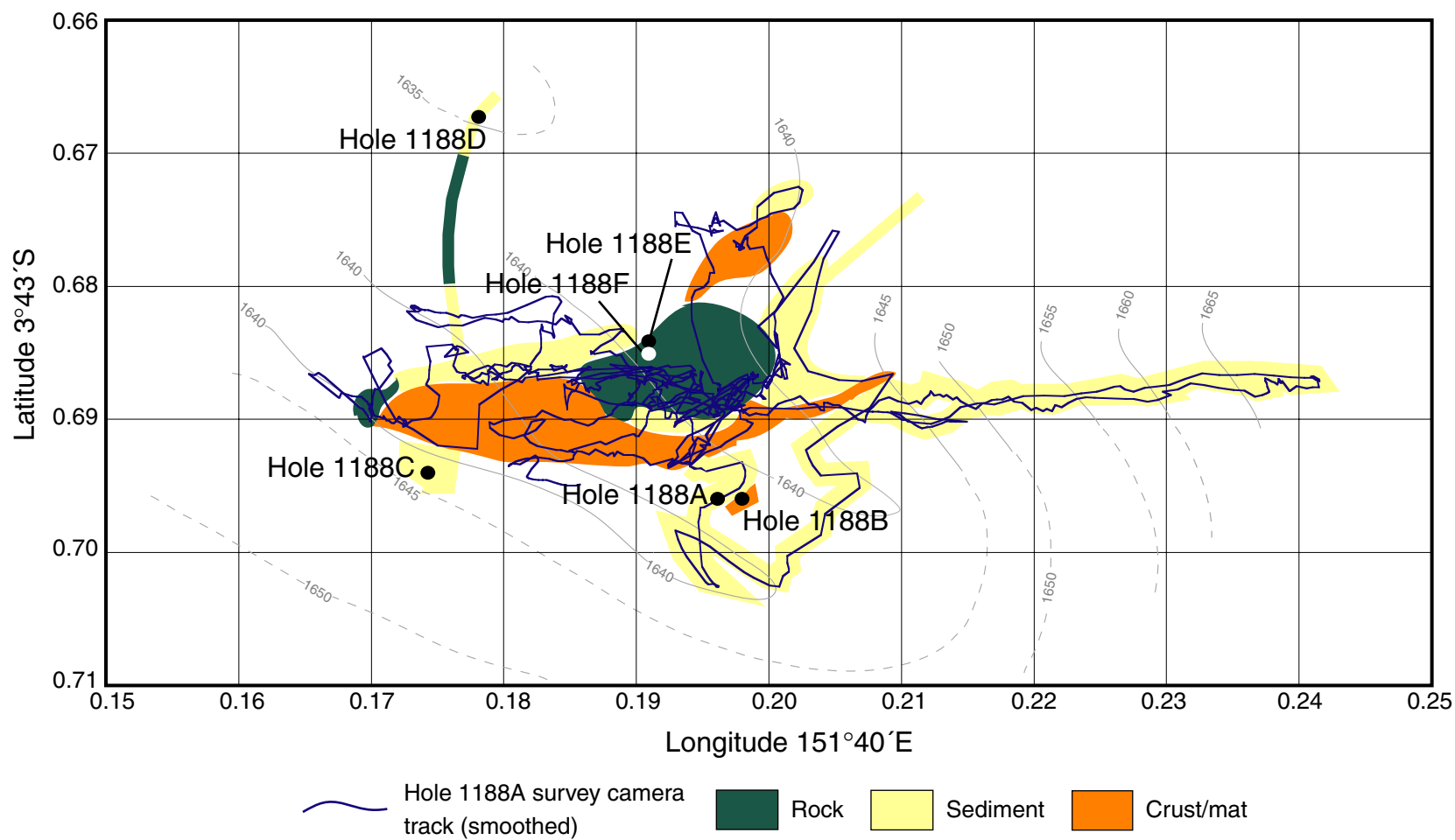
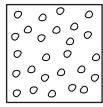
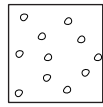


Figure 8

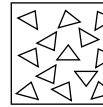
### Lithology



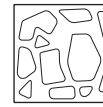
Moderately vesicular volcanic rock



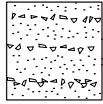
Sparsely vesicular volcanic rock



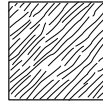
Volcanic breccia



Hydrothermal breccia



Volcaniclastic sediment



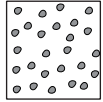
Flow banding



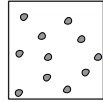
Perlitic



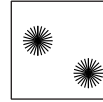
Anhydrite



Moderately amygdaloidal volcanic rock

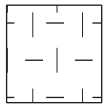


Sparsely amygdaloidal volcanic rock

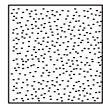


Spherulitic volcanic rock

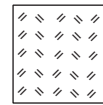
### Alteration



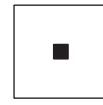
Silicification



Bleaching

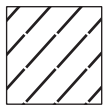


Silica-sulfate-chlorite and green, silica-clay alteration

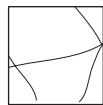


Magnetite enriched

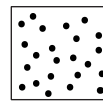
### Mineralization



Massive and semimassive sulfide



Stockwork/veins/stringers



Disseminated

Figure 9



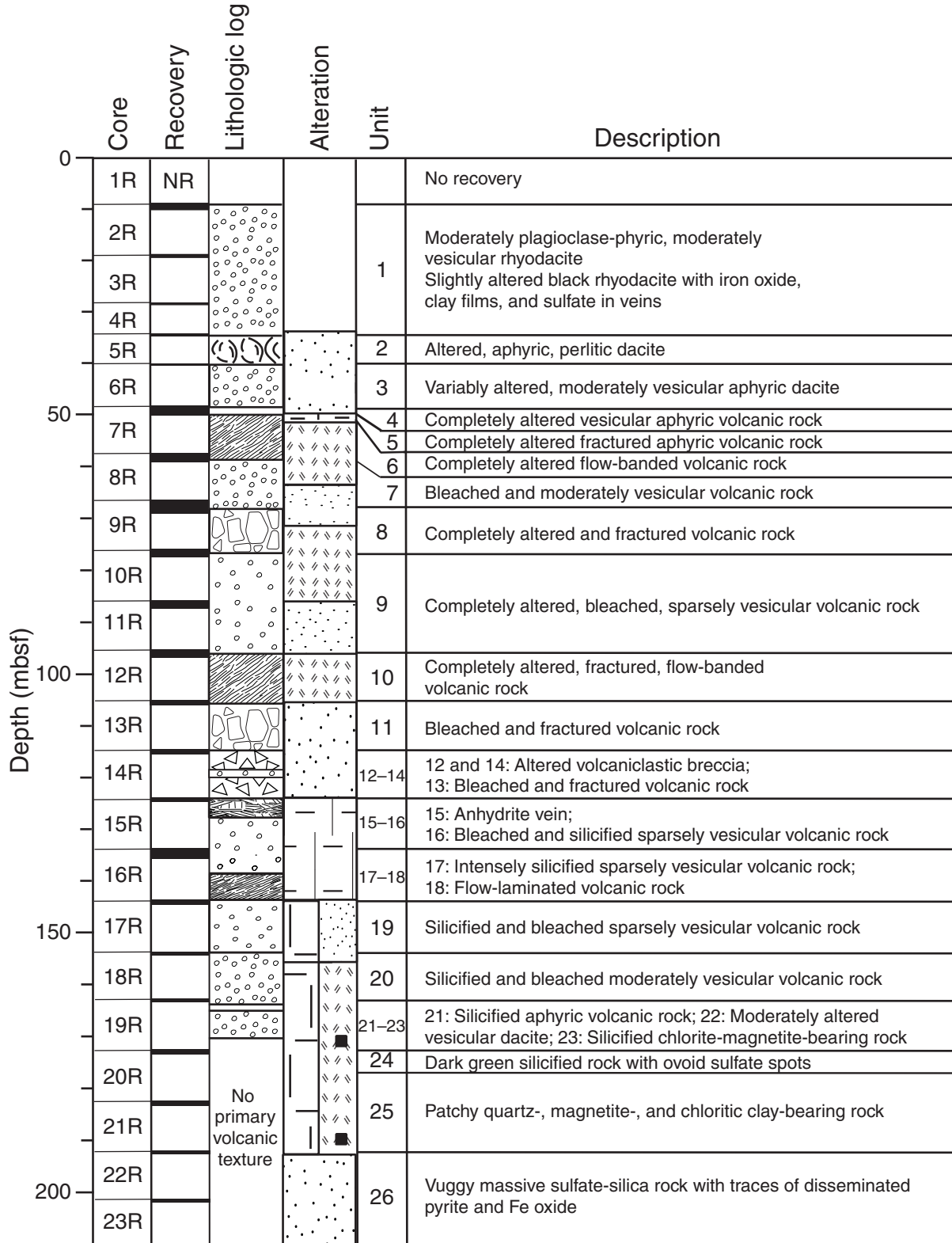


Figure 10A



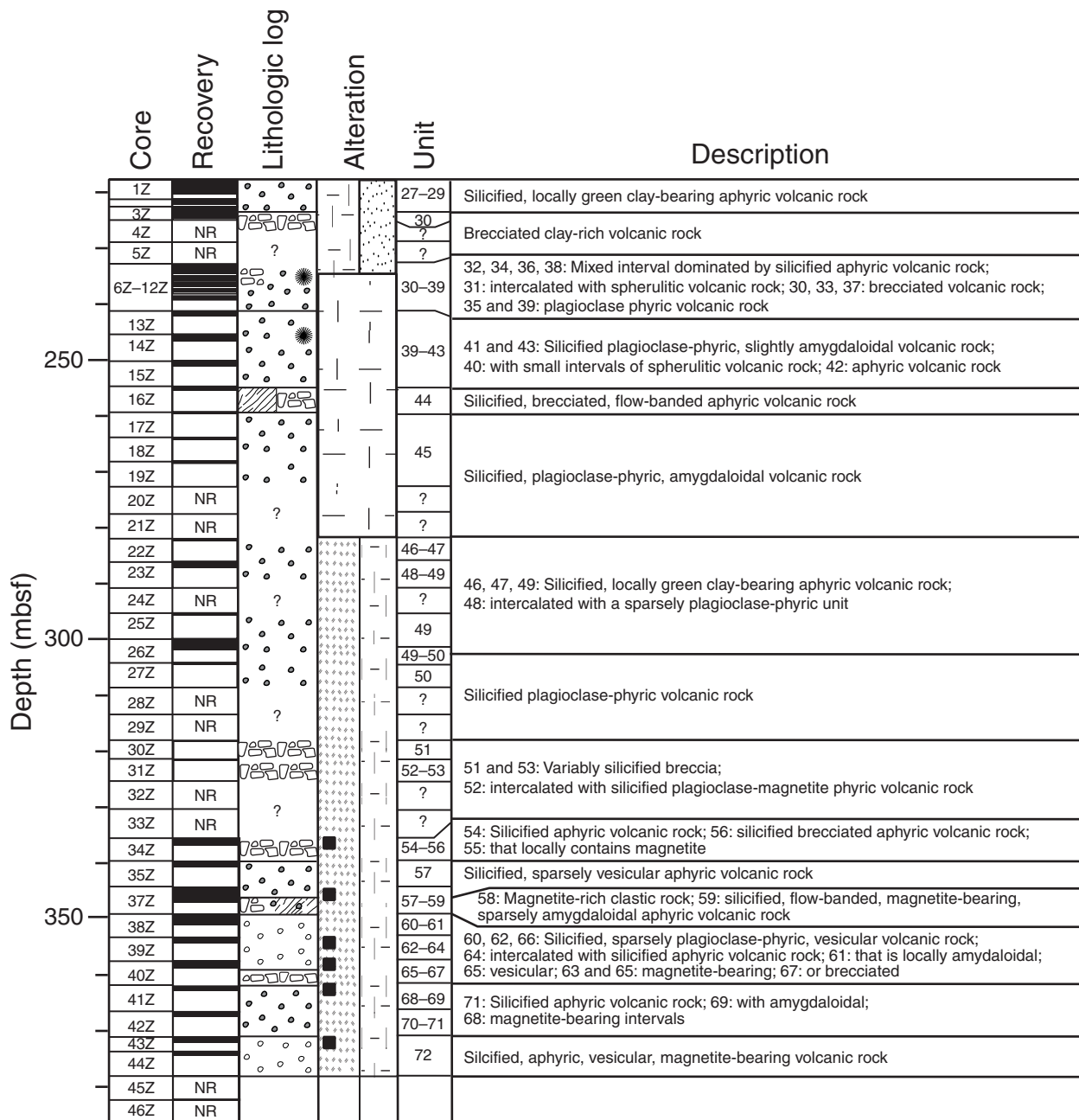


Figure 10B

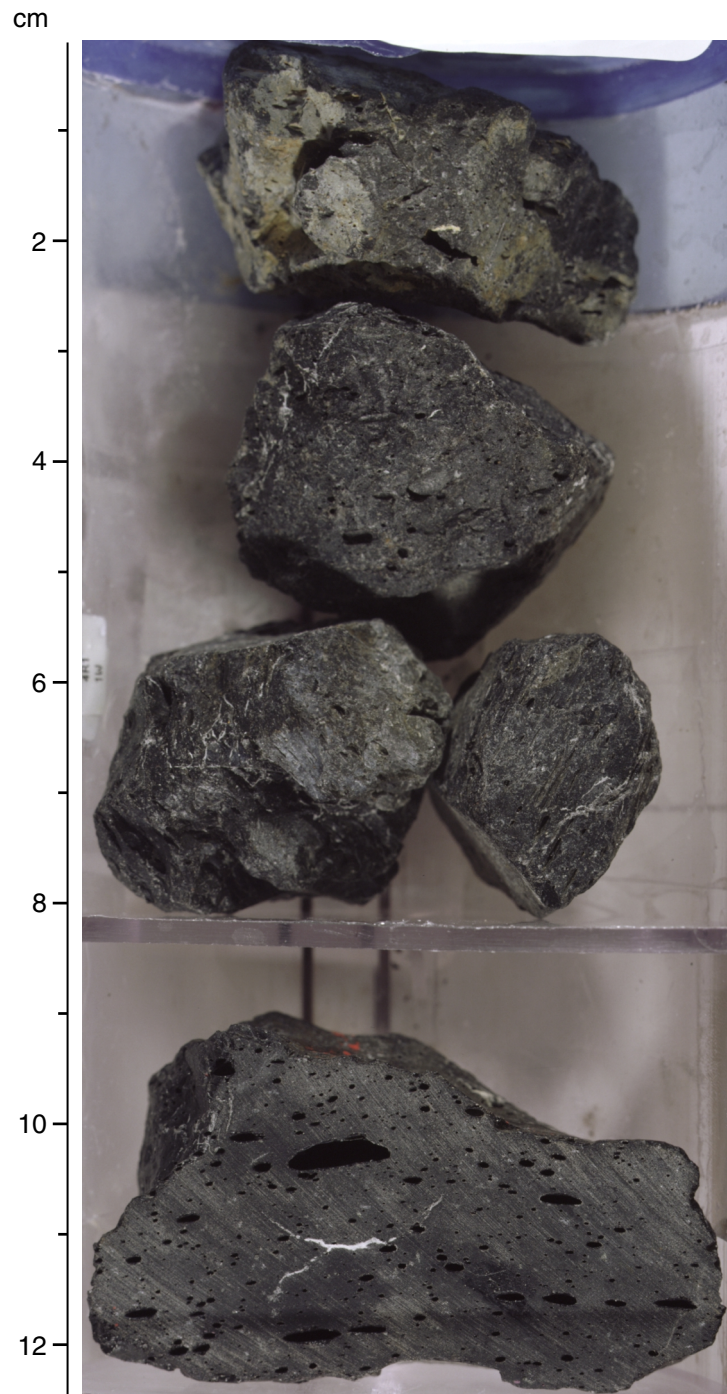


Figure 11

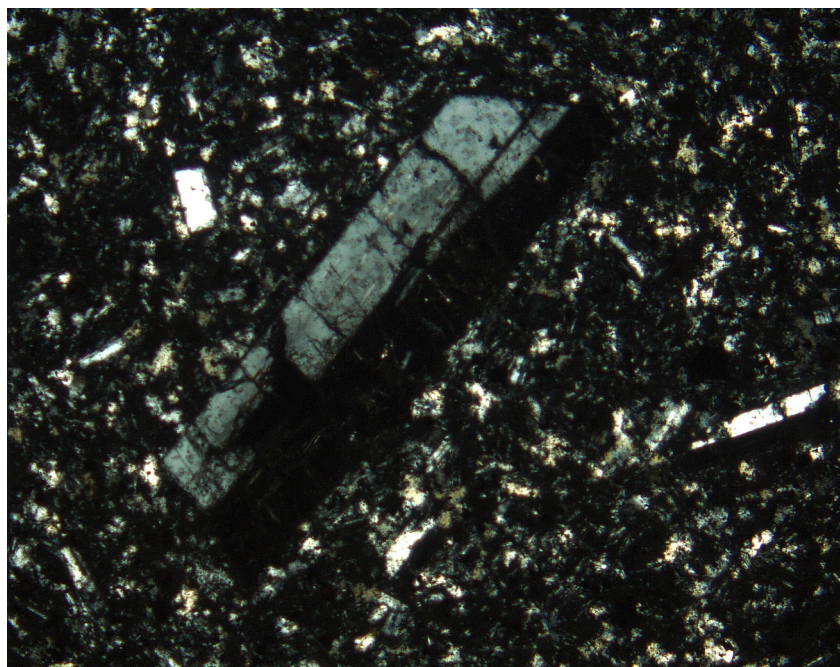


Figure 12



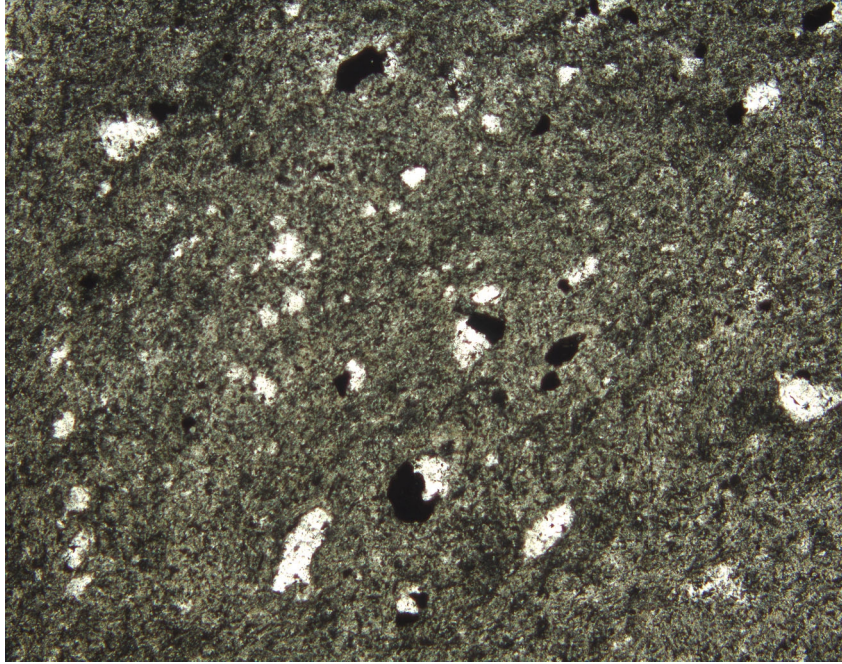


Figure 13

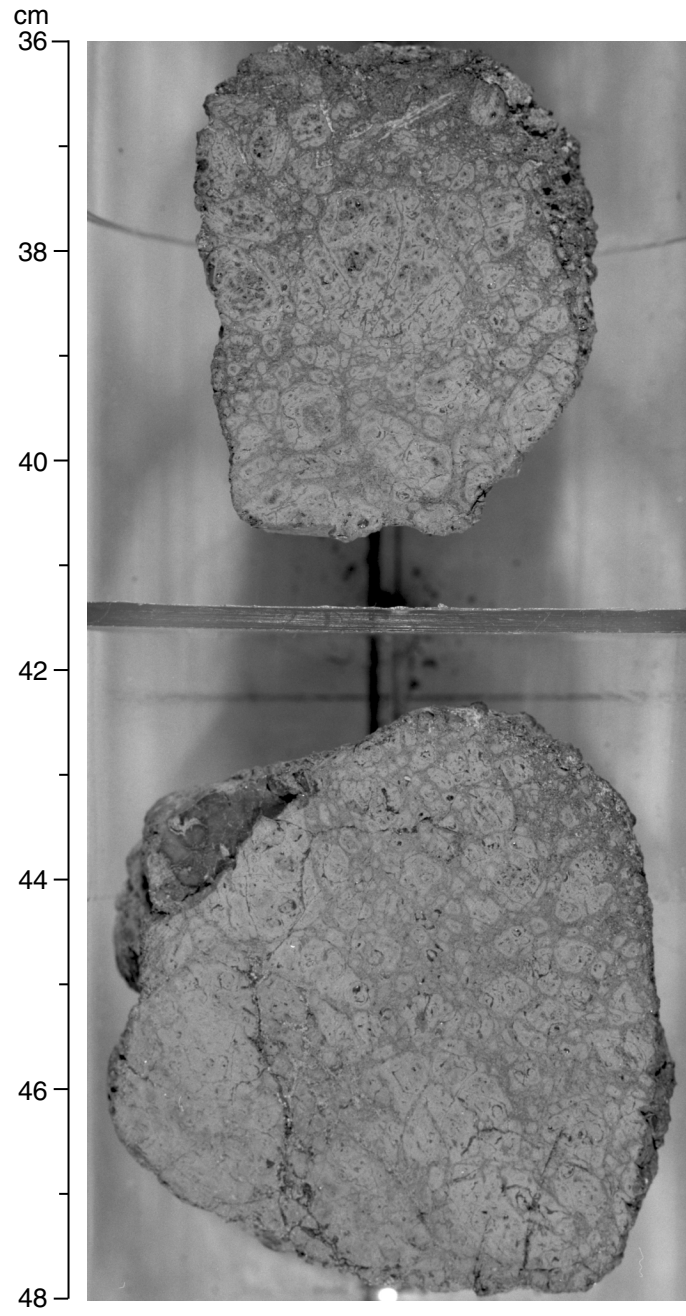


Figure 14A

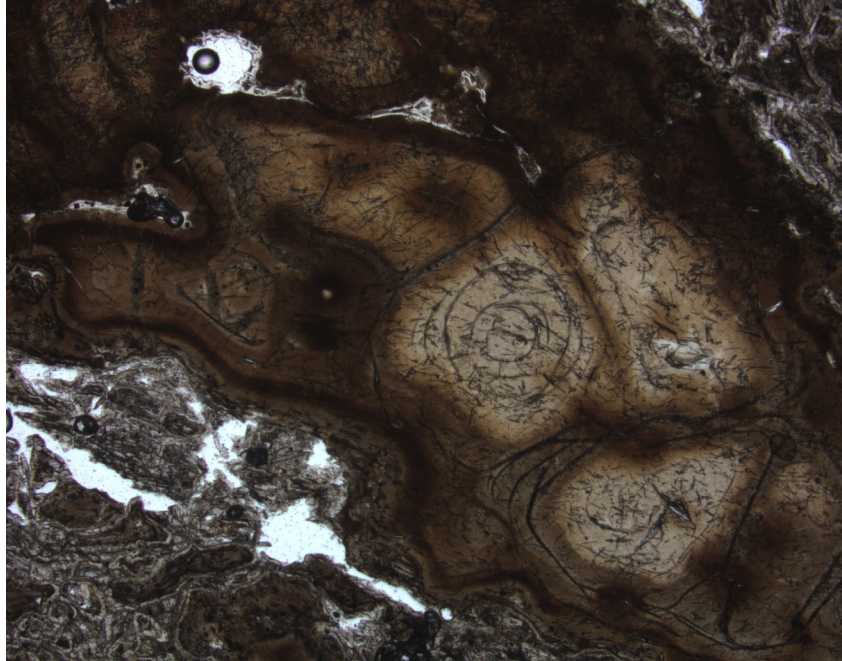


Figure 14B

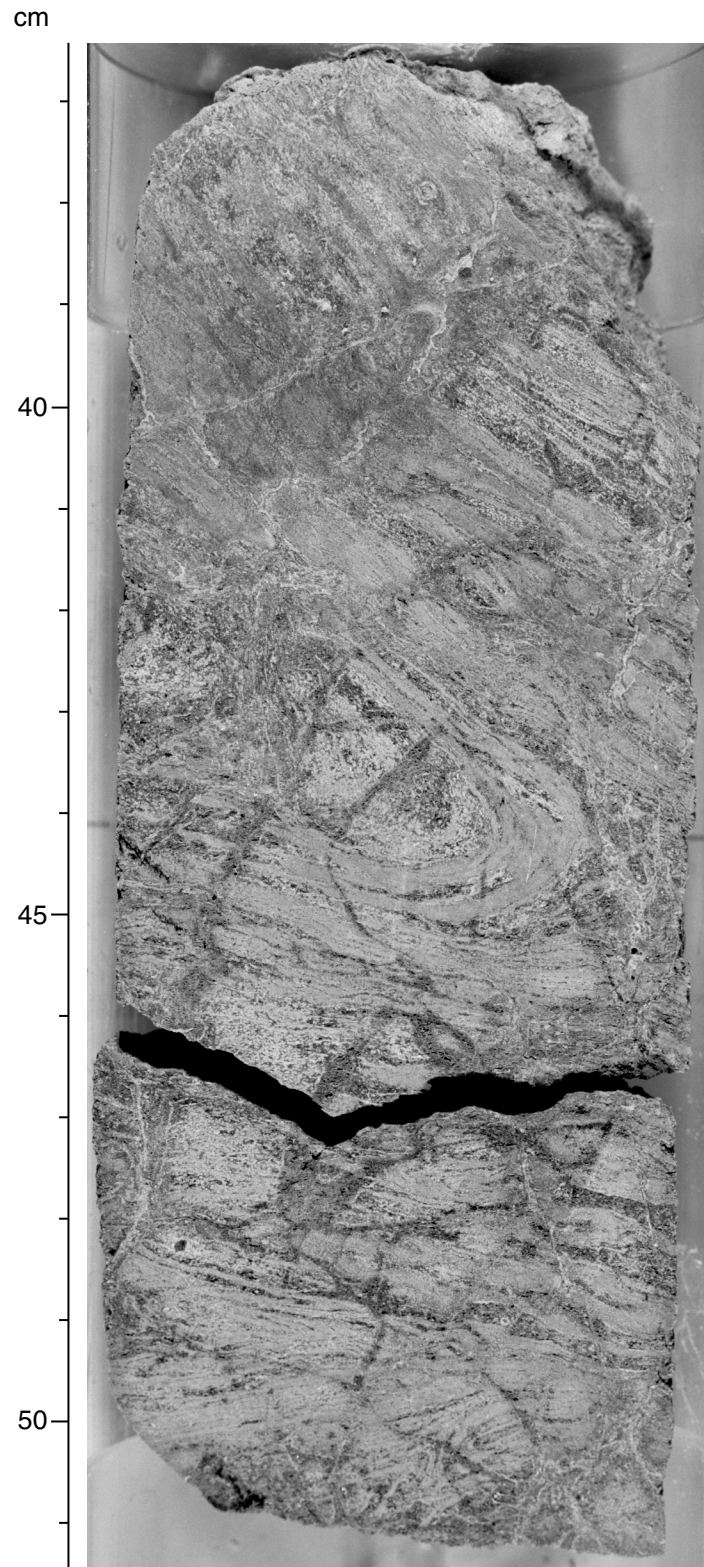


Figure 15A

Interval 193-1188A-12R-2, 36-53 cm



Figure 15B



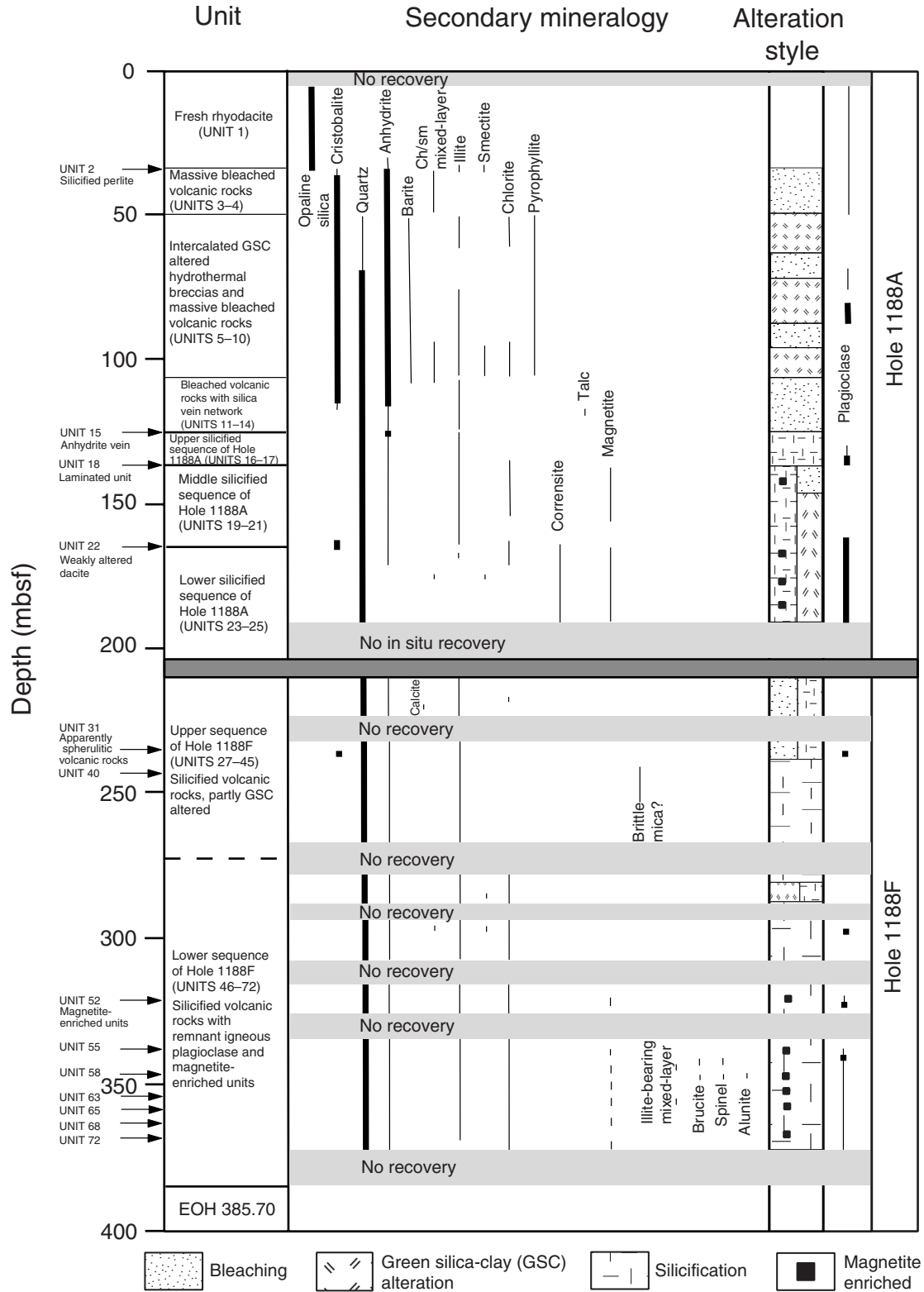


Figure 16

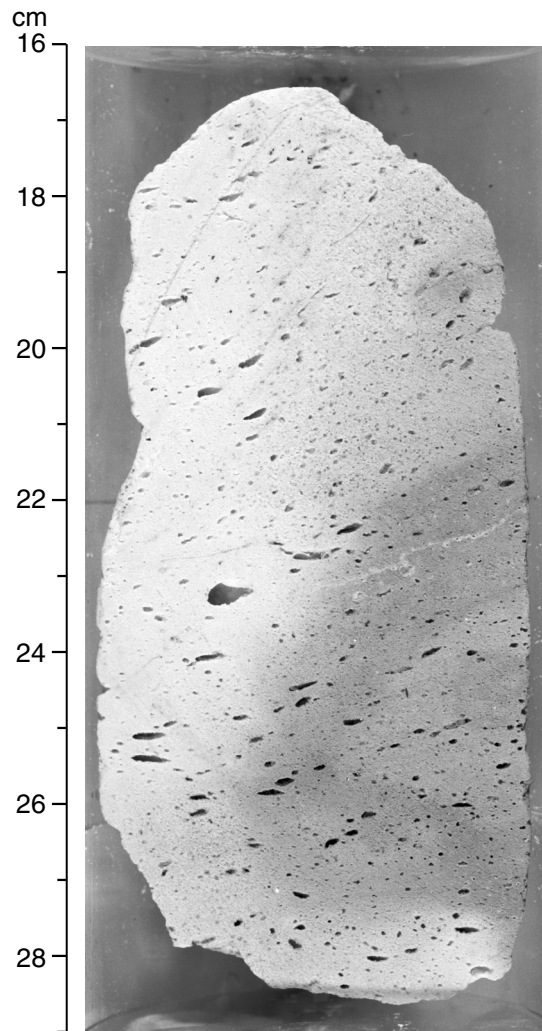


Figure 17

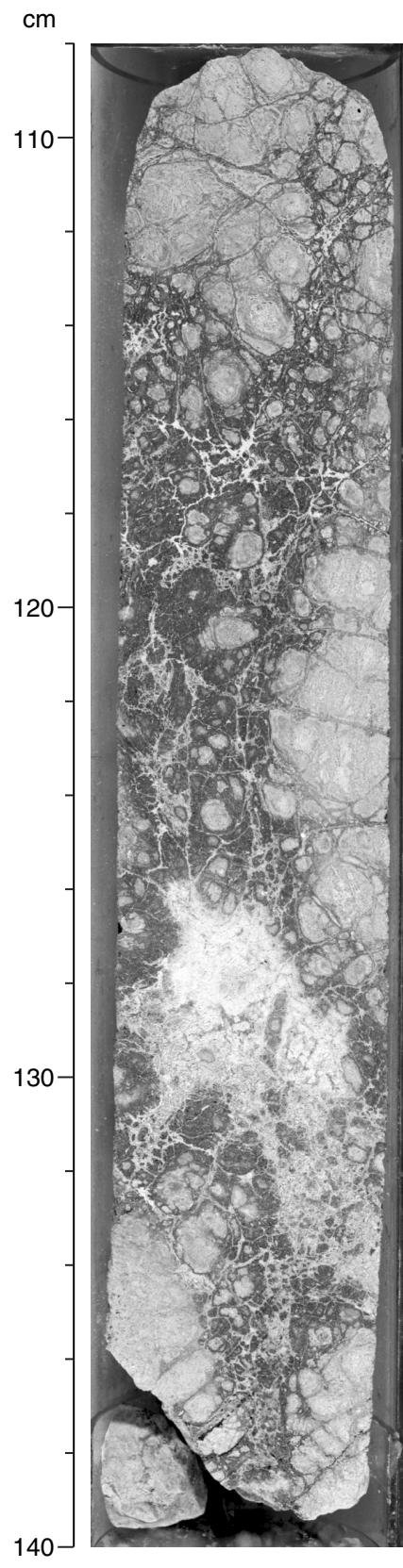


Figure 18

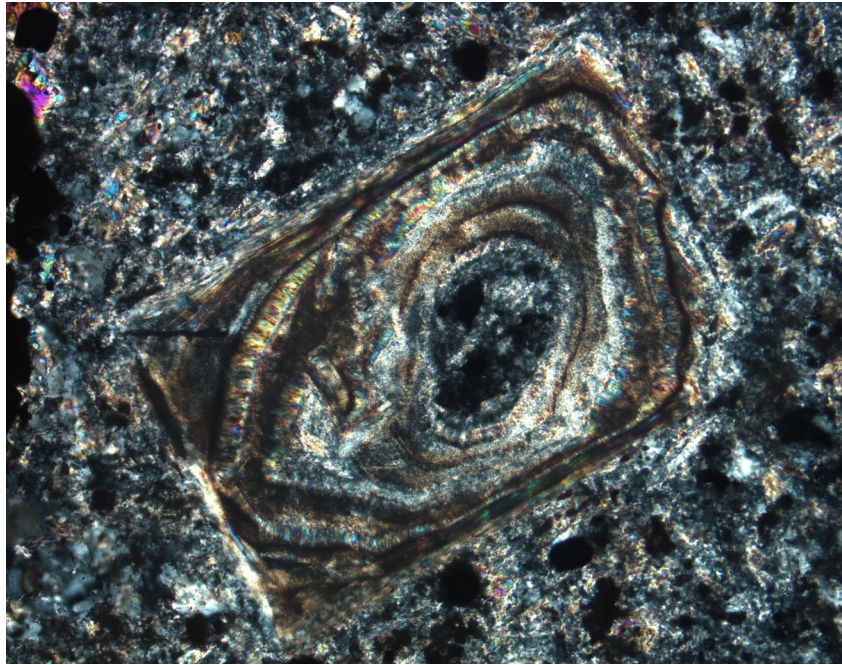


Figure 19

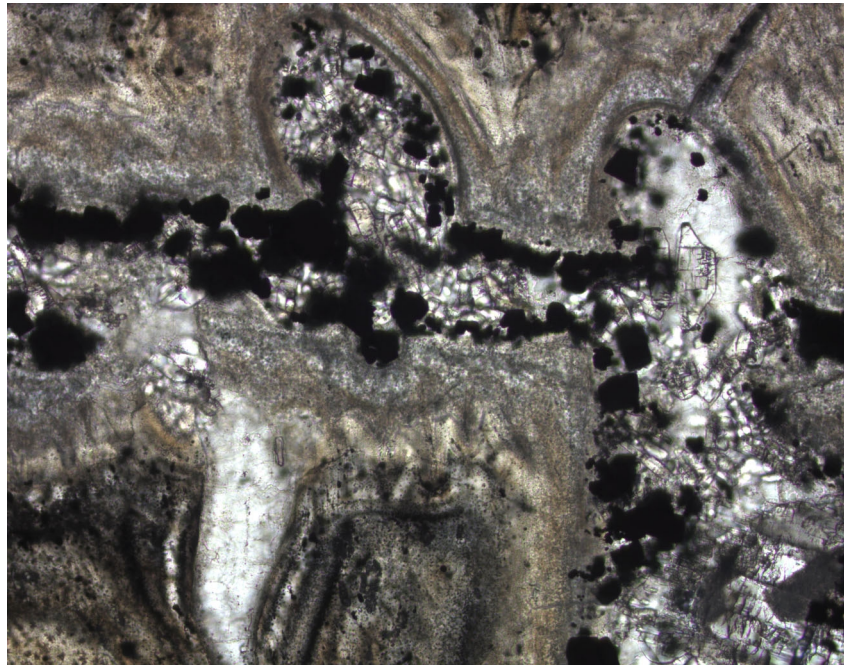


Figure 20



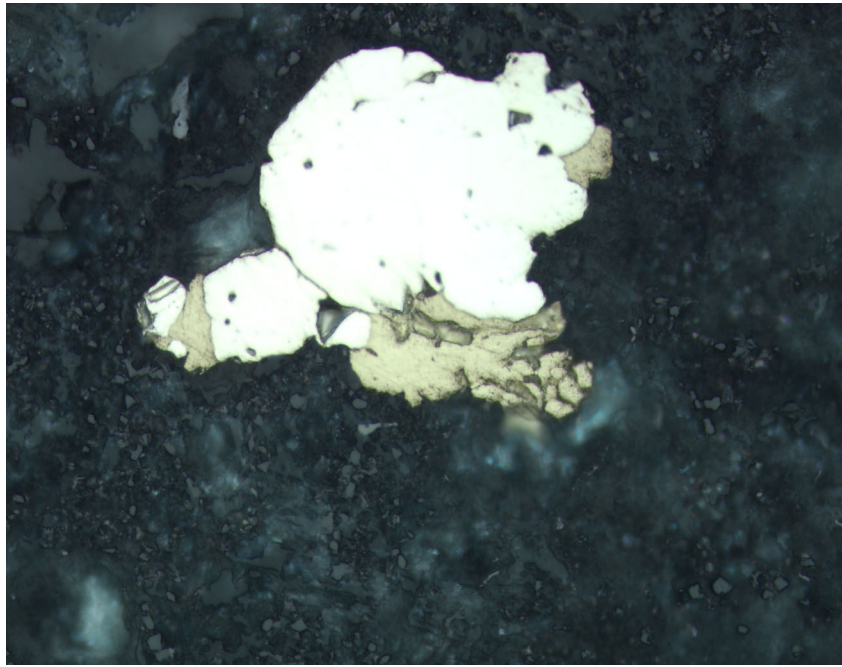


Figure 21

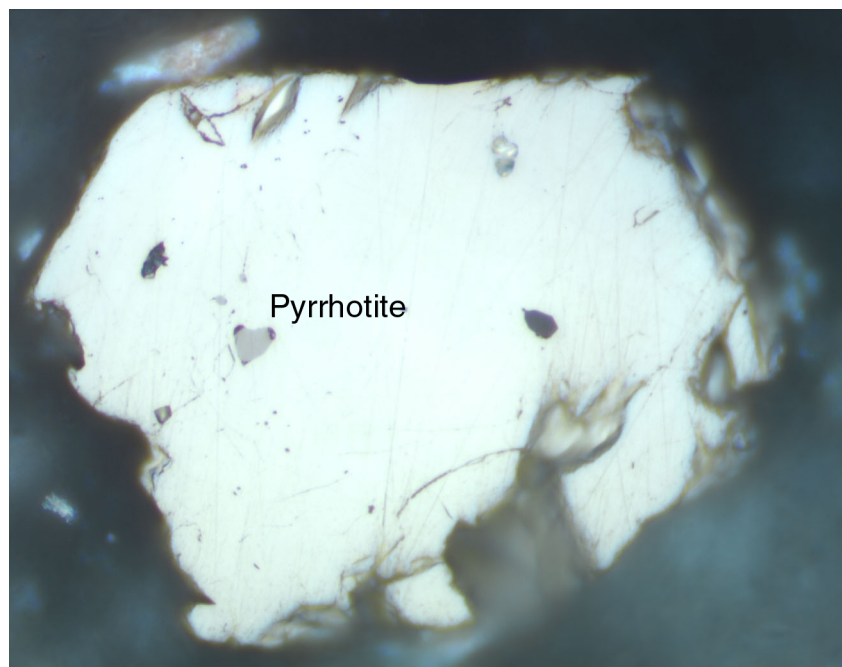


Figure 22

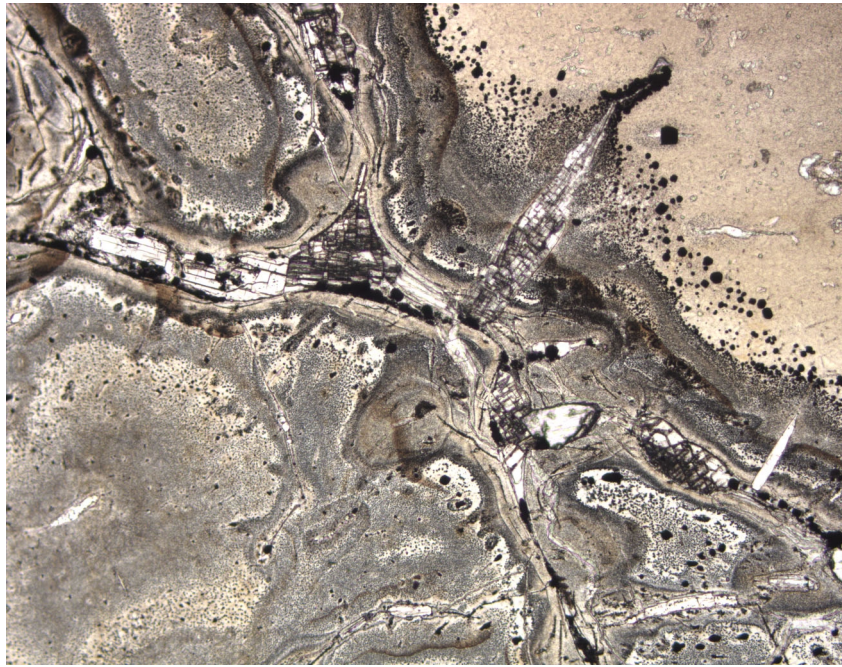


Figure 23



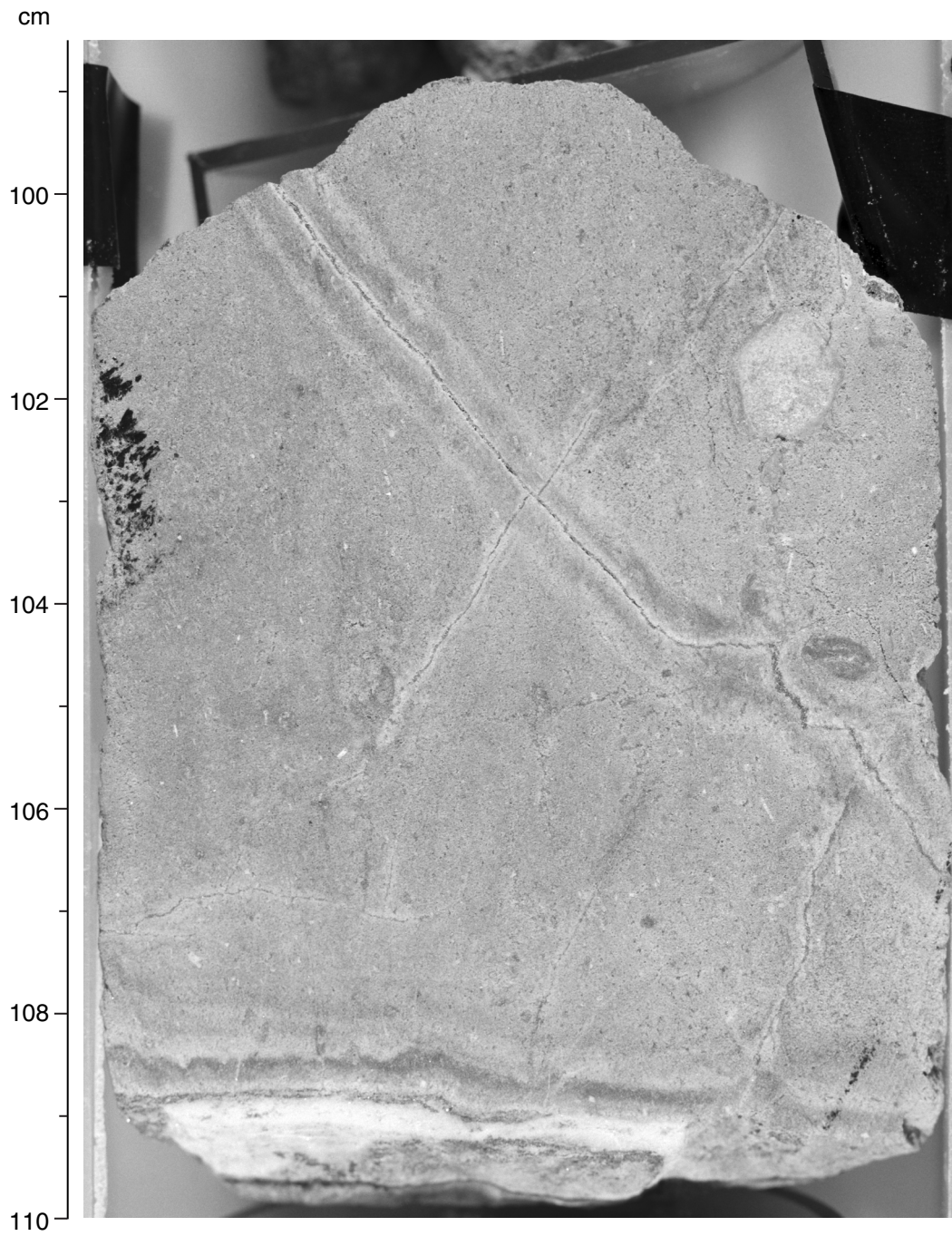


Figure 24A

Interval 193-1188F-14Z-1 (Piece 6, 96-108 cm)

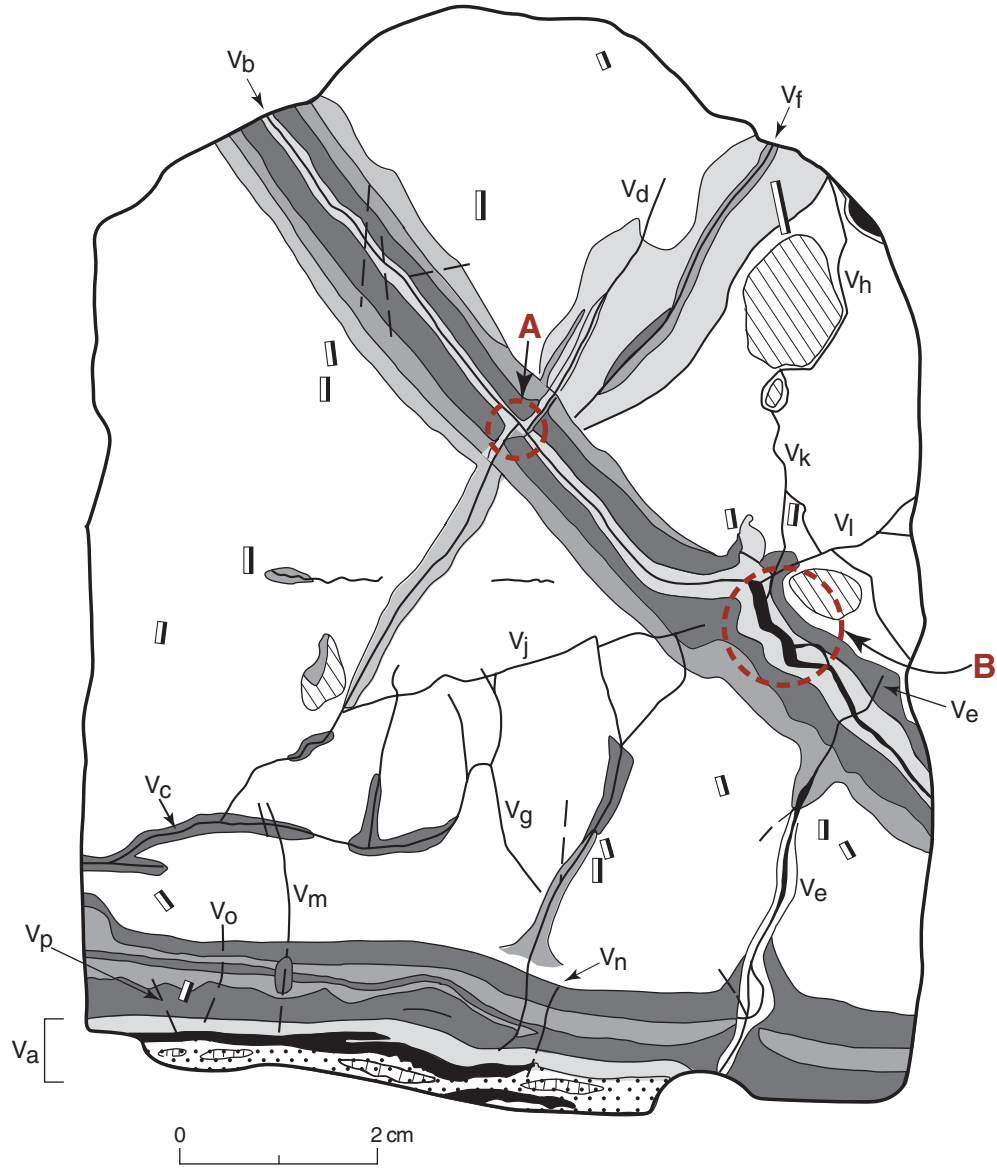


Figure 24B

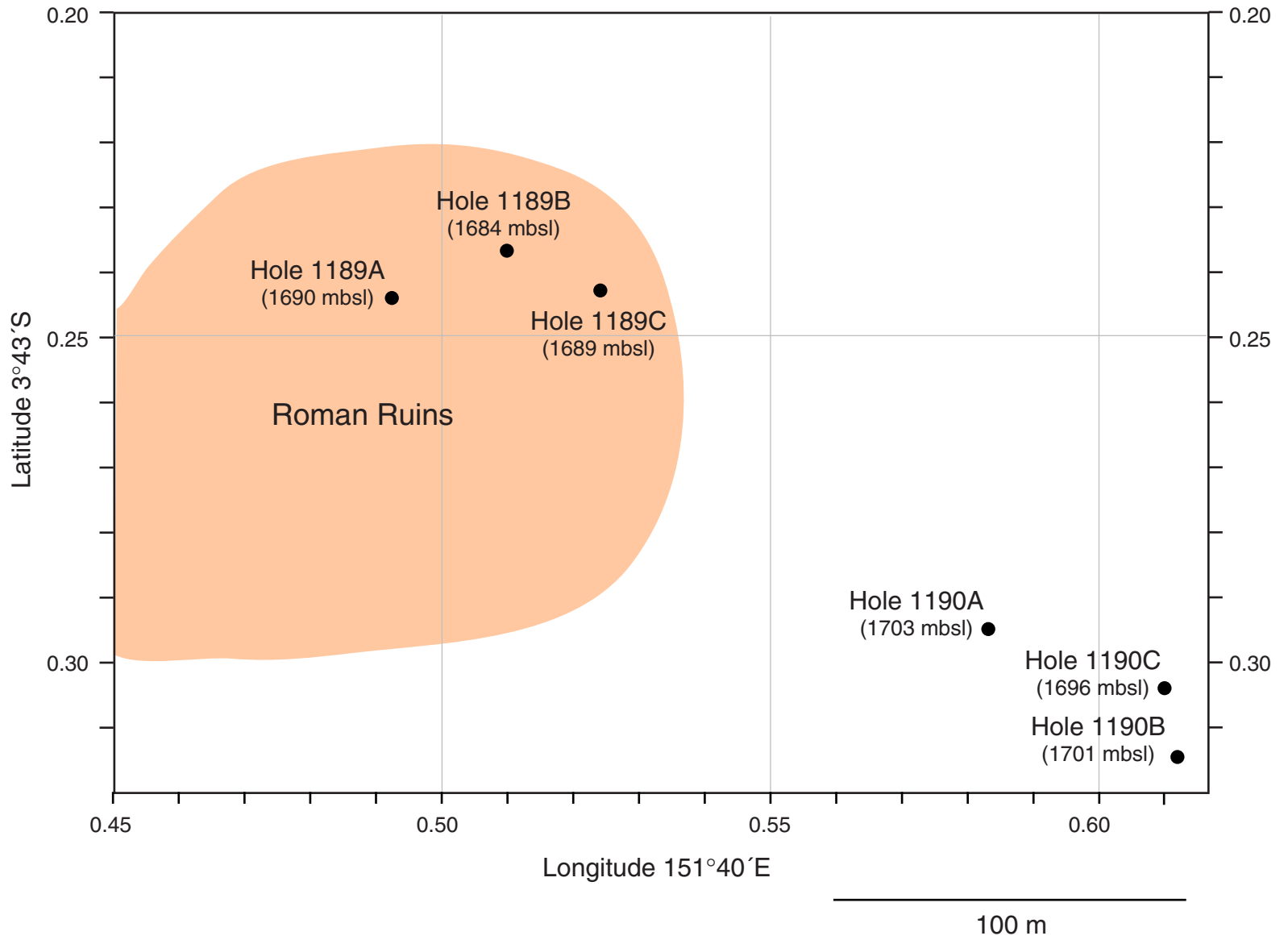


Figure 25

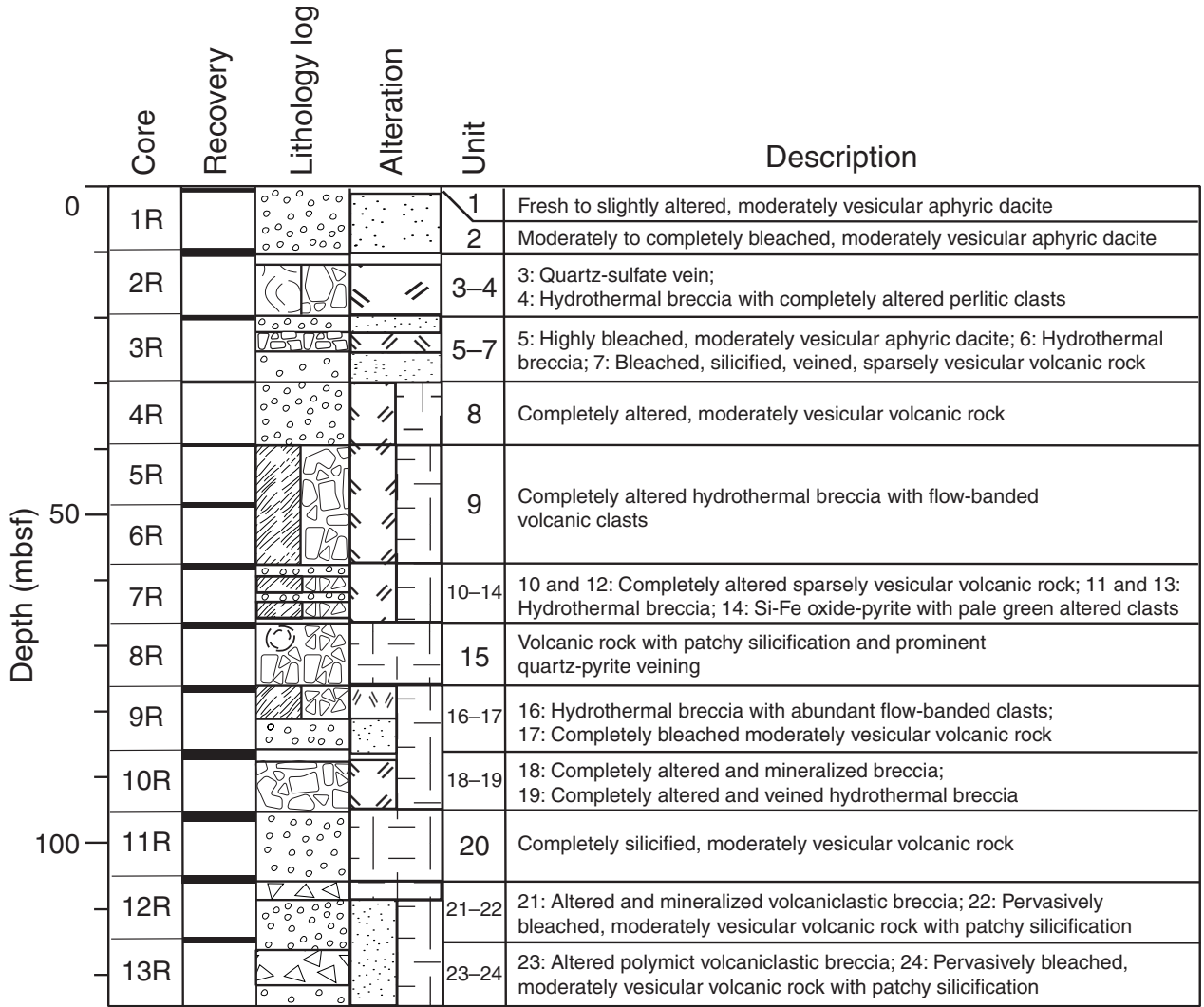


Figure 26A

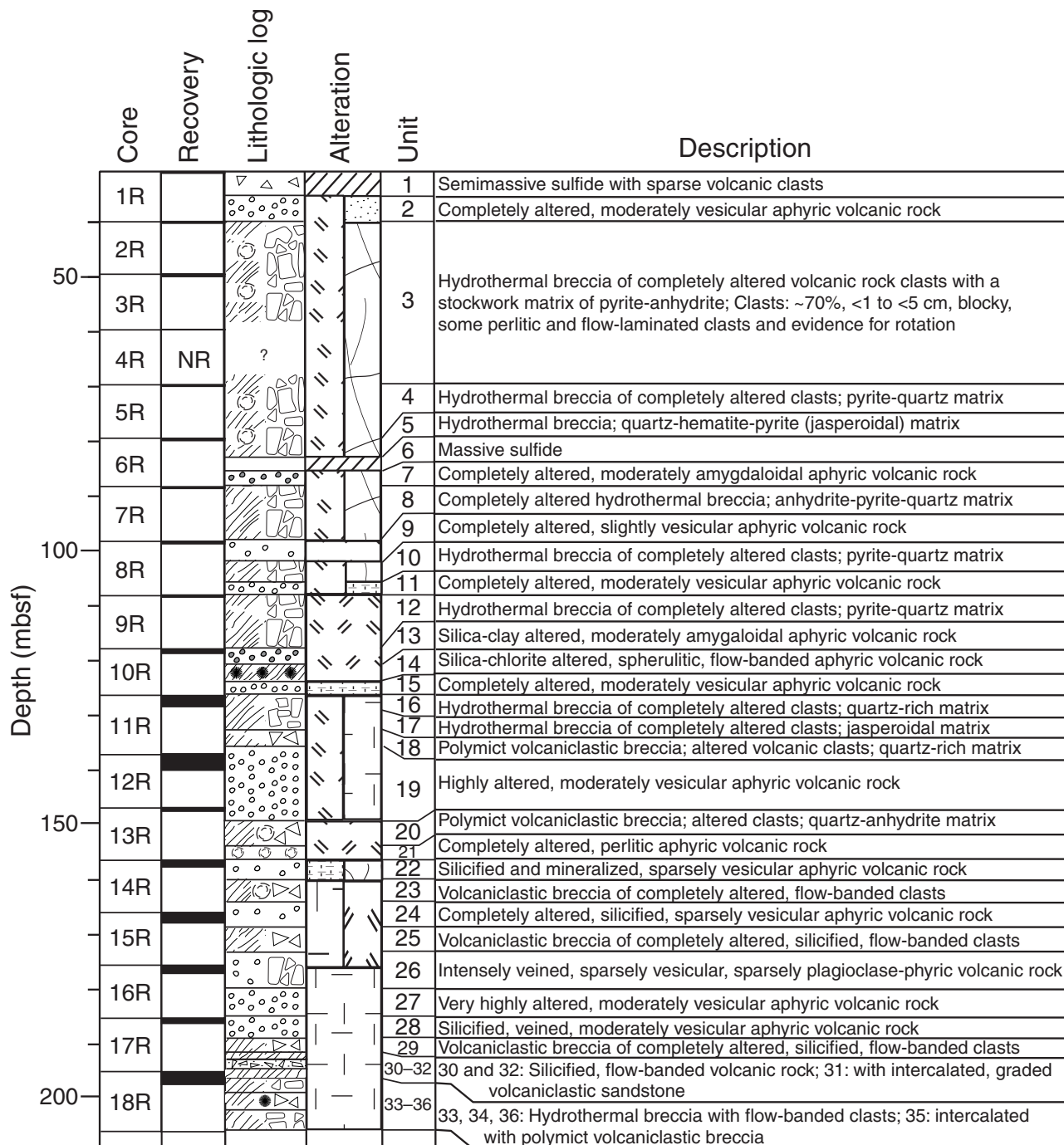


Figure 26B



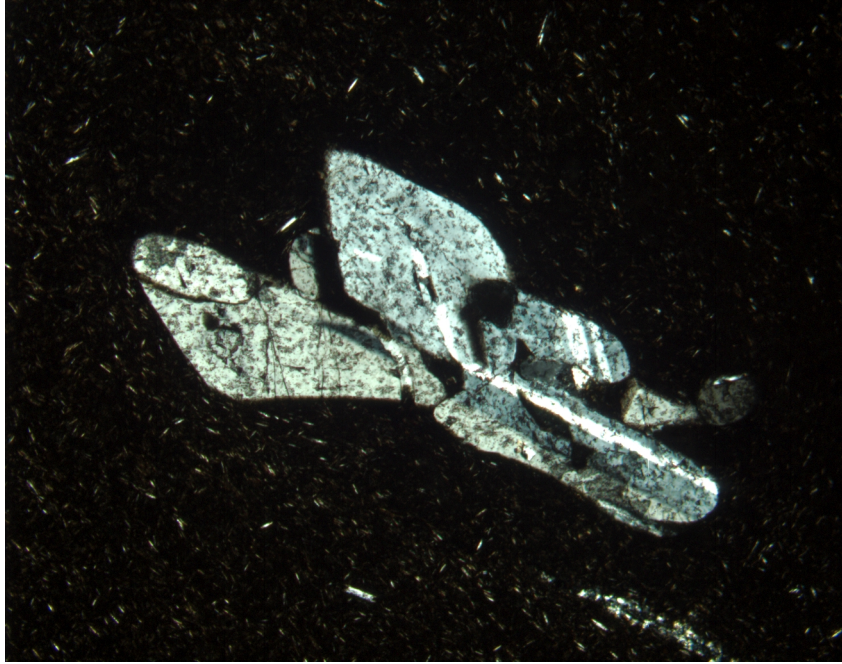


Figure 27

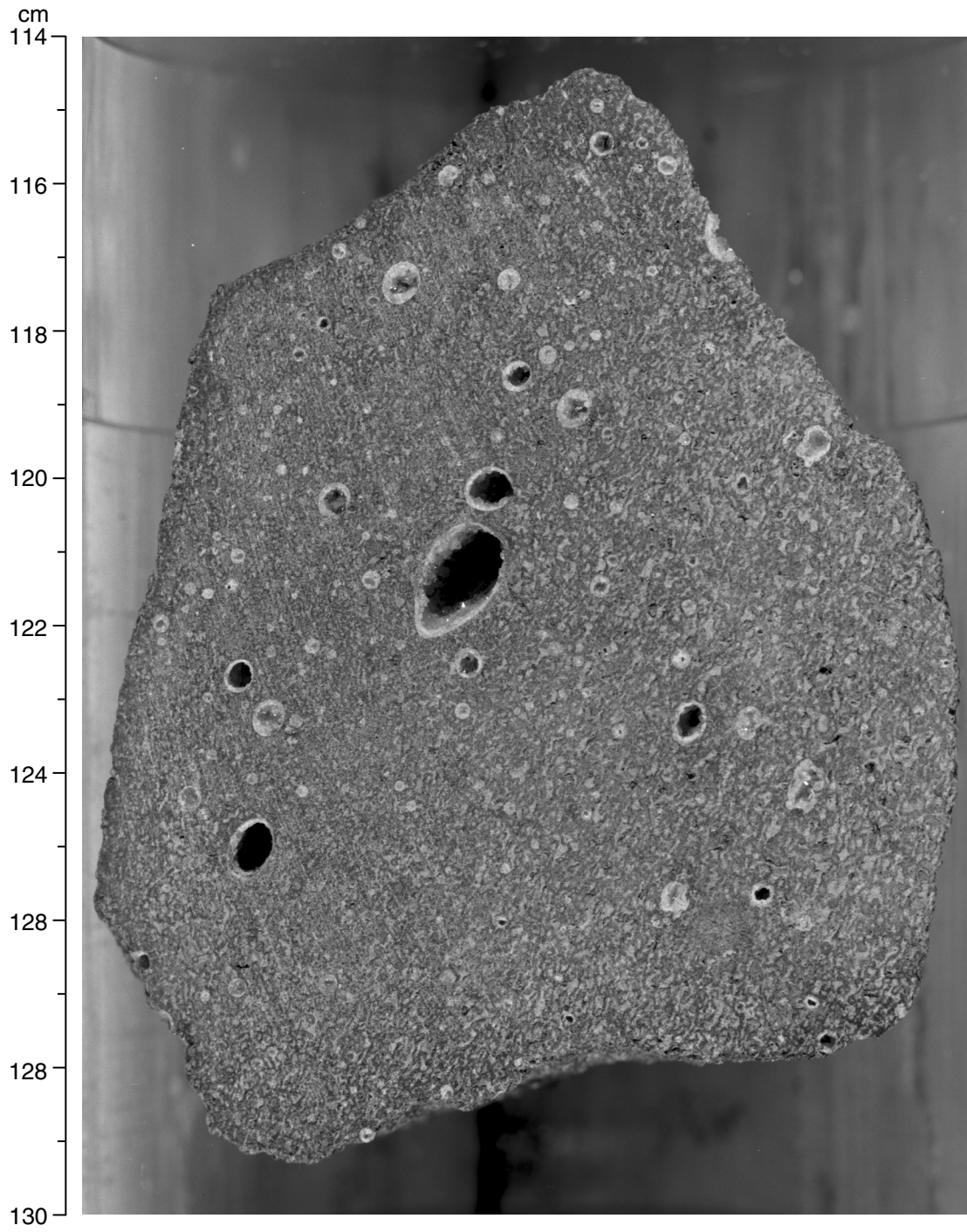


Figure 28

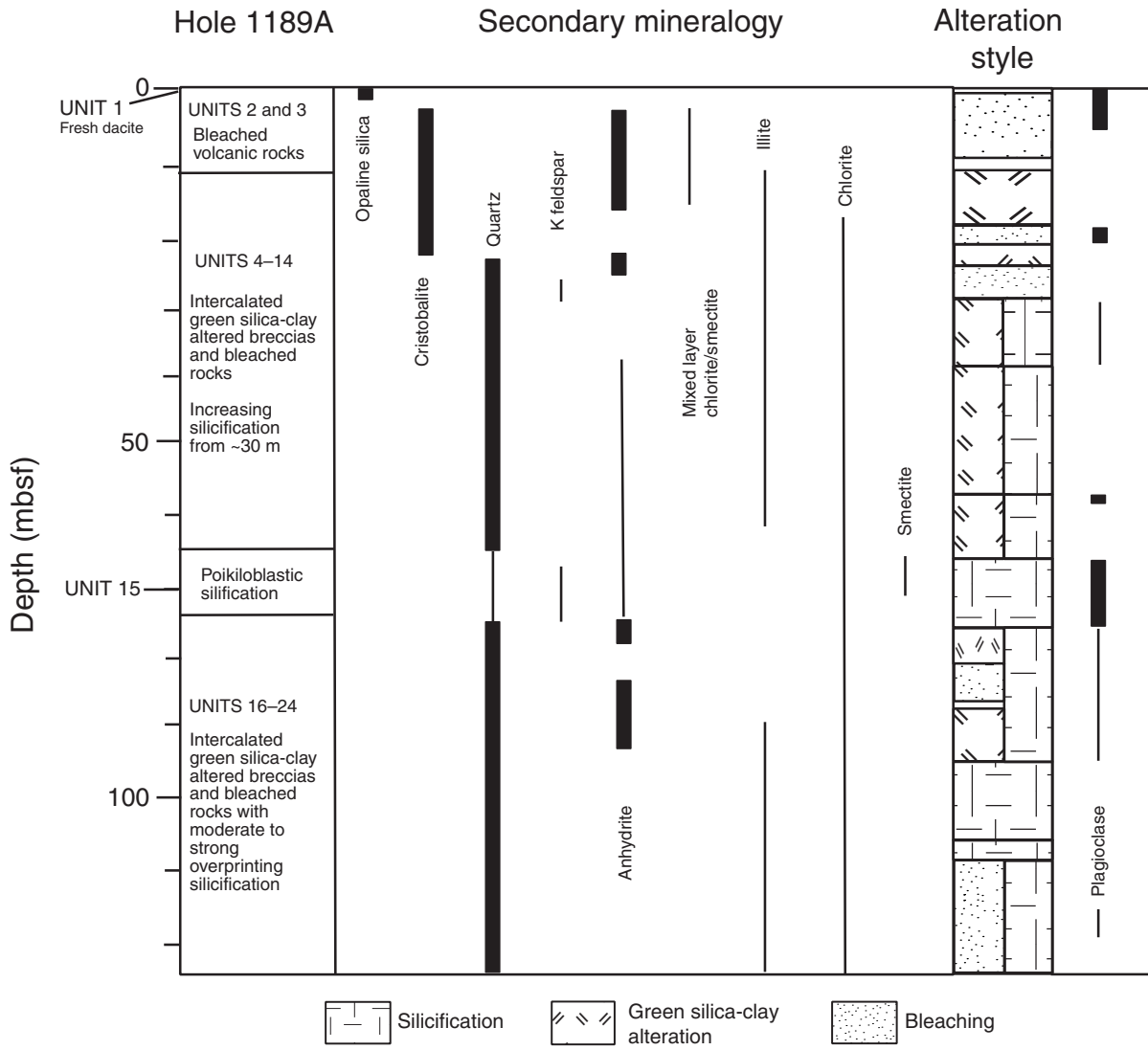


Figure 29A



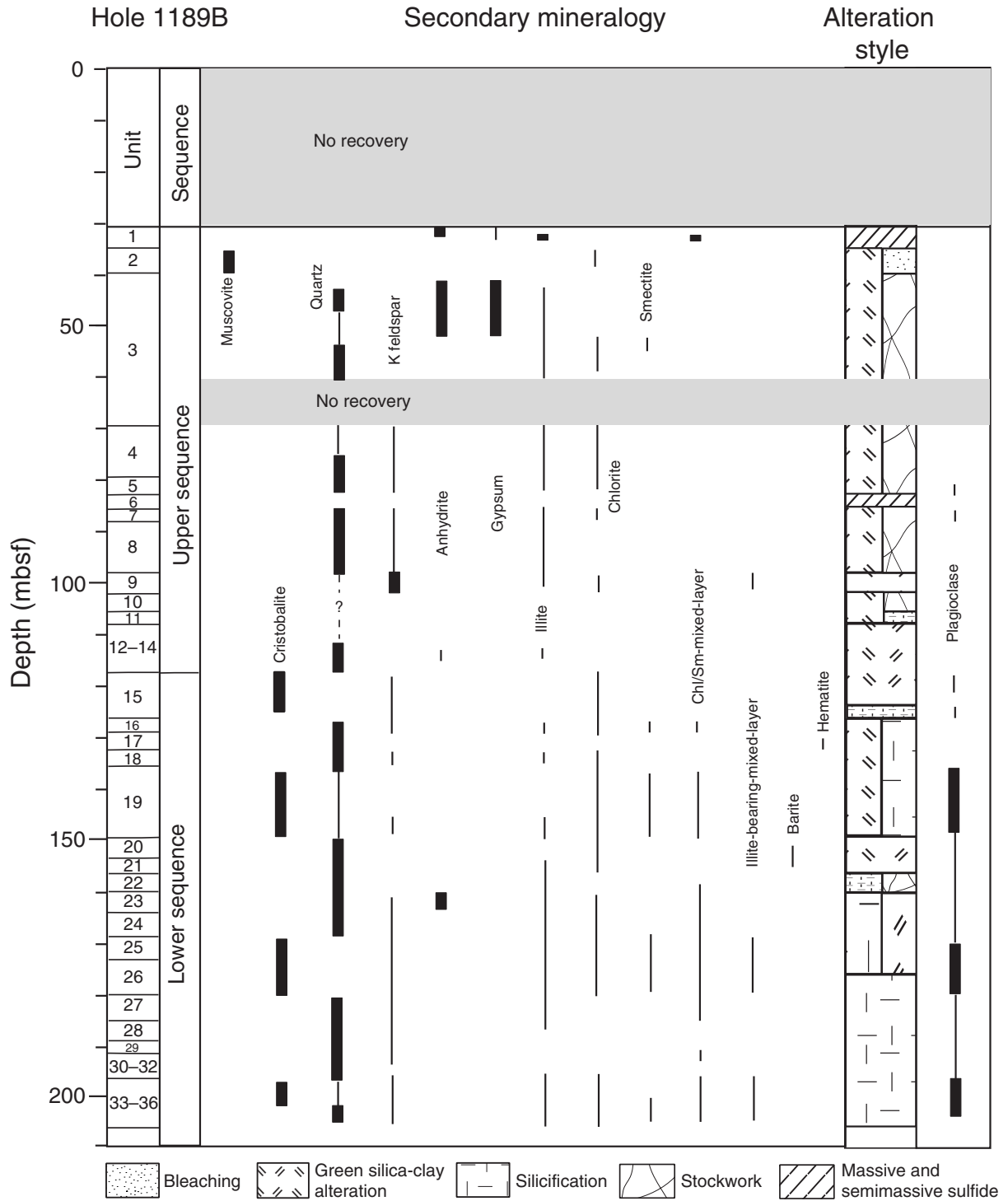


Figure 29B

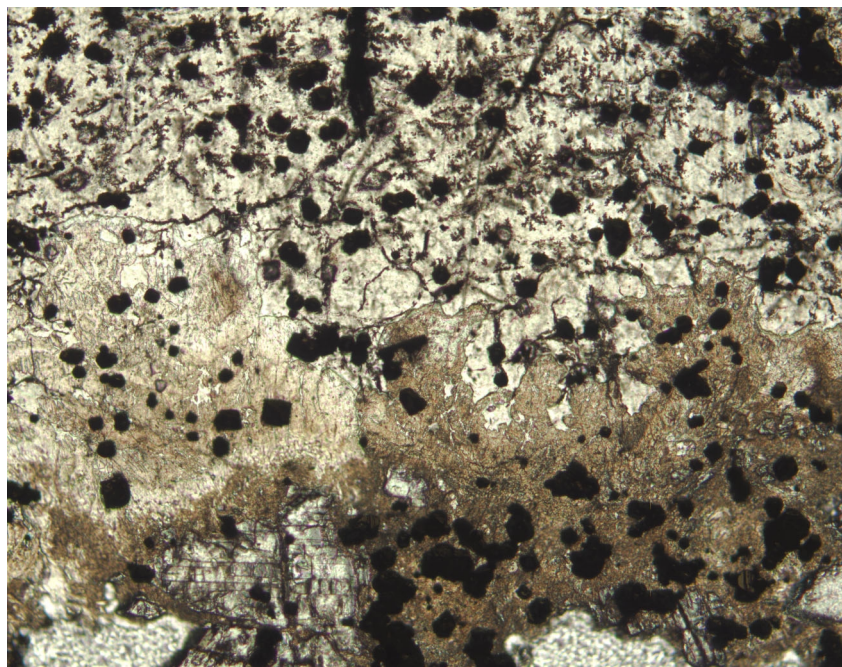


Figure 30

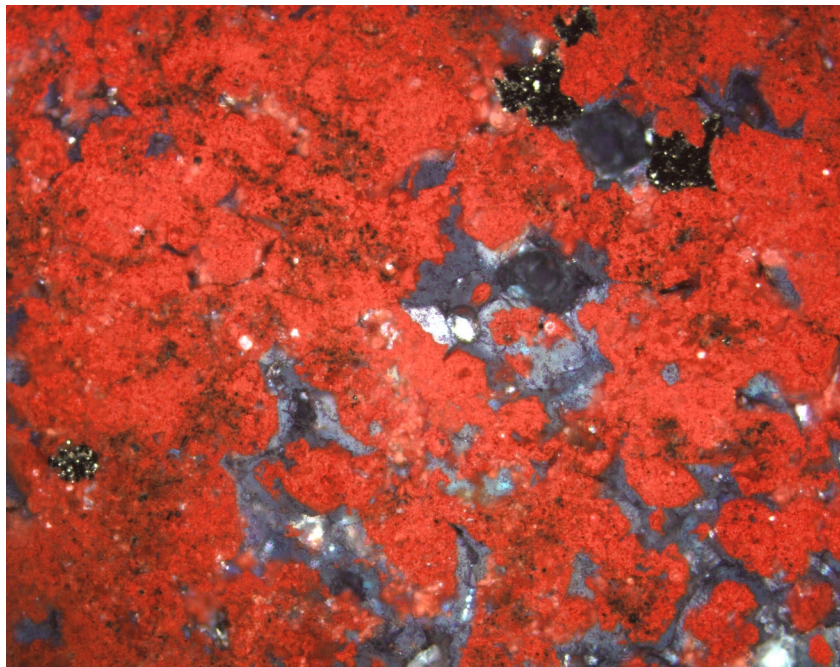


Figure 31

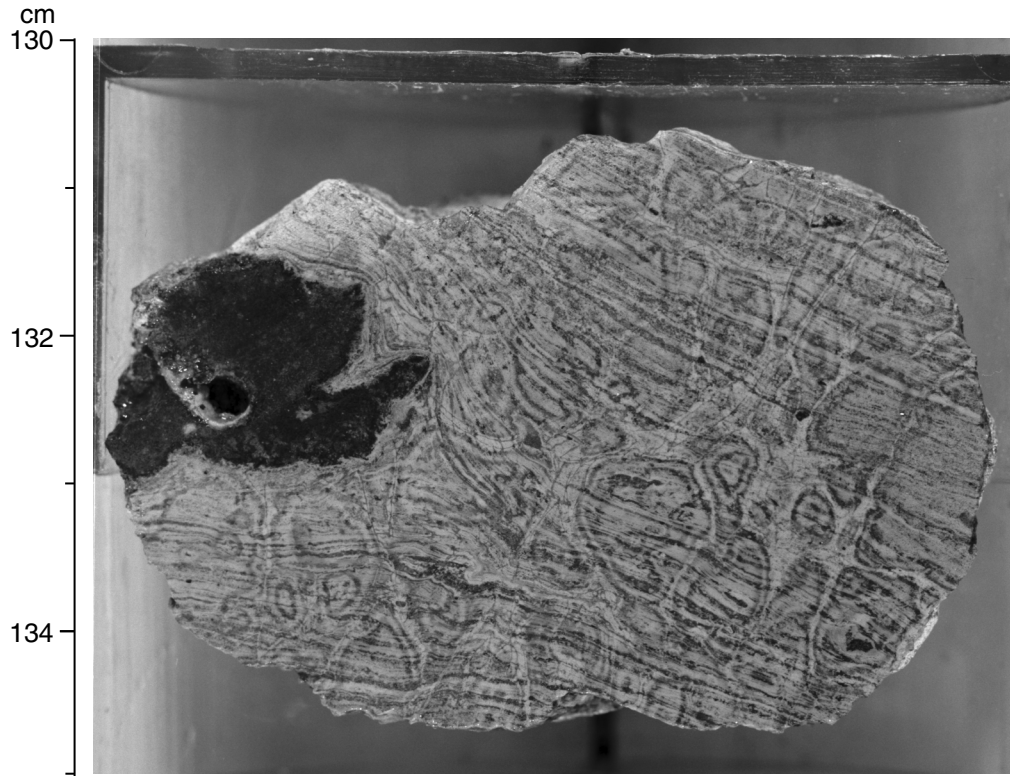


Figure 32



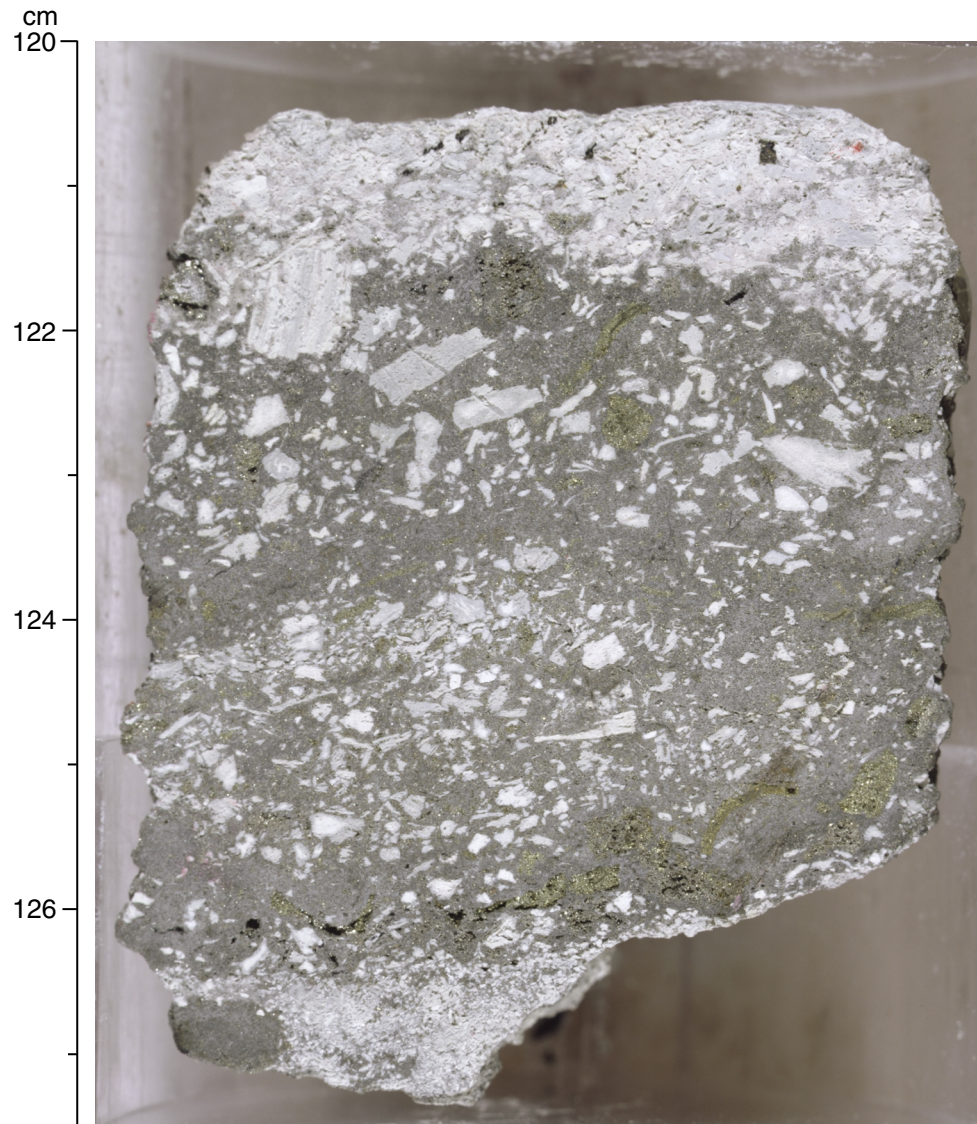


Figure 33A

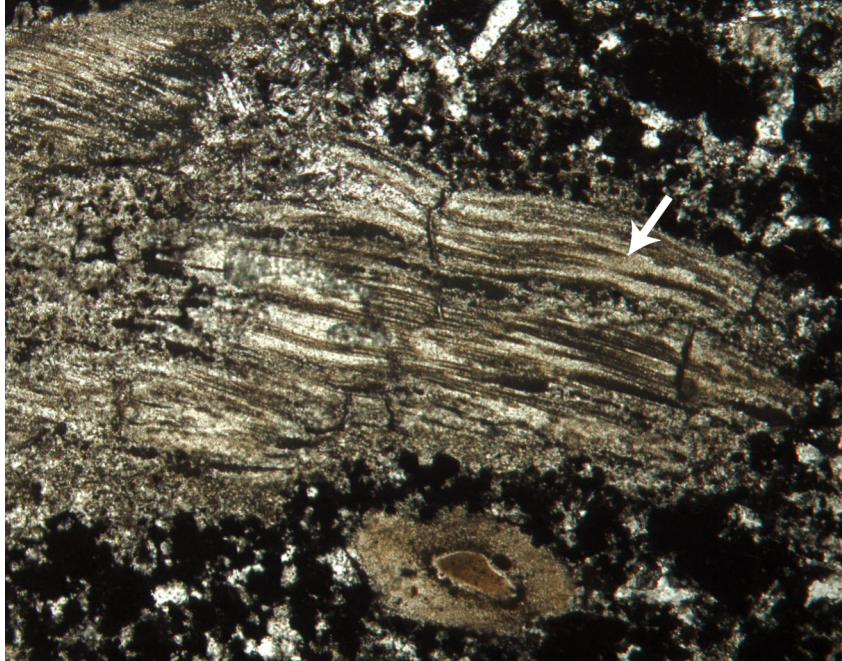


Figure 33B

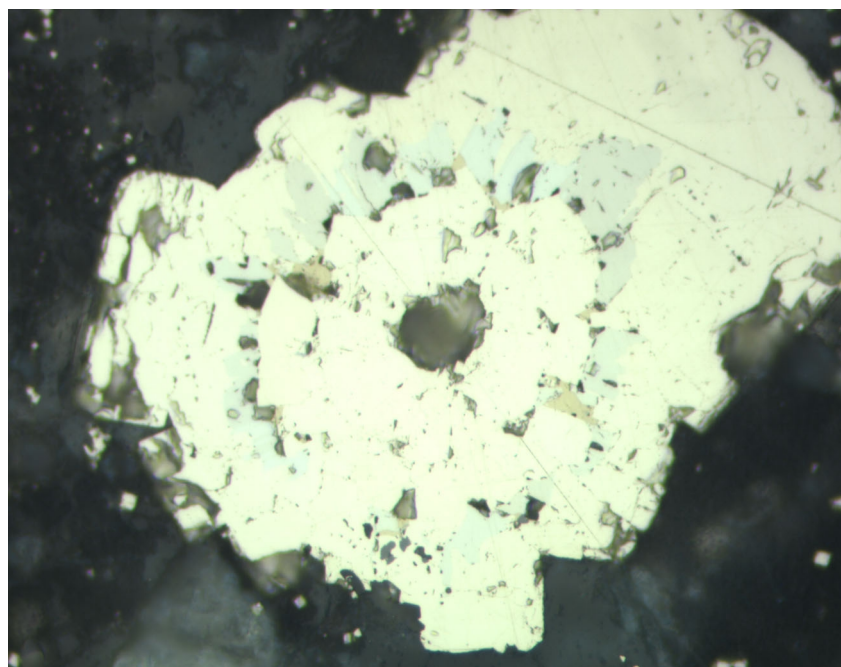


Figure 34



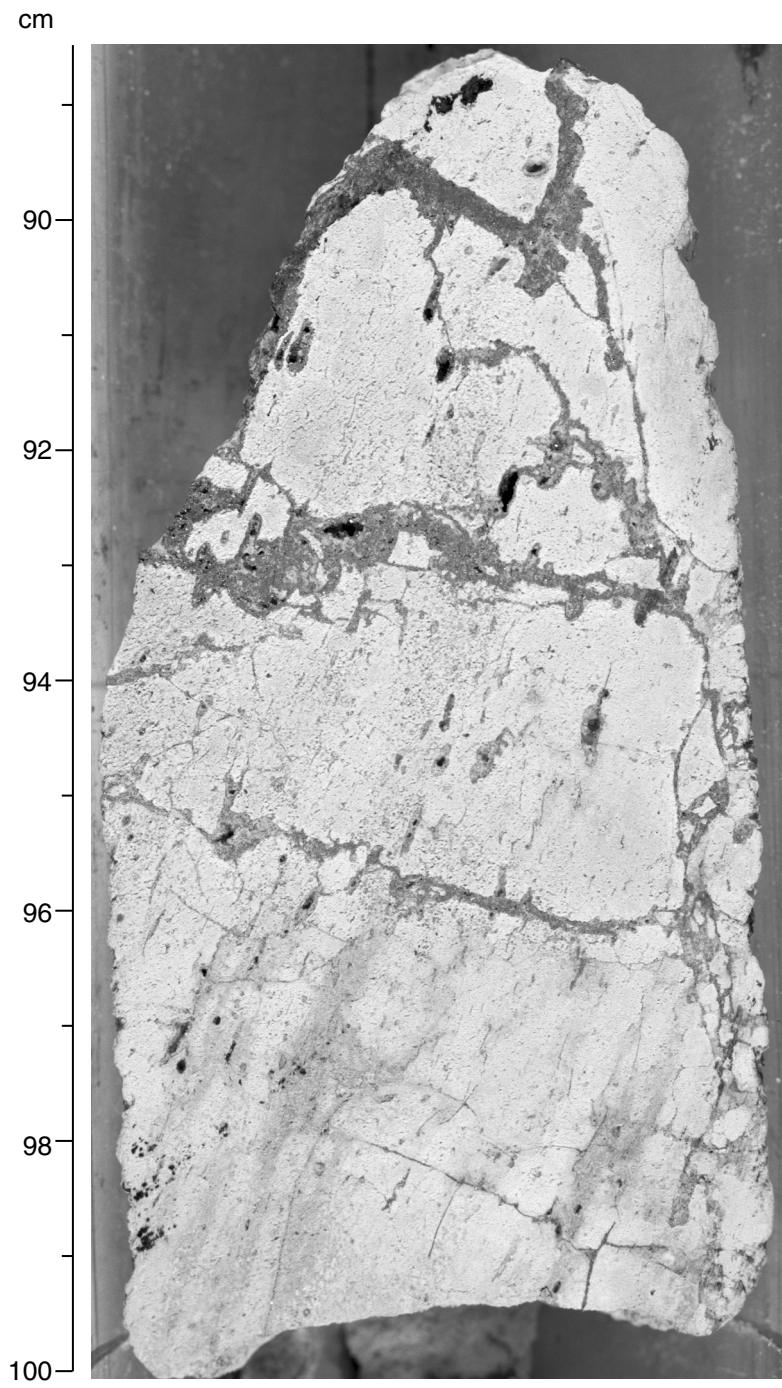


Figure 35



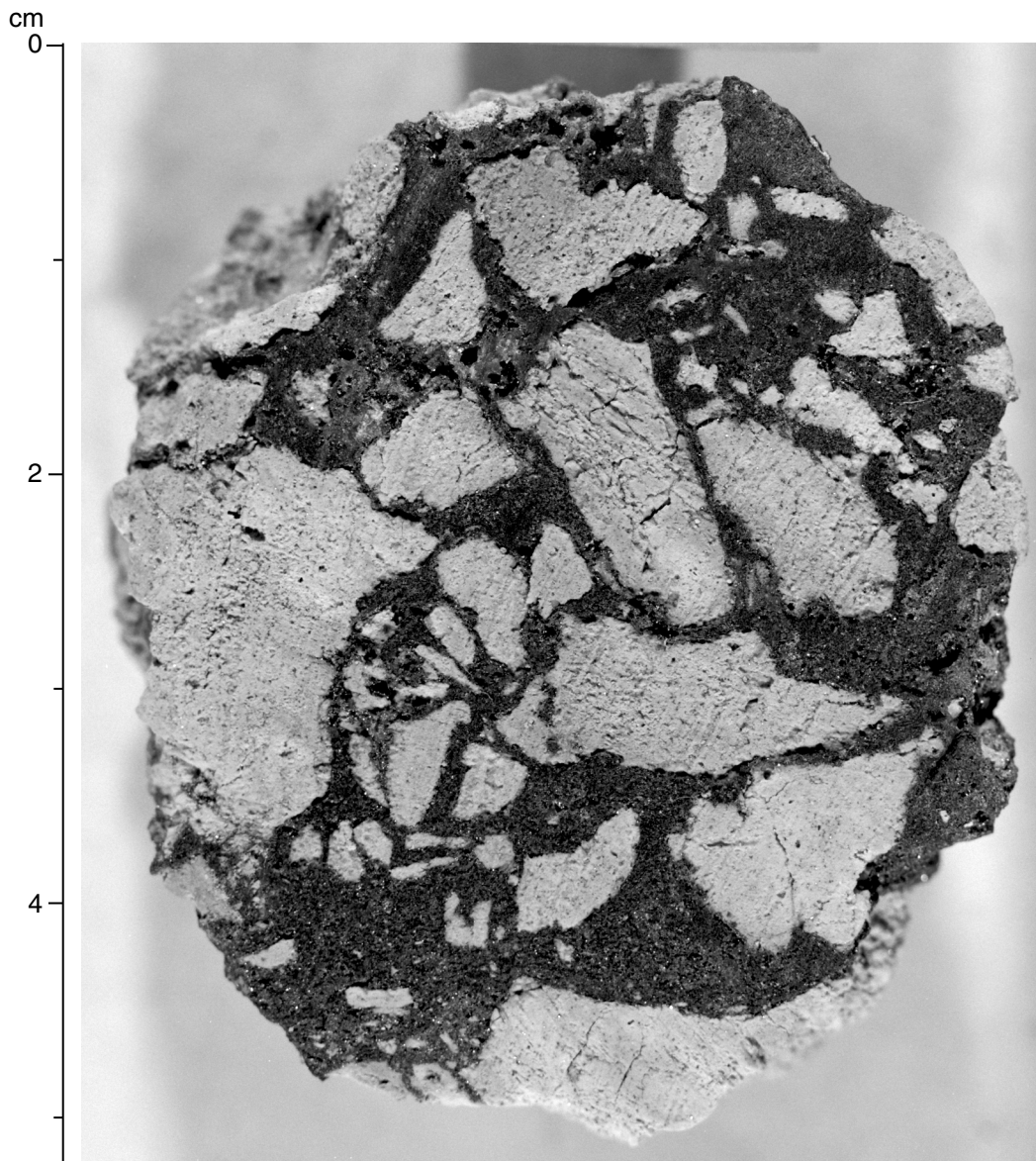


Figure 36

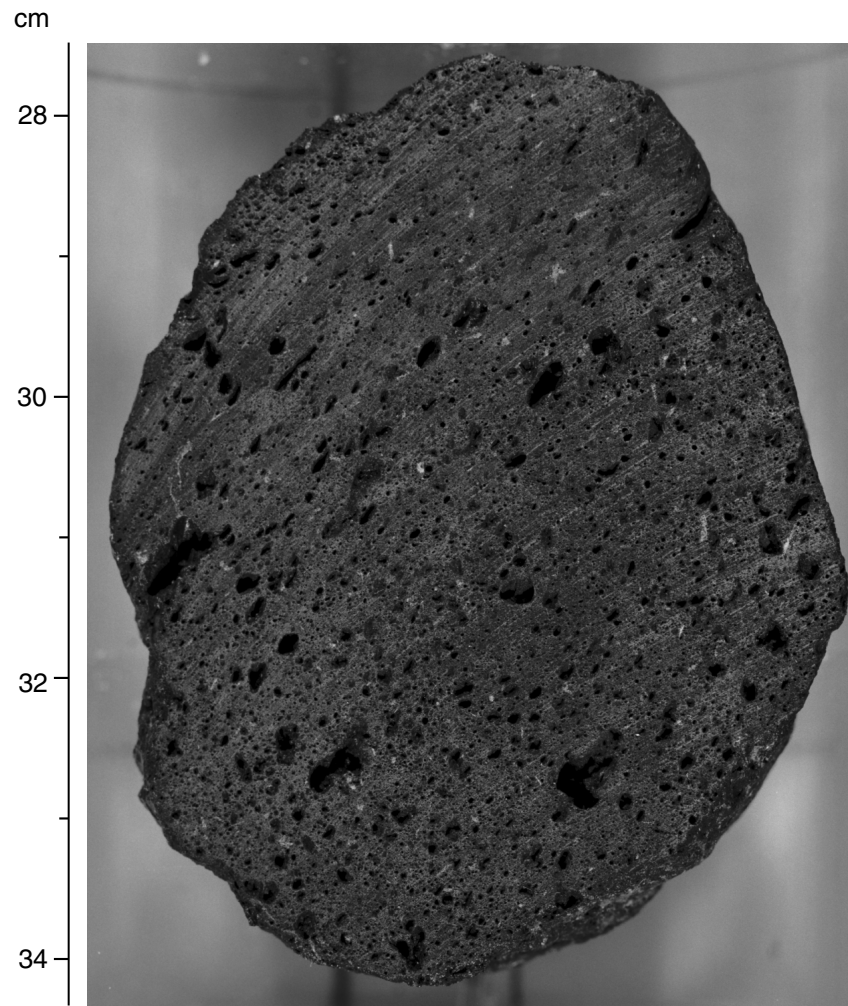


Figure 37

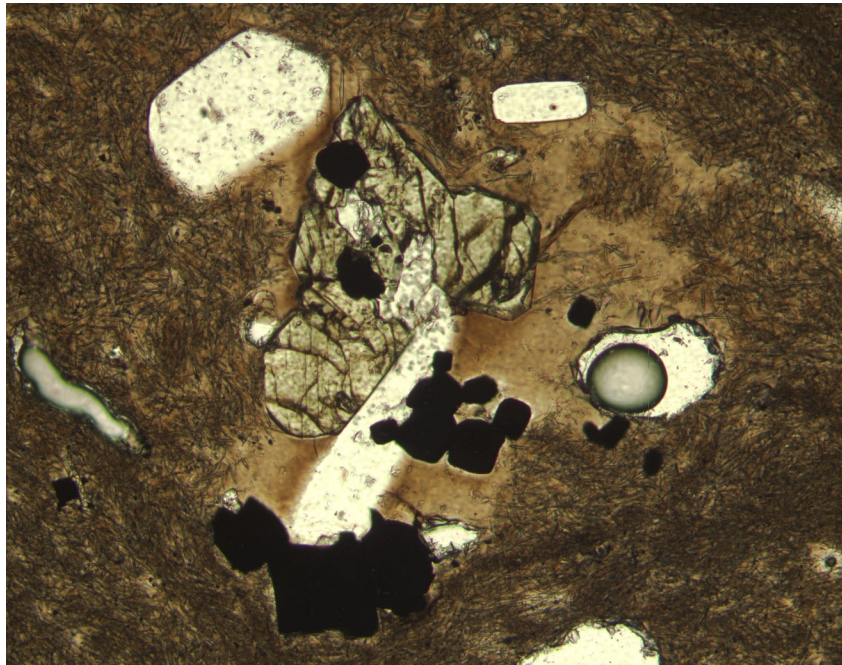


Figure 38

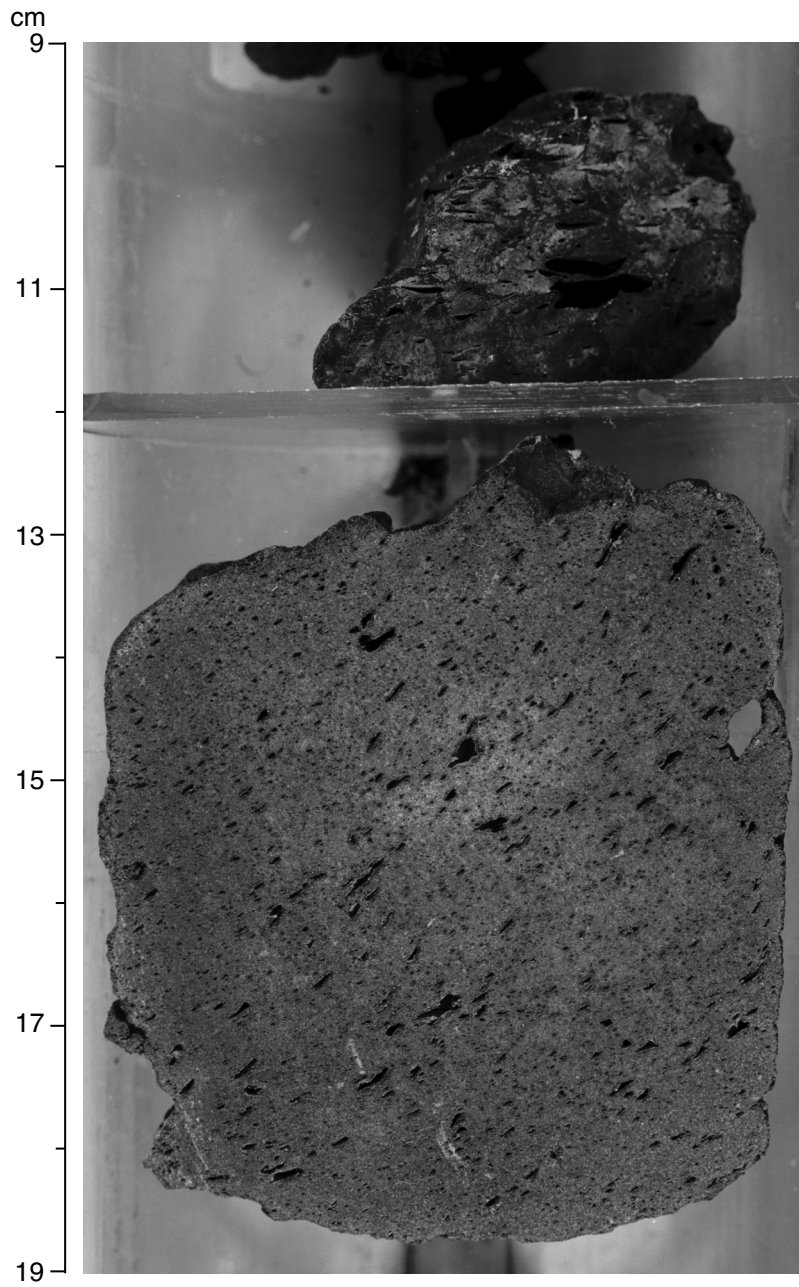


Figure 39

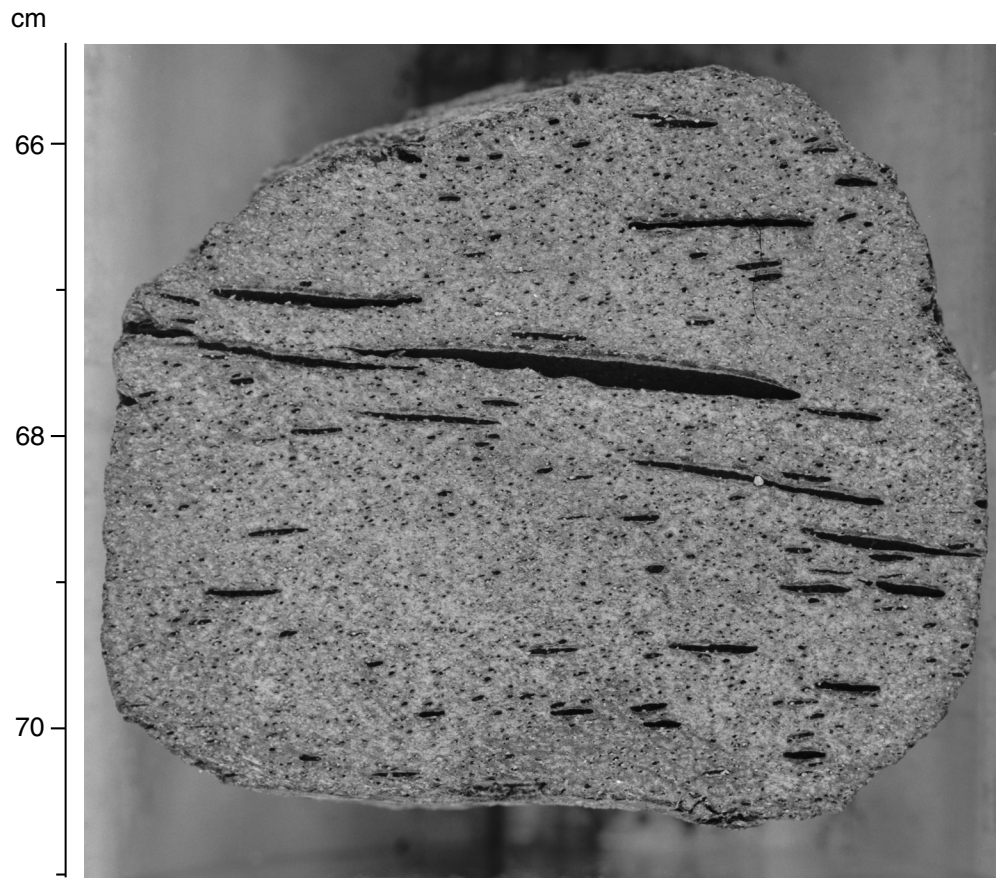


Figure 40



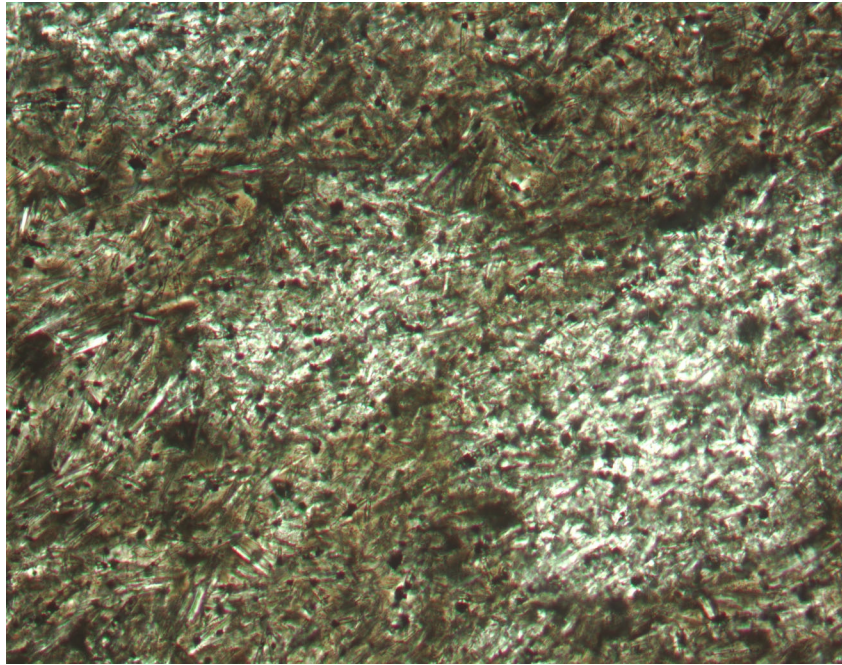


Figure 41

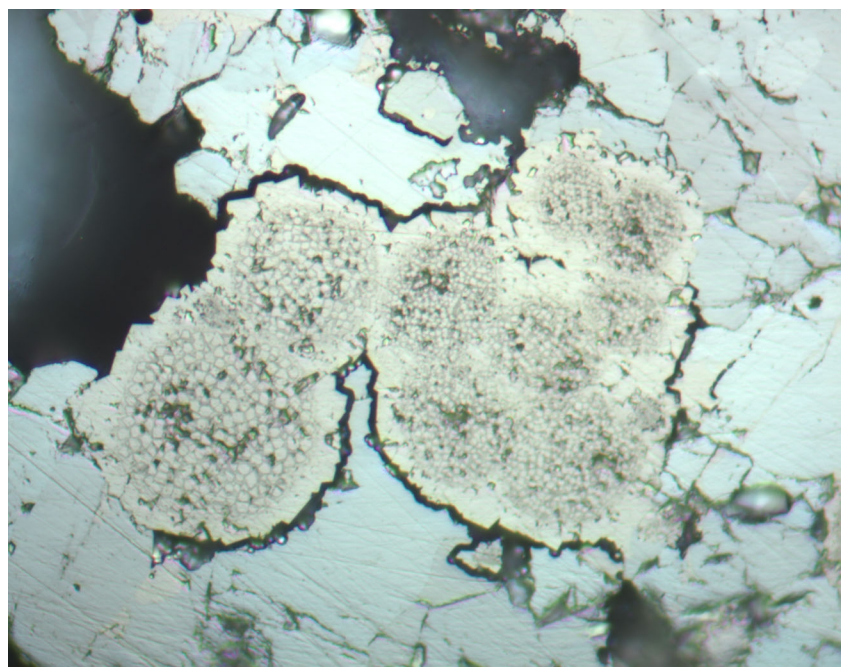


Figure 42